

Assessment of Stiffness in Intact Cartilage Using Contrast-Enhanced Computed Tomography (CECT)

by

Reza Nickmanesh

B.A.Sc., Sharif University of Technology, 2012

A THESIS SUBMITTED IN PARTIAL FULFILLMENT OF THE
REQUIREMENTS FOR THE DEGREE OF MASTER OF
APPLIED SCIENCE

in

The Faculty of Graduate and Postdoctoral Studies

(Biomedical Engineering)

THE UNIVERSITY OF BRITISH COLUMBIA

(Vancouver)

August 2015

© Reza Nickmanesh, 2015

Abstract

Introduction: Osteoarthritis (OA) is the most prevalent joint disease in Canada, affecting millions of people. OA begins with softening of cartilage and is characterized by progressive loss of the tissue resulting in joint impairment. Because cartilage's primary function is mechanical, and because OA disrupts cartilage's mechanical function, there is a substantial need for a non-invasive method to assess cartilage mechanics. Contrast-enhanced computed tomography (CECT) using charged contrast agents is an imaging method developed to quantify Glycosaminoglycan (GAG) content of cartilage. Since GAG is a key determinant of cartilage compressive stiffness, CECT measurements may be correlated with cartilage stiffness. The objective of this study was to determine whether CECT using a novel cationic contrast agent (CA4+) is correlated with cartilage stiffness in intact human joint surfaces.

Methods: Six human femoral condyle compartments with intact healthy cartilage (ICRS grade 0 or 1) were used. Cartilage stiffness was measured across the surface in a Mach-1 testing system (Biomomentum, Montreal) using an indentation test. The samples were then immersed in CA4+ solution for 48 hours and then scanned at 41 μ m resolution in a hr-pQCT scanner (Xtreme CT, Scanco, Zurich). The averages of CECT attenuations at the sites of the indentation tests were computed for both superficial cartilage (600 μ m depth) and for the full thickness of cartilage. Correlations between stiffness and CECT attenuation were assessed with scatter plots and Pearson's correlation coefficient.

Results: A significant and positive correlation was observed between stiffness data and mean CECT attenuations in superficial cartilage across all samples, with correlation coefficients ranging from $r=0.4$ to 0.72 , and $p<0.01$. When data from all locations were pooled ($n=221$), the correlation coefficient was $r=0.55$ and a regression line fitted to the data predicted stiffness from CECT measurements with an error of 20% of the stiffness range. However, correlations between stiffness and CECT attenuations in full-depth cartilage were substantially lower and not significant in half of the tested specimens. CECT identified regions of reduced cartilage stiffness and the expected depth dependent changes in GAG concentration.

Conclusion: CECT of superficial cartilage using CA4+ provides a surrogate measure of compressive cartilage stiffness in intact joint surfaces.

Preface

I was responsible for the study design, data analysis, presenting data and writing the manuscript. Dr. David Wilson provided guidance for the development of the experimental methodologies and provided revisions for the writing of the thesis. This work is covered by UBC clinical research ethics board (certificate H08-02599).

Table of Contents

Abstract	ii
Preface	iii
Table of Contents	iv
List of Tables	vii
List of Figures	viii
List of Acronyms	xii
Acknowledgement	xiii
1 Introduction	1
2 Literature Review	4
2.1 Knee Joint.....	4
2.2 Articular Cartilage.....	5
2.3 Cartilage Biomechanics	7
2.4 Osteoarthritis (OA).....	10
2.5 Osteoarthritis (OA) Treatment	11
2.6 Clinical Osteoarthritis (OA) Evaluation.....	12
2.7 Advanced Osteoarthritis (OA) Imaging	14
2.7.1 MRI	14
2.7.2 CECT.....	15
2.7.2.1 Principle of X-ray and CT	15
2.7.2.1 Principle of CECT	16
2.7.2.3 Application of CECT to Assess GAG	17
2.7.2.4 Application of CECT to Assess Cartilage Mechanics.....	19
2.8 Summary	20
3 Material and Methods	21
3.1 Sample Preparation	21
3.1.1 Sheep Samples.....	21
3.1.2 Human Samples.....	21
3.2 Mechanical Testing	22
3.2.1 Mechanical Testing Apparatus.....	22

3.2.2 Indenter and Positioning of Indenter in Testing Locations	23
3.2.2.1 Indenter.....	23
3.2.2.2 Positioning.....	24
3.2.3 Indentation Test Protocol	24
3.2.3.1 Surface Localization Procedure.....	24
3.2.3.2 Surface Orientation Determination.....	25
3.2.3.3 Normal Indentation.....	25
3.2.3.4 Cartilage Stiffness Calculation	26
3.3 CECT Imaging	27
3.3.1 Equilibration in Contrast Agent Solution.....	27
3.3.2 Sample Preparation for Scan	28
3.3.3 CT Scan Protocol.....	28
3.3.4 [CA4+] Computation from CECT Measurements	28
3.3.5 Image Processing.....	29
3.3.5.1 Cartilage Surface Segmentation	29
3.3.5.2 CECT Mapping of Articular Cartilage	29
3.3.5.3 Determination of Testing Location in CECT Scans.....	30
3.3.5.4 Regions of Interest for Calculating CECT Attenuation.....	31
3.3.5.6 Thickness Measurement	32
3.4 Statistical Analysis	33
4 Results	34
4.1 Sheep Samples	34
4.2 Human Samples	36
4.2.1 Qualitative Comparison between Stiffness and CECT Measurements	37
4.2.2 Correlation Analysis between Stiffness and CECT Measurements	40
4.2.3 Spatial Variation and Depth Dependence of CECT Measurements.....	43
4.2.3 Effect of Compartment (Medial/Lateral).....	44
4.2.4 Effect of Cartilage Grade	46
4.2.4 Effect of Thickness Variations on Stiffness Measurements.....	46
5 Discussions	49
5.1 Motivation and Contributions	49
5.2 Significance and Findings	49

5.2.1 Comparison of Indentation and CECT Results with Literature	49
5.2.2 Selecting the Wrong Region of Interest Confounds the Results	50
5.2.3 Predictive Potential of CECT for Stiffness Measurement.....	51
5.2.4 Why Would We not Expect $r=1$ between CECT and Stiffness Measurements?.....	52
5.2.4 CECT Advantages over MRI Methods	52
5.2.5 Challenges to Implement CECT in Clinical Practice	53
5.2.6 CECT Offers an Aternative for Histology Assessment in Cartilage Repair Studies.....	53
5.3 Strengths.....	53
5.4 Limitations	55
5.5 Future Directions.....	56
5.6 Conclusion.....	57
References.....	58
Appendices.....	68
Appendix A: Validation of the Time Required for CA4+ to Reach Equilibrium.	68
Appendix B: Variation of Mean X-ray Attenuation with Changes in Contrast Agent Concentration	80
Appendix C: Repeatability of Indentation Stiffness Measurement.....	83
Appendix D: Validation of Articular Cartilage Thickness Measurement Using CECT	86
Appendix E: Registration Accuracy.....	89
Appendix F: Repeatability of CECT Measurements	91
Appendix G: Estimation of the Young's Modulus of Cartilage using Indentation and CECT Measurement of Thickness	95
Appendix H: Comparison between Different Measures of Cartilage Stiffness (Instantaneous, Equilibrium, and Dynamic Stiffness).....	97
Appendix I: Accuracy Assessment of the Normal Displacement in the Indentation Protocol	101
Appendix J: Calibration Certificate for the Load-Cell and the Control Report for all Stages.....	104

List of Tables

Table 2.1: Kellgren Lawrence grading of radiographic OA	13
Table 2.2:International Cartilage Repair Society (ICRS) grading system based on cartilage lesions.	13
Table 2.3: Comparison between commonly used methods for osteoarthritis diagnosis.	14
Table 4.1: Stiffness and CECT measurements in human cartilage samples	37
Table 4.2: The correlation coefficients between stiffness measurement and mean CECT attenuation (superficial and full-depth) in human cartilage samples.	37
Table 4.3 : Correlation coefficients between stiffness and thickness data in human cartilage samples. Mean±SD values of thickness is presented in the second row.....	47
Table A.1: The correlation coefficient between the pattern of GAG distribution at measured time points and the equilibrium state.	75
Table C.1: Mean, SD, and CV of stiffness measurement for each testing location.....	84
Table E.1: Estimation error for determination of coordinates in image space.....	90
Table F.1: Mapping of CECT attenuation (averaged over 0.6mm) in two scans representing two complete equilibration and imaging cycles in one specimen.....	92
Table H.1: Correlation analysis among different measures of cartilage stiffness	99
Table I.1: Comparison between the surface normal vector and the net displacement vector.....	103

List of Figures

Figure 2.1: Anterior view of the knee.	4
Figure 2.2: Articulating surfaces of the knee joint.....	5
Figure 2.3: Illustration of cartilage constituents and zonal variations along cartilage depth.....	7
Figure 2.4: Viscoelastic behavior of articular cartilage under two common loading protocols: stress relaxation and creep.	8
Figure 2.5: Common configurations for mechanical testing of articular cartilage: unconfined compression test, confined compression test, and indentation test.	9
Figure 2.6: Immediate and equilibrium load responses of cartilage to displacement.	10
Figure 2.7: Normal versus OA knee joint representation in x-ray images.....	12
Figure 2.8: The principle of contrast-enhanced computed tomography of articular cartilage.....	17
Figure 3.1: Top view of the testing chamber of the mechanical tester.	22
Figure 3.2: Mechanical testing setup.	23
Figure 3.3: 1 mm diameter and 0.35 mm diameter spherical indenters.....	24
Figure 3.4: Indentation test protocol.	26
Figure 3.5: normal force-normal displacement curve in indentation.....	27
Figure 3.6: Image processing algorithm used for mapping CECT attenuation.....	30
Figure 3.7: Locating indentation sites in CECT image.....	31
Figure 3.8: Definition of the region of interest (ROI) corresponding to the indentation test on CECT images.	32
Figure 4.1: Maps of CECT attenuation in 2 sheep cartilage samples.	34
Figure 4.2: Scatter plots of stiffness versus CECT measurements	35
Figure 4.3: Correlation analysis of the combined data in sheep samples.	35

Figure 4.4: Maps of CECT attenuation and stiffness measurements.....	38
Figure 4.5: Scatterplots of stiffness vs. mean CECT attenuation (0.6 mm depth) in all medial cartilage compartments.....	40
Figure 4.6: Scatterplot of pooled stiffness measurement vs. mean CECT attenuation (0.6 mm depth).	41
Figure 4.7: Scatterplots of stiffness vs. mean CECT attenuation (full-depth) in all medial cartilage compartments.....	42
Figure 4.8: CECT maps of human cartilage surface.....	43
Figure 4.9: Variation of CECT attenuation along cartilage thickness.....	44
Figure 4.10: Scatterplots of stiffness vs. mean CECT attenuation (0.6 mm depth) in all medial cartilage compartments.....	45
Figure 4.11: Scatterplots of stiffness vs. mean CECT attenuation (0.6 mm depth) in all lateral cartilage compartments.....	45
Figure 4.12: Scatterplots of stiffness versus mean CECT attenuation (0.6 mm depth) in grade 0 and 1 testing locations.....	46
Figure 4.13: Distribution of articular cartilage thickness across samples.....	47
Figure 4.14: Scatterplot of stiffness vs. thickness in human cartilage samples.....	48
Figure 4.15: Scatterplots of stiffness vs. mean CECT attenuation (0.6 mm depth) in all testing locations and testing locations with thickness >2mm.....	48
Figure A.1: Top view of the sample used for the diffusion experiment.....	69
Figure A.2: Diffusion behavior of the cationic contrast agent (CA ⁴⁺) into superficial human femoral cartilage.....	70
Figure A.3: Diffusion behavior of the cationic contrast agent (CA ⁴⁺) into full-thickness human femoral cartilage.....	71

Figure A.4: Topographical maps of CECT attenuation, reflecting contrast agent concentration in superficial cartilage.	72
Figure A.5: Topographical maps of contrast agent concentration in full-depth cartilage.	73
Figure A.6: Mean CECT attenuation of superficial cartilage in each region of interest plotted as a function of immersion time.....	74
Figure A.7: Mean CECT attenuation of full-depth cartilage in each region of interest plotted as a function of immersion time.....	74
Figure A.8: CA4+ concentration in articular cartilage as a percentage of the immersion solution concentration, plotted as a function of immersion time.....	75
Figure A.9: Cross-sectional (sagittal plane) CECT images of the human medial femoral cartilage at different time points.	76
Figure A.10: Spatial contrast agent profiles along cartilage thickness as a function of immersion time and the depth-wise GAG concentration.....	77
Figure B.1: Xtreme-CT image of phantom tubes with different levels of CA4+ concentration.	81
Figure B.2: Linear correlation between CA4+ concentration and observed x-ray attenuation in CECT scans.....	81
Figure C.1: Repeatability of stiffness measurements for a series of 16 testing locations on one lateral femoral cartilage compartment	84
Figure D.1: Needle indentation technique for physical measurement of cartilage thickness	87
Figure D.2: Thickness measurements from needle indentation method versus CECT method (Femoral condyle).....	87
Figure D.3: Thickness measurements from needle indentation method versus CECT method (Tibial plateau).....	88
Figure E.1: The metal markers in physical space and image space.....	89

Figure F.1: Mapping of CECT attenuation (averaged over 0.6mm) in two scans representing two complete equilibration and imaging cycles in one specimen.....92

Figure F.2: Repeatability of CECT measurements for a series of 38 testing locations in one lateral femoral compartment.93

Figure H.1: Displacement protocol used for inferring different measures of cartilage stiffness.....98

Figure H.2: Schematic representation of cartilage load response to the multi-functional displacement protocol.....98

Figure H.3: Comparison of different 6 load response profiles across 12 locations on one femoral condyle cartilage99

Figure I.1: Displacement versus time curves in X, Y, and Z directions (Plots A, B, and C, respectively) for the stages of the Mach 1 system during a typical cartilage indentation test..... 102

List of Acronyms

CECT	Contrast Enhanced Computed Tomography
CT	Computed Tomography
dGERMIC	Delayed Gadolinium Enhanced Magnetic Resonance Imaging of Cartilage
E	Young's Modulus
ECM	Extracellular Matrix
FCD	Fixed Charged Density
GAG	Glycosaminoglycan
HFC	Human Femoral Condyle
MRI	Magnetic Resonance Imaging
OA	Osteoarthritis
PG	Proteoglycan
pQCT	Peripheral Quantitative CT
PBS	Phosphate Buffered Saline
PF	Patellofemoral
TF	Tibiofemoral
V	Poisson's Ratio

Acknowledgments

I would like to express my sincere thanks to Dr. David Wilson for his priceless guidance and support during my studies. His insightful feedback has been a key part of my learning experience.

I would also like to thank all of the students, faculty and staff at the Center for Hip Health and Mobility for making my graduate study memorable.

I am grateful for the assistance given by our collaborators at the Boston University, particularly Dr. Rachel Stewart.

I am grateful for the support given by the staff at Biomomentum Company, particularly Dr. Martin Garon.

Finally, I would like to thank my beloved family and friends for continuous support and being there beside me through hard times.

1 Introduction

Osteoarthritis (OA) is the most prevalent joint disease and a leading cause of disability that adversely affects the lives of more than 5 million Canadians. OA begins with softening of cartilage and is characterized by progressive loss of the tissue resulting in chronic pain and dysfunction of the joint. The prevalence of the disease is predicted to rise from 1 out of 9 Canadians to 1 out of 4 by the year 2030 [1]. The economic burden is crippling, estimated to cost socially \$ 195.2 billion between the years 2010 and 2015 [1].

Many aspects of OA are not well understood, mainly because monitoring the disease *in vivo* is difficult. Current methods for monitoring OA are not sensitive enough to changes, and the disease is not diagnosed until its advanced stages, at which point it is irreversible. At this time there is no effective cure for OA. Treatment of the affected joint in advanced OA is limited to control of symptoms (pain and inflammation), which has no effect on the progression of OA. In most OA cases, the only viable option for the patient is total joint replacement surgery, which often requires revision after 10-15 years [1].

There is a substantial need for an imaging method that can non-invasively assess mechanical properties of cartilage. The function of cartilage in the joints is mechanical, and thus mechanical parameters such as stiffness are the most important measures of cartilage health. The most widely used current method for measuring cartilage stiffness is to probe the tissue during arthroscopy, which is invasive and has shown poor repeatability [63], [64]. A surrogate, noninvasive *in vivo* measure of cartilage stiffness would be very useful for studying changes in cartilage mechanics with OA progression and treatment. Such a method would also be potentially useful for early diagnosis of cartilage degeneration.

Current methods can assess various quantitative measures of articular cartilage but have limitations. The most commonly used method for assessment of cartilage status is radiography. This method lacks the ability to image the cartilage directly. In radiography, cartilage degeneration is detected as the narrowed space between the bones in the joint. Radiography therefore identifies OA when gross cartilage loss becomes evident, which indicates an advanced and irreversible stage of OA. MRI, in contrast to radiography, is able to visualize cartilage directly and thus assess its morphology. Several quantitative MRI techniques have been developed for non-invasive assessment of cartilage

composition and structure [2],[3]. Of particular interest is delayed gadolinium-enhanced MRI of cartilage (dGEMRIC), a technique that assesses glycosaminoglycan (GAG) content of articular cartilage using an anionic contrast agent [4],[5],[6]. dGEMRIC has been successfully used *in vivo* [7],[8],[9] and *in vitro* [10],[11] to differentiate between normal and degenerated cartilage, and the dGEMRIC measure has been found to be associated with the mechanical stiffness of cartilage [12],[13],[14]. However, the reliability of dGEMRIC for reflecting GAG content and mechanical properties has been questioned in several investigations [2],[15],[16]. Furthermore, the use of MRI for assessment of cartilage has some limitations including high cost, long acquisition time, low resolution, and difficult interpretation of the MRI signal.

Contrast-enhanced computed tomography (CECT) using charged contrast agents is a non-invasive imaging technique developed to quantify GAG content of articular cartilage. Since CT imaging is x-ray based, unenhanced cartilage is not visible on CT images. In CECT, contrast agents are used to enhance the contrast of cartilage in CT images. Most CECT has been done with anionic contrast agents. Electrostatic repulsion between the anionic contrast agent and negatively-charged GAG molecules results in accumulation of contrast agents within cartilage in inverse proportion to GAG content. These accumulations are reflected in x-ray attenuation in CECT images, which then becomes an index of GAG content. Recently, a novel cationic contrast agent (CA4+) has been developed to be used along with CECT method [17],[18]. Using CA4+, the cationic contrast agent is attracted to negatively-charged GAG molecules and accumulates within the cartilage in direct proportion to GAG concentration. CA4+ has shown higher sensitivity to GAG content of cartilage compared to its anionic counterparts [19],[18] and has been validated against histology assessments and mechanical measurements in plugs of animal cartilage [20],[21],[22].

CECT attenuation using the novel cationic contrast agent (CA4+) has potential to be used as a surrogate measure for cartilage stiffness. To reach that goal, the correlation between CECT measurements and cartilage stiffness must be determined. Two key limitations of previous studies linking CECT attenuation and cartilage stiffness are 1) that they have not assessed human tissue and b) that they have used cartilage plugs instead of intact cartilage surfaces. Stiffness measured in the intact surface of cartilage is more representative of cartilage behavior in *in vivo*. The indentation testing method allows investigators to map the stiffness across the cartilage surface with high spatial resolution, while preserving the physiologic environment of the tissue.

The objective of the present study was to determine the association between CECT using a cationic contrast agent and stiffness measures from indentation testing in intact human cartilage.

The following specific questions were also addressed:

- Is the relationship between stiffness and CECT measurements different in medial and lateral femoral cartilage?
- Is the relationship between stiffness and CECT measurements different in normal (ICRS grade 0) and nearly-normal (ICRS grade I) cartilage?
- How does the depth over which CECT attenuation is averaged (superficial versus full-depth cartilage) affects the relationship between stiffness and CECT measurements?
- How does variation in cartilage thickness influence stiffness measurements in our indentation protocol?

2 Literature Review

2.1 Knee Joint

The knee is a weight-bearing joint that facilitates movement between the thigh and the shank. It is the largest joint in the human body. The knee joint is composed of muscles, ligaments, meniscus, bones, and articular cartilage (Figure 2.1).

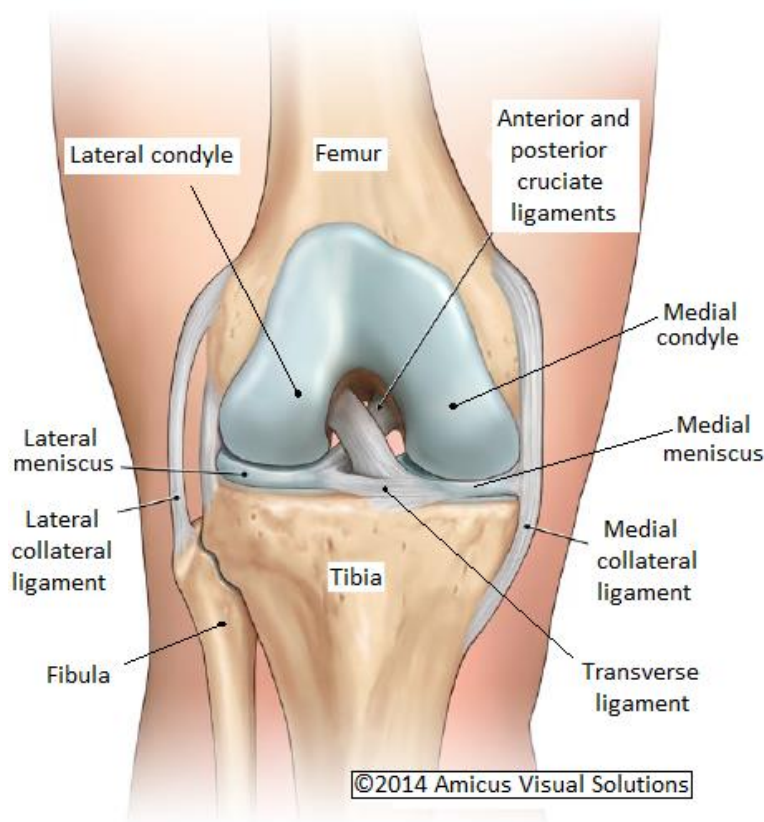


Figure 2.1 Anterior view of the knee.

©Reproduced with permission from Amicus Visual Solutions.

The knee consists of two main articulating joints: the tibiofemoral (TF) and patellofemoral (PF) joints. The TF and PF joints distribute and transmit load during physical activities. In the TF joint, the medial and lateral tibial plateaus articulate with the femoral condyles. In the PF joint, the posterior surface of the patella articulates with the anterior surface of the distal femur where the medial and lateral femoral condyles meet. In total, there are five articulating surfaces in the knee

joint: 2 femoral condyles, 2 tibial plateaus, and the patella (Figure 2.2). All articulating surfaces are covered by articular cartilage.



Figure 2.2 Articulating surfaces of the knee joint.
©Reproduced with permission from Medical Multimedia Group.

2.2 Articular Cartilage

Articular cartilage covers the ends of the bones in diarthrodial joints such as the knee. This tissue permits smooth motion to occur between the bones by providing a well-lubricated and low-friction articulating surface [23]. Furthermore, articular cartilage transmits and distributes the loads in the joint. Cartilage contains no blood vessels or nerves [23], and thus suffers from limited capacity for repair and regeneration [24].

Articular cartilage has two main components: extracellular matrix (ECM) and chondrocytes (cartilage cells). ECM is a porous and permeable matrix consisting mainly (60-80%) of water, most of which is bound to ECM proteins called proteoglycans [25]. The rest of its solid weight is comprised of proteoglycans (4-7%) and collagen (15-22%). In normal and healthy cartilage, chondrocytes comprise only 1-5% of the volume of articular cartilage. The interplay among articular

cartilage components (in particular proteoglycan and collagen) plays a key role in the mechanical behavior of cartilage [26].

Proteoglycan (PG) has a major role in the compressive stiffness of the cartilage [25]. Proteoglycans are made of a core protein to which negatively-charged glycosaminoglycan (GAG) side chains are attached. The large proteoglycans, called aggrecans, bind to each other with linking proteins to form massive PG aggregates [27]. The formation of these giant aggregates results in immobilization of PGs in the cartilage matrix and prevents detachment under loading condition. The resulting negative fixed charged density (FCD) absorbs water, and there is substantial resistance to fluid flow out of the ECM due to the porous structure of the cartilage matrix. The incompressible fluid trapped in the ECM provides cartilage with its ability to withstand compressive loads [25]. Additionally, the high concentration of the negatively-charged side chains of PG generates electrostatic repulsion force among the chains. These two mechanisms contribute to the load-bearing capacity of the cartilage under compression.

The collagen network primarily provides the tensile strength of the cartilage [28]. It also resists excessive expansion of the ECM that occurs otherwise due to the swelling pressure applied by PG and water [29]. The cartilage can be divided into 4 distinct zones along its thickness [29] (Figure 2.3): the superficial zone, the middle zone, the deep zone, and the calcified zone. Collagen fibers run parallel to the articular surface in the superficial zone of the tissue. Often the earliest degenerative signs appear in the superficial zone. In the middle zone, the collagen fibers are mostly in a random arrangement and arch towards the deep zone. Fibrils in this layer transition from a parallel orientation towards a radial orientation. In the deep zone, the fibers are in a perpendicular arrangement to the articular surface and are usually larger in diameter (fibers range between 20-200 nm in diameter). Below the deep zone, often a fourth zone of calcified cartilage is found. In contrast to collagen distribution, the PG content of the articular cartilage increases with depth from the surface, with the lowest and highest concentration in superficial zone and deep zone, respectively [24].

Chondrocytes are the only cells that are found in the articular cartilage. The primary function of these highly specialized cells is to synthesize and maintain the components of the ECM. Chondrocytes can respond to mechanical changes in the environment through degradation and synthesis [24]. Since there are no blood vessels in the cartilage, the flow of water across the surface and through the cartilage transports nutrients to chondrocytes.

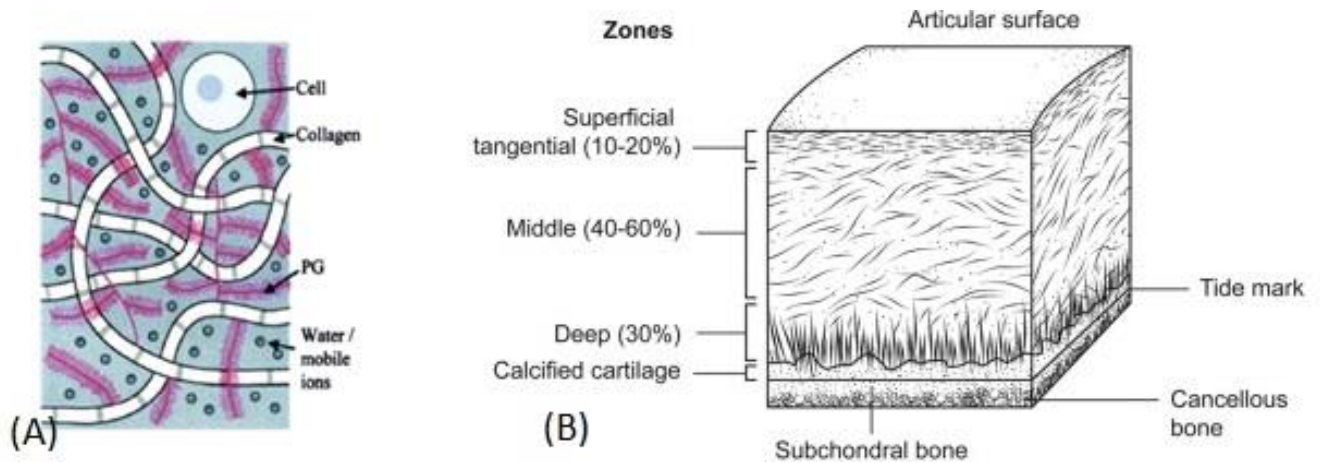


Figure 2.3 Illustration of cartilage constituents (A) and zonal variations along cartilage depth (B).
 © Illustration A is reproduced from [30] with permission from Wolters Kluwer Health, Inc. Illustration B is reproduced from [31] with permission from Elsevier.

2.3 Cartilage Biomechanics

Articular cartilage exhibits viscoelastic behavior under loading [25]. The viscoelastic response of cartilage is tied to the fluid flow in the tissue. There are several experimental methods to investigate the mechanical behavior of articular cartilage under loading. These methods typically use one of two main loading protocols: stress-relaxation or creep test (Figure 2.4). In the stress-relaxation protocol, a displacement is applied at a constant rate and the load response is measured over time. This displacement gives rise to an initial peak load followed by a relaxation period until an equilibrium load is achieved. During the relaxation period, the exudation of water out of the cartilage continues until a balance is reached. In the creep protocol, a step load is applied which produces a rapid increase in deformation. This results in a large flow of water out of the tissue. Following that, the increase in the deformation of cartilage becomes transient because the water cannot escape the matrix immediately. As the rate of deformation slows over time as it approaches the equilibrium state, the rate of water flow out of the cartilage likewise slows.

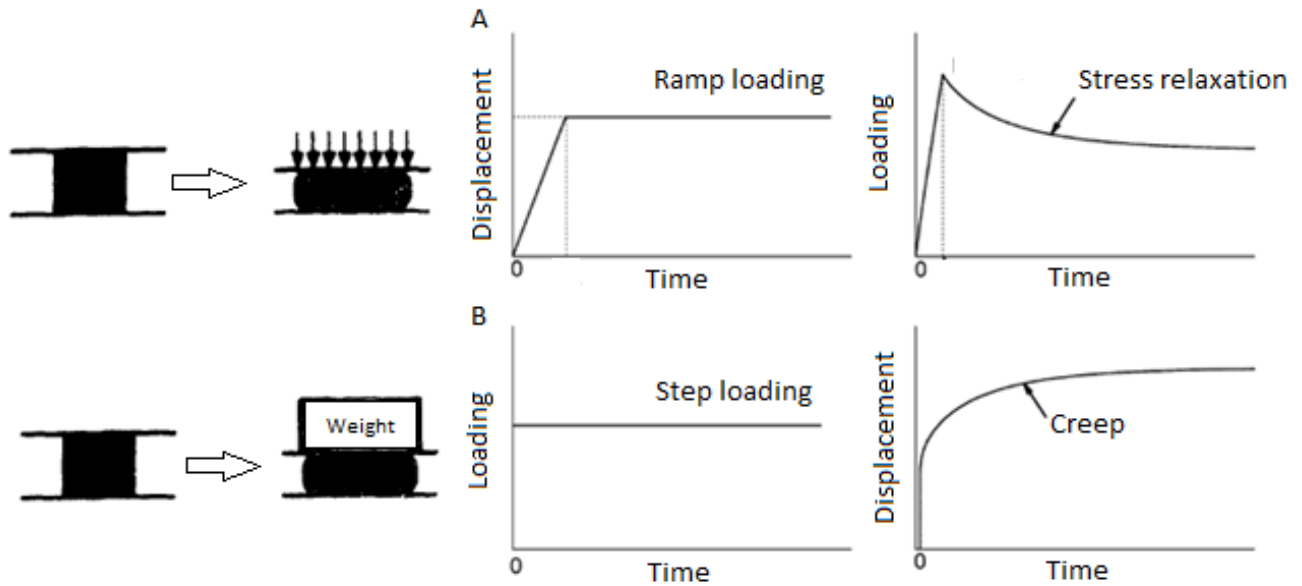


Figure 2.4 Viscoelastic behavior of articular cartilage under two common loading protocols: A) stress relaxation, and B) creep.

The most frequently used mechanical testing configurations for cartilage include confined compression, unconfined compression, and indentation (Figure 2.5). In confined and unconfined compression tests, full thickness cartilage discs are harvested from the joint. In confined compression, the cartilage disc is placed in a chamber that fully confines the lateral edges of the disc and thus prevents lateral flow of water. In unconfined compression, however, the lateral edges of the disc remain free. In a confined compression test, a porous plate is used to apply loading or displacement to the cartilage surface to allow the flow of water out of the cartilage through surface. In unconfined compression, a non-porous plate is commonly used and the flow of water occurs from the periphery of cartilage plug.

Unlike compression tests, indentation test requires no extraction and preparation of small cartilage samples. Mechanical properties can be obtained in an intact cartilage surface. Loading is applied through either a spherical or plane-ended indenter. Indentation testing determines mechanical properties in situ and thus more closely reflects the physiological environment of articular cartilage. The non-destructive nature of indentation testing enables repeated measurements on a sample. However, indentation stiffness of cartilage is affected by thickness variation [32],[33],[34] if the indenter size is larger than thickness, with thinner cartilage exhibits higher stiffness values. Therefore, selecting the right indenter size is an important issue that needs to be considered in indentation test.

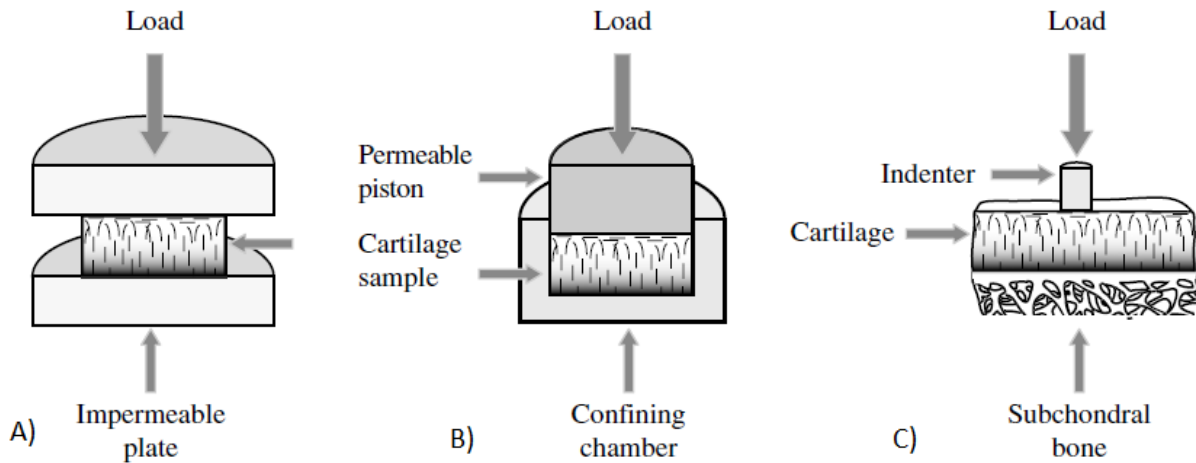


Figure 2.5 Common configurations for mechanical testing of articular cartilage: A) unconfined compression test, B) confined compression test, and C) indentation test.

© Reproduced from [35] with permission from Elsevier

Many numerical models have been developed in an attempt to describe the mechanical behavior of cartilage. These can be used to interpret the results obtained from mechanical testing protocols. The earliest work modeled cartilage as an isotropic, homogeneous, and elastic material. Hayes et al. [32] derived a numerical solution for different boundary conditions of an indentation test, whereby the contact of a spherical or plane-ended indenter with an infinite elastic layer of cartilage attached to an underlying rigid layer (subchondral bone) was modeled. Biphasic theory was introduced by Mow et al. [36] in which cartilage was modeled as a composite material consisting of a porous solid phase (PG and collagen network) and a fluid phase. In biphasic models of cartilage, three major factors are assumed to contribute to mechanical behavior of the tissue: a) intrinsic stiffness of the solid phase, b) the hydraulic pressure within the fluid, and c) the frictional forces between solid and fluid phases. Cartilage has been modeled as isotropic biphasic [36], transversely isotropic biphasic [37], and fibril-reinforced biphasic material [38]. The numerical models were further improved as Lai et al. [39] developed the tri-phasic theory to account for the presence of an ionic phase along with solid and fluid phases in cartilage. These models have been successfully used to fit experimental data collected in confined compression, unconfined compression, and indentation geometries under both stress relaxation and creep protocols.

Experimental and numerical investigations have been carried out to study the mechanical behavior of articular cartilage under various boundary conditions. In general, cartilage behaves as a viscoelastic material and represents different immediate and equilibrium responses when subjected to loading or deformation. Immediate response occurs before enough time has passed for significant fluid flow to occur, and the tissue behaves as an elastic material. If loaded for enough time, however, the fluid will

flow within the tissue and exudate from the tissue. This continues until fluid flow stops and an equilibrium state is achieved, referred to as the equilibrium or long-term load response of articular cartilage. Measures of compressive stiffness can be obtained from both the immediate and equilibrium responses (Figure 2.6). The focus of the present study is on the immediate response of cartilage to a rapidly applied displacement. Immediate stiffness of cartilage has shown to be more sensitive to changes associated with OA and better identifies regions undergoing softening [136]. In addition, immediate stiffness of cartilage was found to have similar variations across a sample compared to equilibrium and dynamic (load response to cyclic loading) stiffness of the tissue (Appendix H). Obtaining immediate stiffness of cartilage using an indentation technique can therefore serve as a quick and sensitive method to infer cartilage stiffness on multiple sites across a sample.

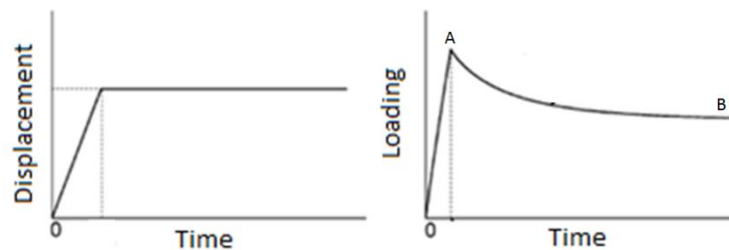


Figure 2.6 Immediate (point A) and equilibrium (point B) load responses of cartilage to displacement.

2.4 Osteoarthritis (OA)

OA is the most prevalent joint disease and a leading cause of disability. 5.7 million (16% of population) Canadians are living with OA in 2015, and this number is estimated to surpass 10.5 million people (25% of population) by 2040. The total economic burden of OA in Canada is reported to be \$195.2 billion between the years 2010 and 2015 [1]. The most commonly affected human joints are the hands and load-bearing joints (hip, knee, and spine) [40].

OA is characterized by the progressive loss of articular cartilage, leading to loss of normal functioning [41]. The signs of OA can manifest at three different levels: biochemistry, morphology, and clinical symptoms. The earliest degenerative changes occur at the biochemical level, with loss of GAG as the primary event [42]. Alterations in the collagen network and an increase in water content are other changes at this level [43]. These changes decrease cartilage stiffness, which in turn accelerate the degenerative process [44]. Articular cartilage is aneural and avascular which decreases its regenerative capacity. When chondrocytes detect the degenerative changes, they accelerate the

synthesis process as a compensatory action to counter degeneration. However, degeneration ultimately prevails over synthesis during OA, which results in progressive loss of articular cartilage [41]. Consequently, articular cartilage undergoes morphological changes such as reduction in thickness and fibrillation of the superficial cartilage, which eventually reaches the subchondral bone [41]. Clinical symptoms of OA include pain, swelling, joint stiffness, and limited range of motion [44]. Although current knowledge of OA can describe the biochemical, morphology, and clinical changes that occur as the disease progresses, some elements of OA progression, such as how changes in cartilage structure and function are linked to OA symptoms, are poorly understood.

OA can typically be classified as primary and secondary. Primary OA develops with no known cause but is generally associated with aging, though there is no clear explanation for the relationship between aging and OA. Secondary OA results from a known predisposing condition, usually mechanical [45],[46],[47]. However, some investigators believe this classification is confusing, since “primary” OA can also originate from mechanical problems [48]. Mechanical factors such as joint deformity [49],[50], obesity [51],[52], and injury [53] are thought to lead to secondary osteoarthritis by causing joint overloading which leads to cartilage degradation.

2.5 Osteoarthritis (OA) Treatment

There is no effective cure to stop OA progression, but there are treatment options that can ease the symptoms and improve the quality of life for the patient. These treatment options include medication, non-medication conservative approaches, and surgical treatment.

In general, medications aim to alleviate OA pain and swelling and have no effect on the degenerative process. Pain killers, anti-inflammatory drugs, and intra-articular injection of steroids are the most commonly used medications for treatment of OA.

Since obesity is a major and modifiable risk factor for OA, an exercise program is commonly prescribed as a means for weight loss and reduction in joint loading. Particular types of physical activities such as muscle strengthening, stretching, and aerobic exercises have been shown to relieve joint pain [54].

Surgical interventions to promote cartilage repair are of particular interest in treatment of OA. Several procedures such as bone marrow stimulation [55], transplantation of autologous chondrocytes [56] or cartilage osteochondral plugs [57], and modification of loading on the joint

through a variety of techniques (e.g. high tibial osteotomy) have been proposed for that purpose. However, these surgical interventions are not effective in advanced stages of cartilage degeneration and their efficacy is dependent on the early diagnosis of OA. Total knee replacement (TKR) is the treatment of choice for patients suffering from impairment of joint function and constant pain not alleviated by the other treatment options. In this procedure, the damaged part of the joint surface is removed and replaced by an implant. The success rate of this surgery is reported to be more than 90% after 15 years [1]. Many patients receiving implants at a young age will require revision surgery [1]. Although TKR is a cost-effective treatment for OA knee, it may not be an ideal choice in young patients because a high level of joint function is expected. In addition, the more active life style of young patients increases the risk of early failure and the need for revision surgery.

2.6 Clinical Osteoarthritis (OA) Evaluation

OA diagnosis is mostly based on clinical symptoms and radiological findings [40]. Articular cartilage is not visible on radiographs since it does not attenuate x-rays well. The Kellgren Lawrence (KL) scoring system is widely used for evaluation of OA severity using radiography. This grading system categorizes OA severity according to particular features such as joint space narrowing (Figure 2.7), sclerosis of subchondral bone, and the presence of osteophytes (Table 2.1) [58]. However, the clinical symptoms and radiographic signs of OA do not always correlate [59]. Furthermore, these clinical and radiological changes indicate an advanced stage of OA. Although computed tomography (CT) can generate 3D images of the joint, it also lacks the ability to directly image the cartilage [60].

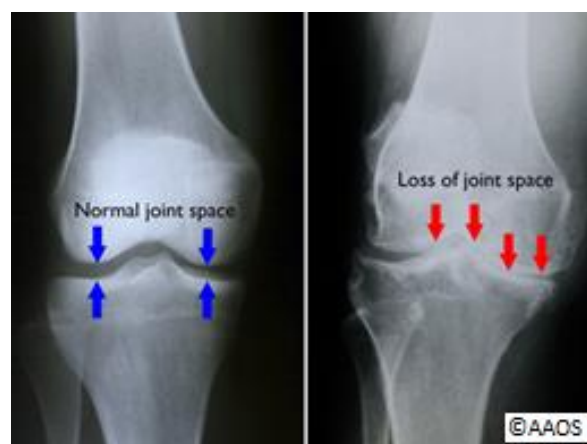


Figure 2.7 Normal versus OA knee joint representation in x-ray images.
©Reproduced with permission from American Academy of Orthopaedic Surgeons.

Table 2.1 Kellgren Lawrence grading of radiographic OA[58].

KL grade	Cartilage description x-ray image
0	no radiographic features of OA are present
1	doubtful joint space narrowing (JSN) and possible osteophytic lipping
2	definite osteophytes and possible JSN on anteroposterior weight-bearing radiograph
3	multiple osteophytes, definite JSN, sclerosis, possible bony deformity
4	large osteophytes, marked JSN, severe sclerosis and definitely bony deformity

The International Cartilage Repair Society (ICRS) system is a long-established grading system for evaluating cartilage health. This grading system requires direct visualization of cartilage and assessment is based on cartilage lesions (Table 2.2) observed by arthroscopy or imaging.

Table 2.2 International Cartilage Repair Society (ICRS) grading system [61] based on cartilage lesions.

ICRS grade	Cartilage status
0	Normal
1	Nearly normal: superficial lesions, soft indentation and/or superficial fissures and cracks
2	Abnormal: lesions extending down to < 50% of cartilage thickness
3	Severely abnormal: lesions extending down to > 50% of cartilage thickness but not into subchondral bone
4	Severely abnormal: lesions extending to subchondral bone

Magnetic Resonance Imaging (MRI) has been used to evaluate OA severity. Unlike radiography and CT, MRI is able to image the cartilage morphology directly and hence detect the extent and the location of cartilage lesions. However, the routine use of MRI in clinical practice is challenging due to its high cost, long acquisition time, and poor resolution.

Finally, arthroscopy is an invasive technique that enables direct investigation of the cartilage surface. In arthroscopy, a fiber optic instrument is inserted into the joint space through a small incision that allows direct visualization of the cartilage surface. The surgeon may use a probe to manually assess relative stiffness across the articular surface. This technique is not routinely used for OA diagnosis but it serves as a gold standard for assessment of cartilage quality. In addition to being invasive, arthroscopy has shown poor intra- and inter-observer repeatability in detecting regions undergoing softening [62],[63]. Table 2.3 summarizes the advantages and disadvantages of the current methods for evaluation of OA.

Table 2.3 Comparison between commonly used methods for osteoarthritis diagnosis.

Diagnostic method	Advantages	Disadvantages
Clinical examination	Accessibility, easy to perform, and low cost	Poor sensitivity, subjective
X-ray imaging	Accessibility, easy and fast to perform, and low cost	Radiation exposure, poor sensitivity, and inability to directly map the tissue
MRI	Direct mapping of the tissue, no radiation exposure	High cost, long acquisition time, hard accessibility, and complicated imaging protocols
Arthroscopy	Direct visualization of cartilage surface, assessment of cartilage functioning	Invasive procedure and subjective

2.7 Advanced Osteoarthritis (OA) Imaging

Detecting OA early enough for successful intervention and assessing prevention and treatment strategies requires imaging that is more sensitive than the clinical imaging methods described above. Advanced OA imaging techniques measure cartilage morphology and composition.

The function of cartilage in joints is mechanical. Hence, in vivo measurement of cartilage mechanics has potential to provide a more comprehensive understanding of cartilage function and the effect of OA on this function. However, most mechanical properties of interest are challenging to measure in vivo. For instance, stiffness of cartilage is a key determinant of cartilage function and there is no direct measurement technique to measure this mechanical property in vivo. An imaging method capable of non-invasive assessment of cartilage stiffness would be useful for improving our understanding of OA.

2.7.1 MRI

MRI has been widely used for imaging of articular cartilage in both research studies and clinical practice. One main advantage of MRI is its ability to change contrast to highlight different tissue types. This has led to the development of several MRI techniques specialized for imaging of cartilage. This imaging modality therefore offers a means to directly visualize cartilage and allows assessment of different morphologic features of the tissue such as thickness, volume, and surface lesions.

Several semi-quantitative grading methods have been developed for evaluation of cartilage status on MRI images and quantifying the progression of OA [64],[65]. The Boston-Leeds Osteoarthritis Knee Score (BLOKS) is a commonly used scoring method which has been specifically developed for knee OA [66]. This method classifies cartilage degeneration based on the extent of full-thickness loss and the number of regions affected by any cartilage loss. In addition to cartilage, BLOKS grades all other tissues involved in knee OA including the ligaments, meniscus, and bone marrow.

MRI imaging for OA has been further expanded by the advent of quantitative MRI techniques that enable the assessment of articular cartilage composition [67],[3]. These techniques measure different aspects of the structure of cartilage, including GAG distribution, architecture of the collagen network, and water content. T2 mapping has been shown to be sensitive to water content and the collagen network of cartilage [68],[69],[70],[71]. Other techniques such as T1rho mapping [72],[73],[74], dGERMIC methodology [4],[5],[75], and sodium MRI [76],[77] have been proposed for measurement of GAG concentration of cartilage.

Delayed gadolinium-enhanced MRI of cartilage (dGERMIC) has been the most commonly used technique for measurement of GAG concentration in cartilage [75]. dGERMIC relies on the fact that anionic contrast agents (gadolinium) distribute in cartilage, at equilibrium, in an inverse proportion to the negatively-charged GAG molecules due to the electrostatic repulsion. Since the concentration of gadolinium contrast agent shortens the T1 relaxation time, the mapped T1 relaxation time corresponds to the GAG concentration in articular cartilage. dGERMIC indices have been associated with histological measurements of GAG content [78],[79] as well as cartilage mechanical properties [80],[13]. Although several studies confirmed the potential of dGERMIC to differentiate between healthy and OA cartilage [7],[8],[10], questions exist regarding the reliability of dGERMIC for estimation of GAG content [2],[15],[16],[81]. In general, the routine use of MRI techniques for evaluation of OA changes in cartilage has been restricted by the high cost, long acquisition time, and poor resolution of MRI scanners. In addition to those limitations, implementation of MRI techniques requires sophisticated scan protocols and pulse sequences.

2.7.2 CECT

2.7.2.1 Principle of X-ray and CT

Radiography uses electromagnetic radiation, typically x-ray, to visualize the organs and structures inside the body. To create an image, an x-ray beam is generated and passes through the body. Along

its path, the x-ray beam is attenuated (weakened) due to interaction with tissues. The part of radiation that passes through the body is captured by the detectors on the opposite side resulting in a 2D image. The exponential equation below (equation 1) illustrates the rate of x-ray attenuation as it passes through an object:

$$I(x) = I(0) * e^{-\mu x}$$

(Equation 1 : X-ray attenuation formula)

Where $I(0)$ is the initial intensity of the radiation, $I(x)$ is the final intensity of the radiation after passing the object, x is the distance travelled in the object and μ is the attenuation coefficient. The attenuation coefficient is specific to the object and represents the density of the object for a given energy of the radiation. X-ray imaging is able to distinguish between tissues inside the body provided that there is enough difference between their attenuation coefficients.

Conventional x-ray represents the average of the attenuation coefficients in one direction and hence results in a 2D image. Since the structures of interest inside the body, e.g. the knee joint, have complex geometries in 3D space, these 2D x-ray images often do not provide sufficient spatial resolution and information related to the structure. Computed tomography (CT) is a 3D imaging method that uses x-ray beams to generate cross sectional images and provide a 3D representation of the object of interest.

XtremeCT is a recently developed high-resolution peripheral quantitative computed tomography (hr-pQCT) imaging system that can provide 3D images with isotropic voxel resolution as low as 41 μm (XtremeCT, Scanco Medical AG, Switzerland). Similar to CT modalities, the principle of hr-pQCT imaging is based on the measurement of the x-ray attenuation coefficients within the object. In this imaging modality, the x-ray source and detector are rotated around the object to acquire a series of attenuation profiles in 360 degrees to create one cross-sectional image (slice) of the object. Subsequently, the data from these 2D images are processed to reconstruct a 3D matrix representing the variation of attenuation coefficients within the object.

2.7.2.1 Principle of CECT

Since articular cartilage does not attenuate x-ray radiation very well, CT imaging cannot be used to visualize unenhanced cartilage. However, contrast agents can enhance the density and attenuation of

cartilage on CT images. Contrast agents have been used for years with radiography to enhance cartilage attenuation and capture the morphology of the tissue [82],[83],[84].

In an approach similar to dGERMIC (above), CT using charged contrast agents has been developed in an effort to measure GAG concentration within the cartilage [85],[86]. When the cartilage is exposed to an anionic contrast agent, the contrast agent diffuses within the tissue in an inverse relationship to GAG concentration due to the negative charge on the GAGs. The contrast agent causes higher attenuation of x-rays, which results in brighter regions in the image where it collects, such as regions with low GAG. The attenuation can be used to measure the distribution of contrast agent and hence the distribution of GAG. With cationic contrast agents, the positively-charged contrast agent is attracted by the negatively-charged GAG molecules. This electrostatic attraction results in higher accumulation of contrast agent in regions with higher GAG concentration (Figure 2.8). The GAG depletion that occurs during Osteoarthritis progression can be detected using CECT imaging.

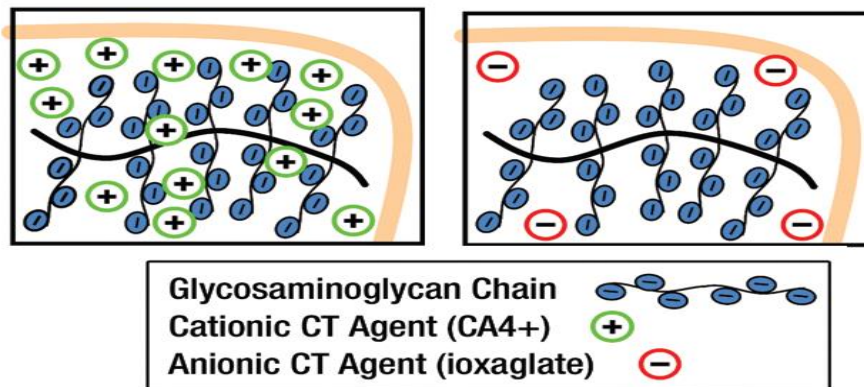


Figure 2.8 The principle of contrast-enhanced computed tomography of articular cartilage. Anionic contrast agents are repelled by the negatively-charged GAG molecules and thus concentrate in an inverse proportion to GAG concentration within the tissue. In contrast, cationic contrast concentrates proportionally to GAG concentration. ©Reproduced from [19] with permission from Radiological Society of North America.

2.7.2.3 Application of CECT to Assess GAG

Cockman et al. [85] used a gadolinium-based contrast agent with computed tomography to visualize cartilage and quantify its GAG content in bovine nasal cartilage disks. The method was able to monitor changes associated with trypsin degradation. However, the use of iodine-based contrast agents along with CT has become more frequent due to their desirable physiochemical properties and

better enhancement of cartilage [87]. Palmer et al. [86] reported the first use of an anionic iodine-based contrast agent (Hexabrix320) along with CT and found a strong correlation between CECT attenuation and GAG content in bovine articular cartilage. The relationship between CECT attenuation using anionic contrast agent and GAG concentration, as obtained from histology, has been further confirmed in several investigations in bovine [88],[89],[90], rat [91], and human [92] cartilage samples. CECT has also been shown to detect mechanical injury in bovine articular cartilage subjected to impact test [93].

The potential of CECT with an anionic contrast agent for in vivo examination of cartilage degeneration in experimental OA in small animals has been demonstrated [94],[95],[96]. Injection of chemical, surgical intervention, and strenuous exercise were three methods employed to induce OA in those experiments. CECT imaging of OA joints over time monitored the changes of cartilage structure in different stages of OA. These findings suggested that CECT is a promising alternative to destructive histological assessment for longitudinal OA studies. These findings, along with ex vivo investigations on human cadaver knees [97],[98] suggested the possibility of using CECT routinely in clinical practice. The clinical application of CECT (anionic contrast agent) for measuring cartilage composition has been investigated for the first time in vivo [99]. In that experiment, one normal and one OA knee were imaged before and following administration of an anionic contrast agent (Hexabrix320) at multiple time points (up to 120 minutes). The contrast agent concentration was detectably higher in OA cartilage than intact cartilage, reflecting the lower concentration of GAG as a consequence of OA progression.

Recently, a novel cationic contrast agent (CA4+) has been proposed for use in CECT. It has been evaluated in vitro [21],[100],[20] and in vivo in rabbits [19]. Carrying a positive charge, the CA4+ is attracted to negatively-charged GAG molecules and accumulates into cartilage in concentrations proportional to GAG distribution. Compared to conventional anionic contrast agents, CA4+ is more sensitive to GAG changes and yields higher correlations with GAG concentration in bovine osteochondral cartilage plugs [100],[18],[17],[19]. Furthermore, due to the higher uptake of CA4+ in cartilage, this cationic contrast agent can be used in relatively lower concentrations, and provides better visualization of cartilage and thus easier segmentation. In contrast with anionic agents which are reported to be washed out of joint space quickly, cationic contrast agents remain in the joint long enough to provide sufficient time for imaging [19]. These findings make CA4+ an appealing alternative to anionic contrast agents for evaluation of articular cartilage GAG content.

2.7.2.4 Application of CECT to Assess Cartilage Mechanics

The relationship between CECT attenuation and mechanical properties of articular cartilage has been assessed in few investigations. CECT using anionic contrast agent was associated with the equilibrium modulus in bovine cartilage plugs [90]. In this study, osteochondral cartilage plugs were harvested from bovine patellae. X-ray attenuation in superficial and full-depth cartilage was measured using CECT as an index for GAG concentration. The equilibrium Young's modulus was measured using a stress relaxation protocol in unconfined compression. A significant ($p < 0.05$) and negative correlation ($r = -0.51$ and -0.49 for superficial and full-depth GAG measurements, respectively) was found between CECT measurements and equilibrium Young's modulus. A similar conclusion was achieved in another study that measured the stiffness of bovine cartilage plugs using an unconfined compression test with two opposing cartilage surfaces. Mean x-ray attenuation for the full depth of cartilage significantly and strongly correlated with mechanical stiffness. In tests of ovine tibial plateau [101], an arthroscopic probe was used to measure instantaneous stiffness. The CECT method using an anionic contrast agent was used to measure GAG concentration in superficial and full-depth cartilage. However, only CECT in superficial layer of cartilage demonstrated significant correlation with instantaneous stiffness measurements.

The utility of CECT using the recently developed cationic contrast agent (CA4+) for indirect assessment of cartilage mechanical properties was first examined in bovine cartilage plugs [102]. In that study, a stress relaxation test was used to assess cartilage stiffness. A torsional friction test was also performed to determine the coefficient of friction. The average x-ray attenuations in full-depth cartilage were computed to determine contrast agent and thus GAG concentration. A significant correlation was found between CECT measurements and Equilibrium Young's modulus as well as CECT measurements and coefficients of friction. The potential of CECT using CA4+ to predict Equilibrium Young's modulus was further confirmed in mouse cartilage [22].

In summary, due to the mechanical function of cartilage, the mechanical properties (particularly stiffness) of the tissue are the most relevant measures for assessment of cartilage quality. The relationship between changes in cartilage composition and OA status is not fully understood; hence validation of imaging methods against mechanical measures instead of histology assessments offers a more thorough understanding of cartilage status. However, relatively few studies examined the ability of CECT imaging for revealing mechanical properties of articular cartilage, all of which tested animal cartilage samples. A major limitation of those studies is that cartilage plugs were typically

used for mechanical and imaging experiments which may not truly mimic the cartilage behavior in *in vivo* condition. If CECT imaging is to be used for *in vivo* measurement of cartilage mechanical properties and for OA studies, validation of this method against stiffness measurement in human cartilage samples is an essential step.

2.8 Summary

- OA is the most prevalent joint disease. Detecting OA early enough for successful intervention and assessing prevention and treatment strategies requires imaging that is more sensitive than currently available methods.
- The function of cartilage in the joint is mechanical. Therefore, *in vivo* measurements of cartilage mechanical properties such as stiffness provide an important assessment of cartilage function.
- Several MRI techniques have been developed for quantitative assessment of cartilage composition and structure. In particular, dGEMRIC has been successfully used to measure GAG content of articular cartilage. Since GAG plays a key role in compressive stiffness of cartilage, this technique was also able to indirectly assess mechanical properties of the tissue. However, MRI has limitations including high cost, low resolution, long acquisition time, and the need for complicated imaging protocols.
- Analogous to dGEMRIC, contrast-enhanced computed tomography (CECT) imaging using charged contrast agents has been developed for quantitative assessment of cartilage GAG content. A recently developed cationic contrast agent (CA4+) has shown greater sensitivity to GAG content of cartilage than its anionic counterparts. The potential of CECT using CA4+ for prediction of cartilage mechanical properties has been investigated in animal cartilage plugs, but not in human tissue or intact cartilage surfaces.
- Indentation tests have many advantages for measuring cartilage stiffness, since they allow testing on intact cartilage surfaces. This method preserves the physiologic environment of the cartilage and more closely resembles *in vivo* loading condition.
- It is not clear whether CECT attenuation is associated with stiffness in intact human cartilage surfaces. This validation is required to assess the potential of CECT for indirect assessment of cartilage function.

3 Material and Methods

The primary objective of the present study was to determine whether a non-invasive contrast-enhanced CT-based imaging method can predict cartilage stiffness. This chapter describes the following key steps in assessing the association between contrast-enhanced CT measurements and cartilage stiffness:

1. the indentation technique used to measure cartilage stiffness;
2. the CECT imaging protocol and image processing algorithms used to measure cartilage GAG content; and
3. the registration algorithm used to link mechanical and CECT measurements.

3.1 Sample Preparation

3.1.1 Sheep Samples

A total of 4 intact, fresh sheep knee joints (aged 12-20 months) were acquired from a local butcher's on the day of sacrifice. The joints were disarticulated and soft tissues were removed carefully so as not to damage the articular cartilage surface. The proximal tibia and distal femur were transversely cut approximately 20 mm from the cartilage surface. Visual inspection showed no sign of overt degeneration in any of the samples (4 femoral condyles). The samples were then mounted in the testing chamber of a mechanical test system (Mach-1, Biomomentum, Montreal, Canada) (Figure 3.1) using screws, providing a rigid frame for mechanical measurements. To keep the samples hydrated, they were immersed in phosphate buffered saline (PBS) throughout mechanical testing.

3.1.2 Human Samples

Human cartilage specimens were obtained from cadaver knee joints that have been used in a previous experiment. The knee joints had been frozen at -20°C for approximately one year. 5 male cadaver knees were thawed at room temperature for 48 hours. Prior to mechanical testing, the knee joints were disarticulated and all soft tissue structures were removed except cartilage. For both the tibia and femur, a horizontal cut was made (with a band saw) 30 mm from the cartilage surface and a vertical cut separated the medial and lateral compartments. In total we had 25 cartilage surface compartments; 2 femora, 2 tibia, and one patella for each joint. Cartilage samples that showed heterogeneous surface areas with minimal cartilage destruction (fissures, fibrillation, cuts, etc) were

included in this study. The testing locations were therefore classified as grade 0 (normal) and 1 (nearly normal) according to the ICRS scoring system. Grade 0 cartilage is essentially pristine, while grade 1 cartilage includes superficial fissures and cracks and may have a change in color from grade 0 [61]. Based on these criteria, 6 cartilage surface compartments (3 medial femora and 3 lateral femora) were chosen. Human femoral compartments are identified throughout the thesis with a label consisting of the prefix ‘HFC’ (Human Femoral Condyle), followed by a number.

The cartilage samples were mounted in the testing chamber of a cartilage indentation testing system (Mach-1, Biomomentum) using screws providing a rigid frame for testing (Figure 3.1). To prevent dehydration of the samples during the mechanical tests, they were immersed in phosphate buffered saline solution (PBS).

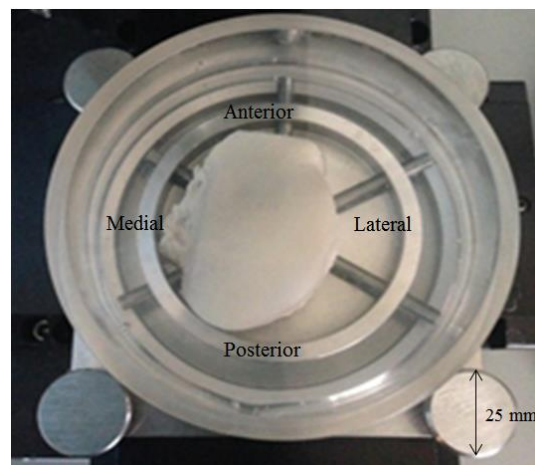


Figure 3.1 Top view of the testing chamber of the mechanical tester.

3.2 Mechanical Testing

This section presents the mechanical testing protocol employed to measure cartilage stiffness using indentation.

3.2.1 Mechanical Testing Apparatus

Indentation testing of articular cartilage specimens was performed using a commercially available mechanical test system (Mach-1, Biomomentum, Montreal, Canada) (Figure 3.2). This mechanical testing system consists of three motor-driven stages (two translational stages for x-y displacement and one vertical stage) and a testing chamber. A 6 axis load cell is mounted on the vertical stage and allows measurement of forces and torques in all directions with a resolution of 3.5 mN over a 70 N range for force measurement and a resolution of 25 μ N.m over a 0.5 N.m range for torque

¹ 6 cartilage surface compartments (HFC1-HFC6) were obtained from 4 different knee joints. HFC1 (medial) and HFC2 (lateral) belonged to the same knee joint. HFC6 and HFC5 were medial and lateral compartments of the same knee joint. HFC3 and HFC4 were medial and lateral compartments of two different knee joints.

measurement [104]. A spherical indenter was rigidly fixed to the load cell. Computer-controlled displacements were applied via a micro-stepping motor. The displacement resolution of the mechanical tester was 0.5 μm [104]. The calibration certificate for the load cell and the control reports for all stages are included in appendix J. Software program modules (LabView, Mach-1 analysis) were used to automate the control of the indenter displacement profiles and continuously record the resulting load and displacement as functions of time.

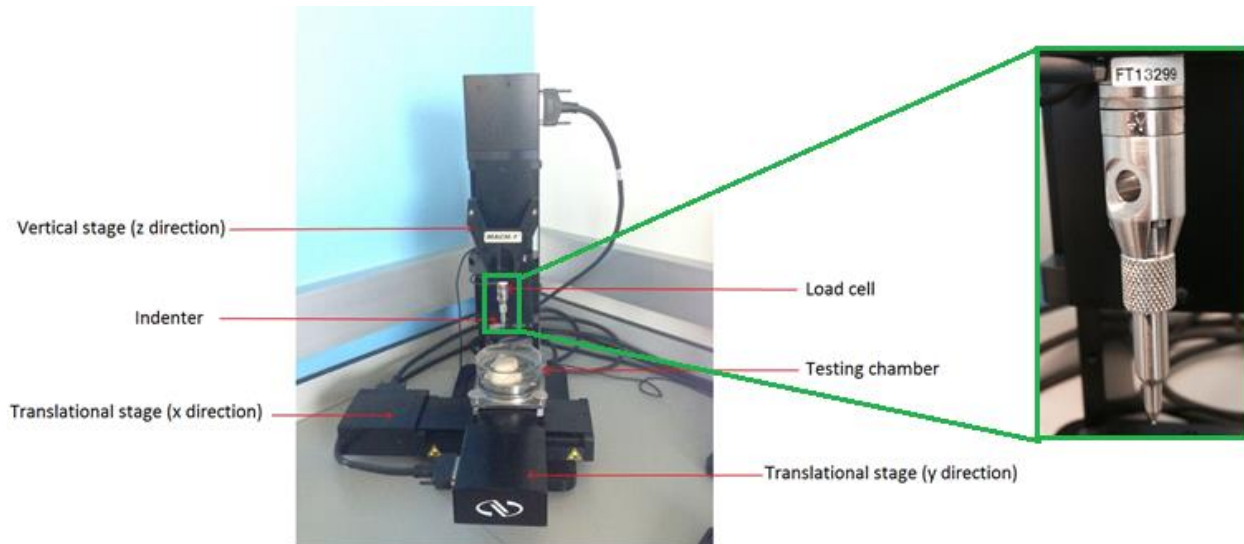


Figure 3.2 Mechanical testing setup.

3.2.2 Indenter and Positioning of Indenter in Testing Locations

3.2.2.1 Indenter

In situ indentation of human samples was performed with a rigid, nonporous, spherical-ended tip indenter with a diameter of 1 mm (Figure 3.3 A). A smaller indenter with a diameter of 0.35 mm was used for testing sheep cartilage samples (Figure 3.3 B). These indenter sizes were selected to minimize the effect of cartilage thickness variation on stiffness measurements [34]. Human and sheep cartilage samples are 1.8-3.3 mm and 0.7-1.3 mm thick, respectively. Selecting these indenter sizes reduces the effect of thickness variation on load response of cartilage to less than 10%, according to the results of a FEM model of indentation [34]. As a result, the measured stiffness can be directly assigned to cartilage composition and structure.

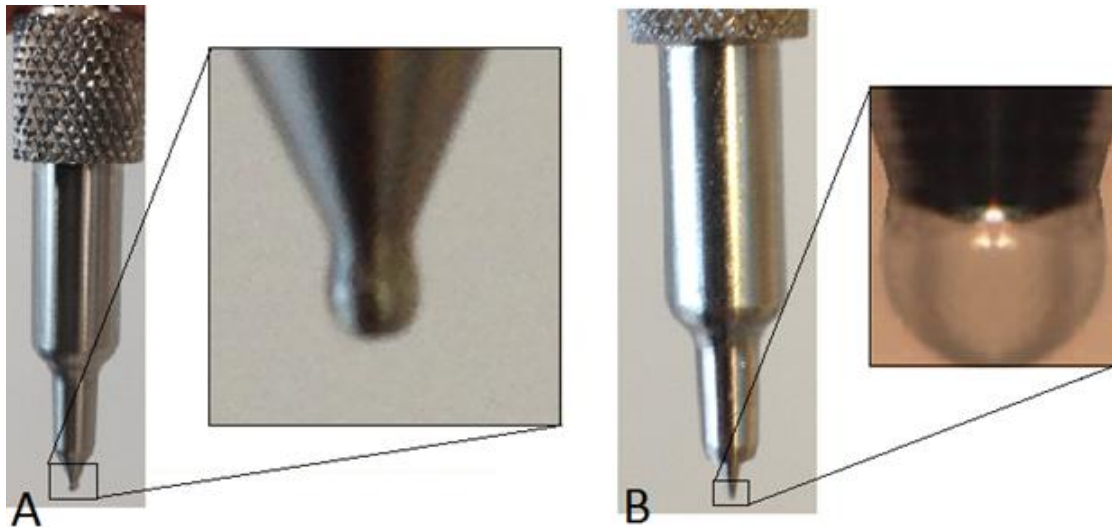


Figure 3.3 A) 1 mm diameter and B) 0.35 mm diameter spherical indenters.
 ©Illustration B is reproduced with permission from Biomomentum Inc.

3.2.2.2 Positioning

To accurately define testing positions a two-step procedure was followed:

I) Mechanical reference definition:

Two metal beads ($d=1\text{mm}$) were attached to the periphery of the specimen (distant from testing locations) using adhesive to serve as mechanical origin markers. The translation stages were adjusted so that the indenter was situated above the markers and their corresponding x and y positions were recorded to define the origin positions in the plane of the translation stages.

II) Displacement to a test location:

Before each indentation test, the indenter was raised and the translation stages were moved so that the indenter was situated above the desired testing locations and the corresponding x and y positions were recorded. This procedure was repeated for all testing positions in each sample. The testing sites were chosen to cover the whole articular cartilage surface. The spacing between testing locations was 2 mm to ensure that the edges of the testing locations did not overlap.

3.2.3 Indentation Test Protocol

3.2.3.1 Surface Localization Procedure

An essential first step in any indentation test is to position the indenter tip at the surface of the sample, since all subsequent displacements will be measured relative to that reference point. The vertical (z) position of the indenter tip when it is just contacting the uncompressed cartilage surface is

termed the zero-point, and the procedure for localizing the tip to the surface is termed surface localization. To localize the surface, the indenter was lowered under manual control until it was approximately 2 mm above the surface. The vertical stage was then moved automatically at 0.5 mm/s until a predefined load increase (stop criterion= 0.1 N) in the vertical direction (z direction) was measured by the load cell, indicating contact of the indenter tip with the cartilage surface. The z coordinate at this point was recorded and defined as the zero point.

3.2.3.2 Surface Orientation Determination

One challenge to using indentation testing for measuring cartilage stiffness is that indentation should be performed perpendicular to the articular surface. The articular surfaces of the human knee joint contain areas with high curvature. The spherical indenter needs to be displaced normal to the articular surface and hence the surface orientation must be determined to define the correct displacement profile. To calculate that, for each tested point, the coordinates of 4 points in the vicinity of the test location ($\Delta x = \Delta y = \pm 1$ mm) were measured using the same procedure. A best-fit plane to the points was found and the angle between the normal of the plane and the vertical direction defined the surface orientation. Testing locations with surface orientation greater than 60° were excluded from indentation testing due to the restrictions of the mechanical tester.

3.2.3.3 Normal Indentation

Once a point on the cartilage surface was identified for testing and the surface orientation had been found, the point was positioned beneath the indenter tip via adjustment of the x-y translation stages. The indenter was then lowered until it reached a tare load of 0.1 N to localize the contact point. For each test, a single pulse indentation was applied (Figure 3.4). The three stages of the tester were translated to move the spherical indenter with a displacement profile along a virtual axis normal to the surface of the sample, and the load (measured with the multi-axial load cell) was continuously recorded. The indentation for human specimens was a 300 μm displacement (nearly 10% strain) at 0.5 mm/s. For sheep samples, the displacement was 100 μm at 0.1 mm/s velocity. This displacement velocity yields nearly elastic response of cartilage by not providing sufficient time for fluid motion; a minimum loading rate of 0.3 mm/s has been suggested for elastic response of human cartilage [12]. The displacement amplitude for the indentation test was selected to keep the stress on the cartilage within the physiological range (2-11 MPa) and minimize the risk of cartilage damage. Our calculation of stress is based on the Hertz equation which estimates the contact region between the

indenter tip and cartilage surface as a circle with radius of $R=\sqrt{rd}$, in which r is indenter radius and d is cartilage thickness. For the range of contact force found in our study (0.34-5.97 N), this contact area corresponds to a range of contact pressure (720 KPa- 12.7 MPa) which is far below the level of stress that could cause damage to the tissue (20 MPa has been suggested in some reports[103][104]). The accuracy and repeatability of normal indentation measurement were determined for a subset of cartilage specimens, and are reported in appendix C and I.

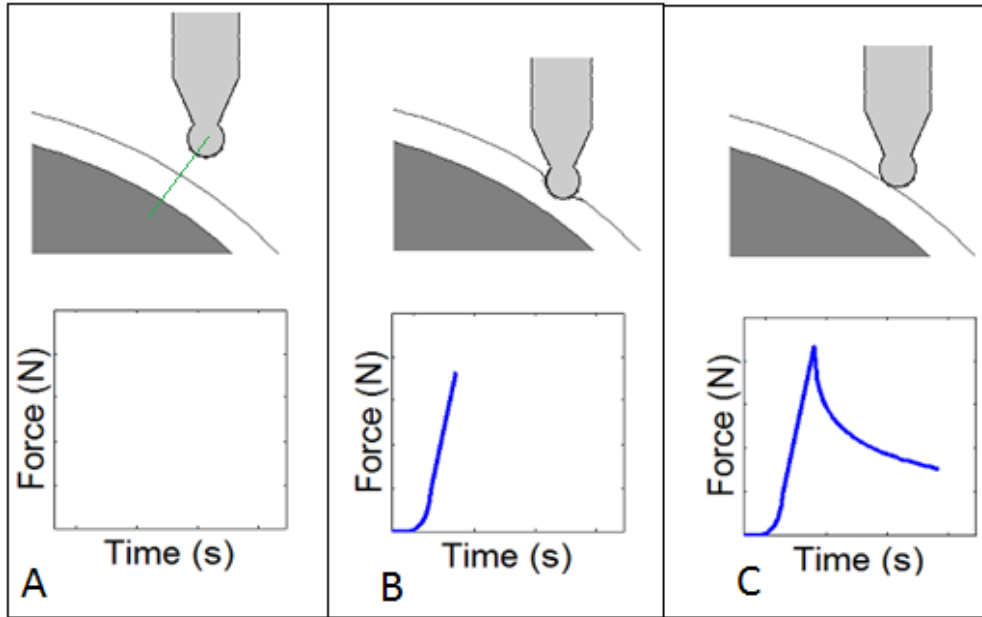


Figure 3.4 Indentation test protocol.

A) the green line is the virtual axis normal to the surface along which the indenter is displaced and the force is measured. B) The indenter is displaced perpendicular to the surface until it reaches the predefined amplitude. C) The indenter is returned to its original position along the normal direction. ©Reproduced with permission from Biomomentum Inc.

3.2.3.4 Cartilage Stiffness Calculation

We calculated the cartilage stiffness as the ratio of peak normal force to normal displacement (equation 2). Figure 3.5 depicts a typical load-displacement curve observed for indentation testing of cartilage, where point A corresponds to the peak normal force. At each testing location, the stiffness was measured twice and the average is reported. The second measurement of stiffness was performed after all testing locations were tested once. The gap between measurements was nearly 30 minutes, which has been determined to be a sufficient time for the cartilage to recover from indentation [107],[108].

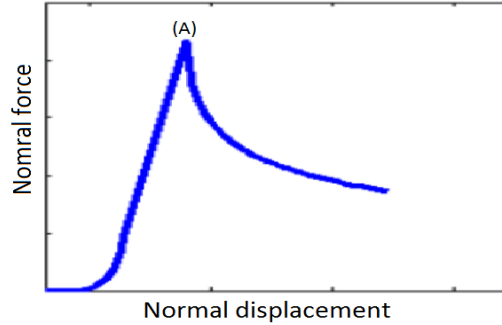


Figure 3.5 normal force-normal displacement curve in indentation.
Point A corresponds to the peak normal force that is used for calculation of cartilage stiffness.

$$\text{Indentation Stiffness} = \frac{\text{peak normal force (N)}}{\text{normal displacement (mm)}}$$

(Equation 2 : Stiffness calculation formula)

3.3 CECT Imaging

3.3.1 Equilibration in Contrast Agent Solution

Following the indentation test, the samples were immersed for 48 hours at room temperature in a 12 mgI/mL (mg of Iodine per mL) solution of CA4+ contrast agent. One complete cocktail protease inhibitor tablet (Roche, Germany) was added to the 50 ml of contrast agent solution to prevent degradation of cartilage during the experiment. CA4+ is an iodine-based cationic contrast agent that has demonstrated higher sensitivity [18],[21] to GAG content of cartilage (due to its 4 positive charges) compared to its anionic counterparts (that typically carry one negative charge [17]). To associate CA4+ concentration with x-ray attenuations, a phantom model was developed and the optimal concentration of CA4+ for our experiment was determined (Appendix A); a 12 mgI/ml concentration provides sufficient contrast between cartilage and bone in CECT images to allow the cartilage to be identified clearly. This contrast agent concentration is significantly lower than those typically used in CECT studies that utilize anionic contrast agent (80-320 mgI/ml). We performed a diffusion study to confirm that 48 hours was enough time for the contrast agent to fully diffuse into the cartilage and reach equilibrium (Appendix A). The volume of contrast agent solution was chosen to be approximately 20 times the cartilage to minimize changes in solution concentration as contrast

agent diffuses into the cartilage. The volume of human cartilage tissue was estimated based on CECT scans obtained from preliminary experiments prior to this study. On average, the volume of cartilage in each compartment was 2.4 ml and therefore 50 ml of contrast agent solution was deemed to be sufficient for our assessments.

3.3.2 Sample Preparation for Scan

Prior to imaging, the samples were removed from the contrast agent solution and the surface was gently dried using gauze to remove excess solution. To prevent dehydration of samples during scanning, they were wrapped in two layers of paraffin film (Parafilm, US). The samples were then centrally positioned and attached to the bore of a CT scanner (XtremeCT, Scanco medical, Switzerland) with tape. Care was taken not to move the two fiducial markers originally fixed prior to mechanical testing during the positioning process.

3.3.3 CT Scan Protocol

Each sample was scanned twice, once prior to exposure to contrast agent (to obtain a baseline image) and once after equilibration in contrast agent. Sequential images of cartilage and subchondral bone in the coronal plane were acquired at an isotropic voxel resolution of 41 μm , 300 μAmp tube current, and 120 kVp voltage in the XtremeCT (HR-pQCT). Each cartilage compartment scan contained, on average, 1000 slices and the corresponding scan time was approximately 90 minutes.

3.3.4 [CA4+] Computation from CECT Measurements

A phantom consisting of contrast agents at 10 levels of concentration was built and scanned to relate CA4+ concentration to CECT attenuation (Appendix B). The CA4+ concentration in cartilage samples can be determined from equation 3:

$$[\text{CA4+}] = a * (\text{HU}_{\text{CA4+, Tissue}} - \text{HU}_{\text{Tissue}}) + b$$

(Equation 3 : Calculation of CA4+ concentration from CECT attenuation)

Where a and b are, respectively, the slope and intercept of the regression line in the phantom study (Appendix B). $\text{HU}_{\text{CA4+, Tissue}}$ is the x-ray attenuation (in Hounsfield units) of the cartilage tissue equilibrated in CA4+ while $\text{HU}_{\text{Tissue}}$ is the attenuation of native tissue without CA4+.

We assumed a constant value for HU_{Tissue} by averaging the cartilage attenuation in each baseline image compared to using specific HU_{Tissue} values for each pixel. Our justification for this assumption is that the CECT attenuation in CA4+ equilibrated cartilage is one order of magnitude greater than the attenuation in native cartilage. In the worst case, when $HU_{\text{CA4+,Tissue}}$ has the lowest value and HU_{Tissue} has the highest value a maximum error of less than 5% is introduced in computation of GAG content compared to using specific HU_{Tissue} values. We made this assumption because the subtraction of CECT images from baseline images requires registering the two sets of scans, which could generate errors in final calculation of CA4+ concentration.

Since CA4+ agents attach to negatively-charged GAG molecules, we hypothesize that in equilibrium state, the concentration of CA4+ is proportional to the GAG concentration inside cartilage.

3.3.5 Image Processing

3.3.5.1 Cartilage Surface Segmentation

An automated threshold-based segmentation algorithm using MATLAB software was utilized to segment articular cartilage in CECT scans (Figure 3.6 C). The optimal threshold values for defining areas corresponding to cartilage tissue were determined using histogram line profiles of high attenuation (cartilage) areas. Using the threshold value specific to each individual sample, initial seed points for the region growing segmentation method were determined. Briefly, a seed point was placed in the cartilage region and compared against neighboring voxels to determine whether voxels should be added to the region. The procedure continued and the region was grown until the cartilage was completely segmented. During the segmentation process, multiple techniques such as erosion, Laplacian filtering, and smoothing filtering were also utilized to ensure accurate segmentation of articular cartilage. In some slices the boundary between cartilage and bone was not determined correctly by the automated procedure, and was manually corrected.

3.3.5.2 CECT Mapping of Articular Cartilage

The segmented cartilage in each compartment was approximated by the best-fit plane (Figure 3.6C). The CECT attenuations were averaged over a specific depth from the cartilage surface and projected to the 2D plane directly at the surface (Figure 3.6D). The depth of interest in our study was 600 μm , which corresponds to the superficial layer of cartilage and the region affected by indentation. Figure 3.6 briefly describes the methodological sequence used to map CECT attenuation in intact cartilage compartments.

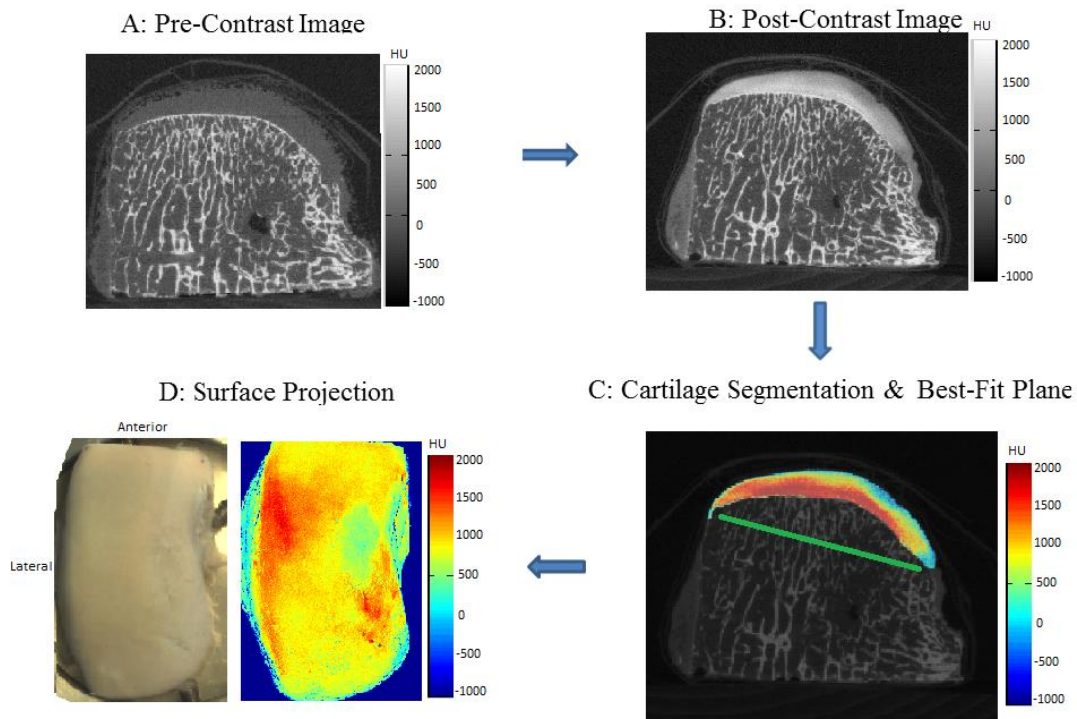


Figure 3.6 Image processing algorithm used for mapping CECT attenuation.

A) Pre-contrast scan of the sheep tibial plateau in the coronal plane. B) Post-contrast scan of the sample: the bright region represents cartilage. C) Cartilage was segmented semi-automatically. The cartilage compartment was then approximated by the best-fit plane (green line). D) Using a surface projection image processing algorithm, the average x-ray attenuations over a depth of 0.6 mm from the cartilage surface was mapped to the plane. A topographical map of x-ray attenuations, as an indirect measure of GAG content, was then generated for each compartment.

3.3.5.3 Determination of Testing Location in CECT Scans

A marker-based registration method was used to locate the indentation testing locations from the mechanical tests in the CECT scans. The first step was a preliminary alignment of the imaged sample in the horizontal plane, similar to its orientation in the mechanical testing chamber. The next steps of the registration were:

- 1) Determination of the two fiducial markers' centroid in the CECT images: this was achieved automatically by thresholding and averaging the coordinates of voxels within the spherical marker.
- 2) Determination of the two fiducial markers' centroid in the physical space: the coordinates of 5 points in x,y, and z directions on the surface of each marker were obtained using the Mach-1 system by replacing the indenter with a needle. The best-fit sphere was identified and the marker centroid was determined accordingly.

3) Registration between the two coordinate systems (image and physical space): the Umeyama method [105] in 2D was implemented to find the transformation matrix that maps the x and y coordinates of markers in physical space to image space. The third coordinate (vertical direction or z) of the testing locations was determined based on the relative distance in z direction between testing locations and marker locations from physical coordinates.

Using the registration method, we could determine CECT attenuation at each point that had been subjected to indentation testing (Figure 3.7). The overall error associated with the registration procedure was less than 250 μm , which was less than 6 voxels (Appendix E).

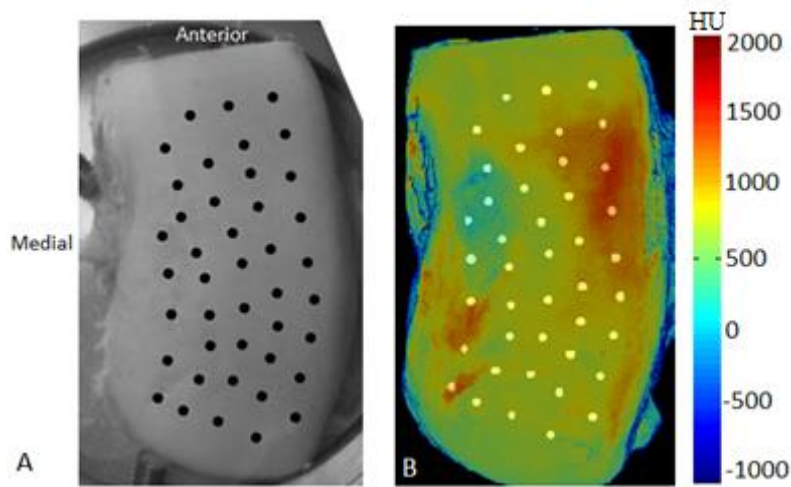


Figure 3.7 Locating indentation sites in CECT image.

The colormap represents GAG distribution across the cartilage surface as measured by averaging CECT attenuation to 600 μm the from cartilage surface. The registration procedure links indentation test sites in physical space (A) and the corresponding locations in the CECT image (B), in this case for a human medial femoral compartment.

3.3.5.4 Regions of Interest for Calculating CECT Attenuation

Regions of interest (ROI) in the CECT images were defined for the calculation of attenuation values (Figure 3.8).

The ROI for each indentation point was oriented normal to the surface. To determine the surface orientation, a cubic volume (100 voxels in length) around each testing location (with the testing location in the center) was identified. The contact coordinates of 4 points surrounding the testing location ($\Delta x = \Delta y = 1$ mm distance or 25 voxels) were measured and the surface orientation was obtained according to the normal of the best-fit plane to the points.

Once the orientation was known, an automated algorithm was used to define ROI in the cartilage beneath each testing location. Each ROI was a 1 mm diameter circle matching the indenter size, centered on the testing location, and extending from the cartilage surface to a depth affected by indentation (twice the indentation amplitude). The depth was chosen according to a FEM study reporting that the stress from indentation decreases by 50% in a depth twice the indentation amplitude [110]. An average of x-ray attenuation was then computed within the ROI for each testing location. The average of CECT attenuations was also computed over full depth of cartilage to determine the variation in correlations with depth of region of interest.

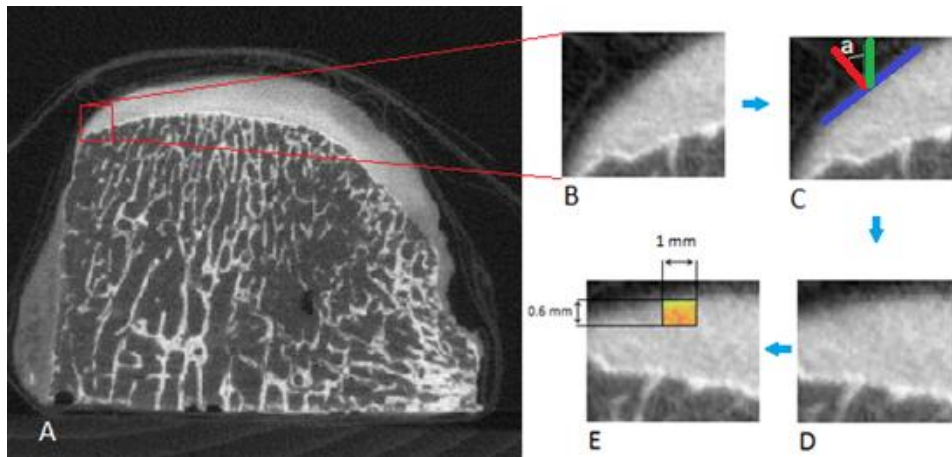


Figure 3.8 Definition of the region of interest (ROI) corresponding to the indentation test on CECT images.

*A) Representative CECT attenuation map for one slice from a femoral cartilage specimen. B) The site of the indentation test is first localized in the image using the registration algorithm and a 100*100 window (with the indentation site in the center) is extracted. C) The blue line represents the best-fit plane to the cartilage surface at the indentation site. The surface orientation is defined as the angle between the normal to the plane (red line) and the vertical direction (green line). D) The window is rotated according to the surface orientation so as to make the cartilage surface horizontal. E) To compute GAG content in the volume corresponding to the region subjected to indentation, the voxels in each testing site were averaged over a depth of 0.6 mm (twice the indentation amplitude) and width of 1 mm (corresponding with indenter diameter).*

3.3.5.6 Thickness Measurement

Articular cartilage thickness was measured at each testing location from the CECT images. We need to measure the cartilage thickness in each testing location to examine the potential confounding effect of thickness on stiffness measurements. Additionally, we were interested in assessing the accuracy of the CECT method in measurements of articular cartilage thickness, an important biomarker that is widely used in studies of OA.

The cartilage surface in each testing location was adjusted horizontally and the shortest distance between the cartilage-air interface and the cartilage-bone interface was computed as the thickness.

Since in some slices the cartilage-bone interface was not easily distinguished by our automated segmentation algorithms, segmented cartilage was manually corrected using an interactive touch-screen tablet to ensure that the boundary between subchondral bone and cartilage is appropriately identified. The cartilage thickness at 4 adjacent points ($\Delta x = \Delta y = 0.5$ mm distance or 12 voxels) was also calculated and the average of the 5 measurements was ultimately reported as the cartilage thickness in the region subjected to the indentation test. To validate thickness measurements obtained from CECT images, a needle indentation method was used to measure the thickness of cartilage in testing locations in a subset of samples. The comparison between the two measurements revealed that CECT is an accurate method (less than 5% estimation error) to measure cartilage thickness non-invasively (appendix D).

3.4 Statistical Analysis

The relationship between stiffness and CECT measurements was examined using correlation analysis. Pearson correlation coefficient (r) was reported to characterize the correlation between measurements. A linear regression model was used to predict stiffness data based on CECT measurement.

We performed ANCOVA analysis to determine whether the relationship between stiffness (dependent variable) and CECT measurement (covariate) differs across cartilage samples. In our ANCOVA analysis, the homogeneity of the slopes of the regression lines was assessed. We also used this analysis to assess the difference in stiffness-CECT relationship (as reflected in the difference between the slopes of the regression lines) among different groups of testing locations that have been categorized based on cartilage health (grade 0 vs. grade 1) and side (medial vs. lateral). To assess the possible confounding effect of thickness on our correlation analysis, ANCOVA was performed to determine whether excluding testing location with thin cartilage ($<< 2$ mm) would affect the relationship between stiffness and CECT measurements.

T-tests were performed to compare the CECT and stiffness measurements across samples. Alpha was set to 0.01 for ANCOVA and t-test analyses. The Fisher r -to- z transformation was performed to assess the significance of the difference between correlation coefficients. We tested the null hypothesis that there is significant difference in measurements (slopes, stiffness, and CECT attenuation). All statistical analyses were performed using commercially available software (MATLAB 2013a and SPSS 22).

4 Results

4.1 Sheep Samples

The number of indentation testing locations was 28 and 31 in the first (FC1) and the second (FC2) sheep cartilage samples, respectively. The mean \pm SD values of stiffness were 1.12 \pm 0.41 (range 0.47 to 2.03 N/mm) for FC1 and 1.84 \pm 0.38 N/mm (range 1.17 to 2.71 N/mm) for FC2. FC2 exhibited significantly higher values for cartilage stiffness compared to FC1 ($p < 0.01$).

Maps of CECT attenuation, reflecting CA4+ distribution, across both cartilage surfaces are shown in Figure 4.1. The mean \pm SD values of attenuation were 1547 \pm 132 (range from 1281 to 1573 HU) for FC1 and 1937 \pm 190 N/mm (range 1573 to 2187 HU) for FC2. Consistent with indentation data, the values of CECT attenuation were significantly higher in FC2 compared to FC1 ($p < 0.01$).

The correlation coefficient between CECT attenuation and cartilage stiffness was $r = 0.55$ for FC1 and $r = 0.47$ for FC2 (Figure 4.2). When the data points across both samples were combined together, the correlation coefficient increased to $r = 0.74$ (Figure 4.3).

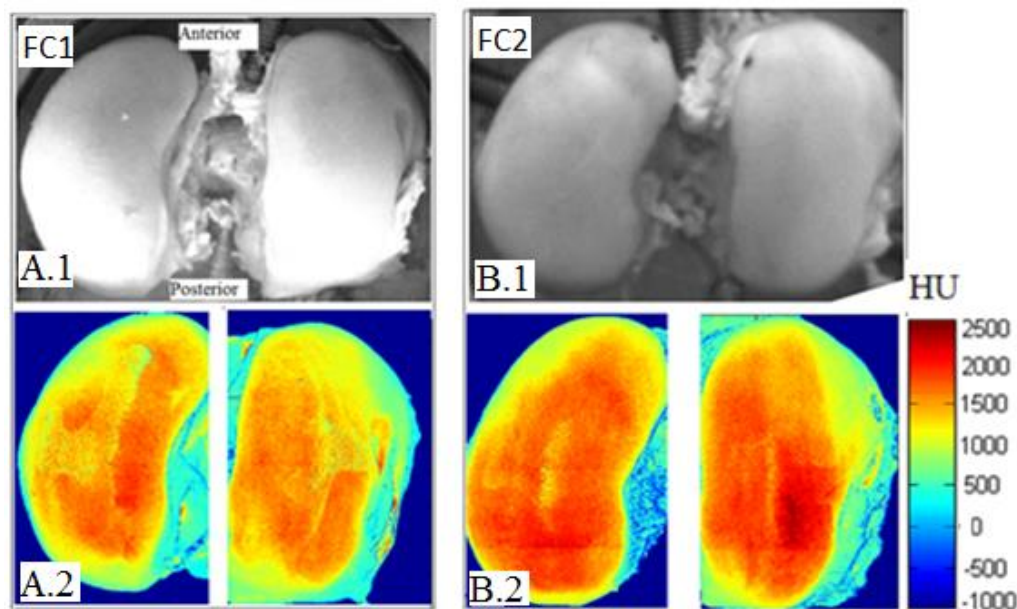


Figure 4.1 Maps of CECT attenuation in 2 sheep cartilage samples.

Top view of the sheep femoral cartilage samples in physical space (A.1 and B.1). CECT maps of cartilage surface (A.2 and B.2). The CECT attenuations are averaged over a depth of 200 μ m and mapped into the cartilage surface. The regions with higher CECT attenuations indicate higher concentration of cationic contrast agent and thereby higher GAG accumulation.

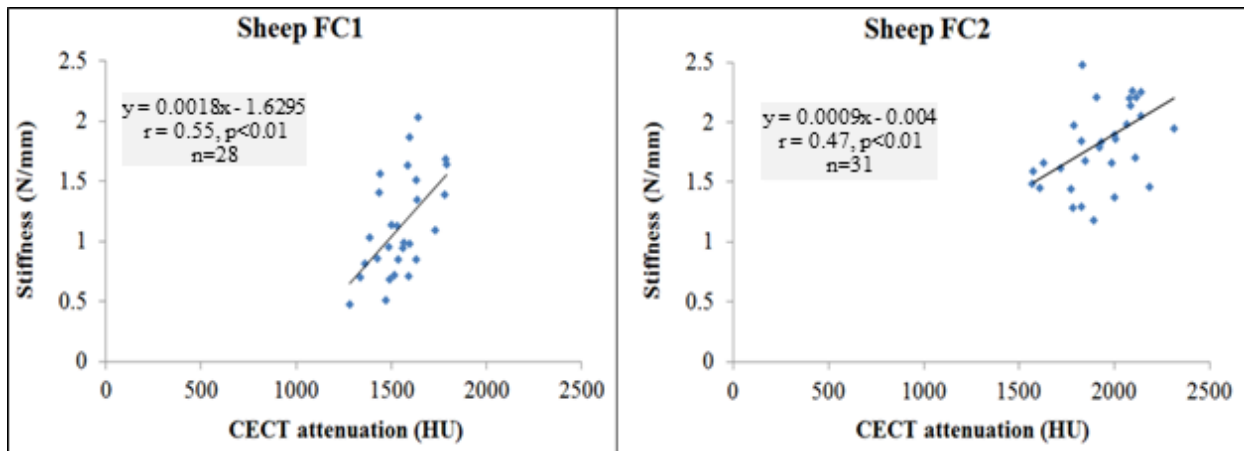


Figure 4.2 Scatter plots of stiffness versus CECT measurements.

Regression line fits describing the relationship between stiffness and CECT attenuation in two sheep femoral cartilage samples. The CECT attenuation is averaged over a cylindrical region of interest with 0.35 mm diameter and depth of 0.2 mm from cartilage surface in each testing locations. A significant positive correlation ($p < 0.001$) was observed in both plots.

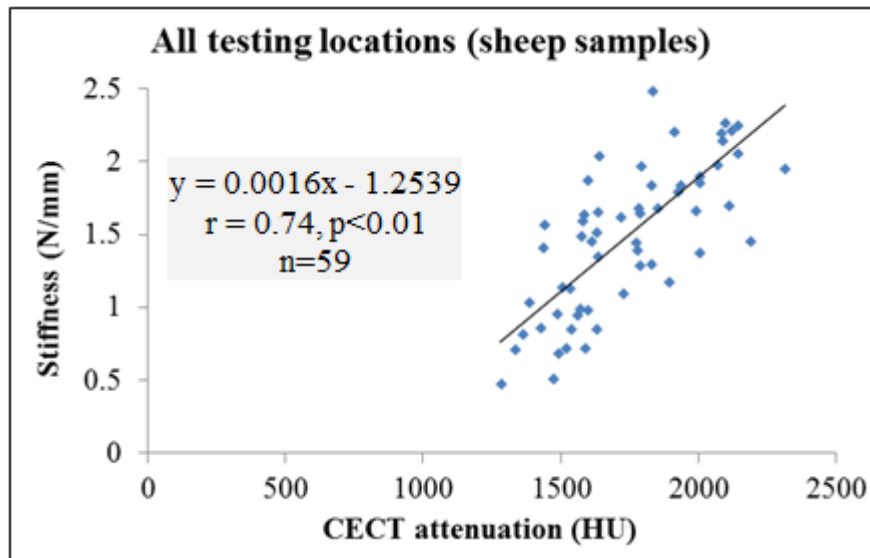


Figure 4.3 Correlation analysis of the combined data in sheep samples.

Regression line fit describing the relationship between stiffness and CECT attenuation when all testing locations are combined together in sheep samples. The CECT attenuation is averaged over a cylindrical region of interest with 0.35 mm diameter and depth of 0.2 mm from cartilage surface in each testing location. A significant positive correlation ($p < 0.01$) was observed in the plot with a correlation coefficient $r = 0.74$.

4.2 Human Samples

Stiffness was assessed at a total of 221 testing locations on the six human femoral condyle cartilage compartments. The mean \pm SD stiffness was 9 \pm 4.3 N/mm, with a range of 1 to 20 N/mm (Table 4.1). The average of stiffness measurements in testing locations classified as grade I was significantly lower than those classified as grade 0 (4.3 versus 9.0 N/mm, $p < 0.01$) according to t-test analysis.

The mean \pm SD values for superficial CECT attenuation were 1140 \pm 210 HU (range 600 to 1800 HU) (Table 4.1). The mean \pm SD values for full depth CECT attenuation were 1515 \pm 325 HU (range 1000 to 2500 HU). T-test analysis revealed that the mean CECT attenuation for superficial cartilage was lower in grade I testing locations than grade 0 locations (973 versus 1165 HU, $p < 0.01$). Likewise, mean CECT attenuation for full depth cartilage in grade 1 was lower than grade 0 locations (1251 versus 1554 HU, $p < 0.01$).

There were significant ($p < 0.01$) and positive correlations between superficial CECT and stiffness measurements in each of the six samples, ranging from $r = 0.4$ to 0.72 (Table 4.2, Figure 4.7). The correlation coefficient between superficial CECT and stiffness for all testing locations from all specimens was $r = 0.55$ (Figure 4.8). The correlation between stiffness and full-depth CECT measurement was lower for every specimen, ranging from $r = 0.04$ and 0.46 , and was not significant in 3 of the 6 samples (Table 4.2, Figure 4.9). The correlation coefficient between full-depth CECT and stiffness for all testing locations was $r = 0.31$ (Figure 4.10).

The relationship between cartilage stiffness and CECT attenuation was fit with a linear model. The model predicted cartilage stiffness with a standard estimation error of 3.59 N/mm, which corresponds to about 20% of the stiffness range (1-20 N/mm) across all samples.

Table 4.1 Stiffness and CECT measurements in human cartilage samples.

Sample	CECT attenuation (HU)		Stiffness (N/mm) <i>Mean ± standard deviation (SD).</i>
	Superficial ROI (0.6 mm depth) <i>Mean ± standard deviation (SD).</i>	Full depth ROI <i>Mean ± standard deviation (SD).</i>	
HFC#1	1131 ± 154	1565 ± 238	8.9 ± 3.7
HFC#2	915 ± 89	1177 ± 101	6.2 ± 2.4
HFC#3	1411 ± 159	1852 ± 279	11.9 ± 5.1
HFC#4	1313 ± 95	1863 ± 260	8.4 ± 2.3
HFC#5	1014 ± 87	1322 ± 122	6.5 ± 2.4
HFC#6	1046 ± 111	1367 ± 226	11.4 ± 4.8
All data	1140 ± 210	1515 ± 325	9 ± 4.3

Table 4.2 The correlation coefficients between stiffness measurement and mean CECT attenuation (superficial and full-depth) in human cartilage samples.

	All	HFC#1	HFC#2	HFC#3	HFC#4	HFC#5	HFC#6
Superficial CECT attenuation vs. stiffness	0.56 ^{**}	0.64 ^{**}	0.67 ^{**}	0.72 ^{**}	0.4 ^{**}	0.52 ^{**}	0.6 ^{**}
Full-depth CECT attenuation vs. stiffness	0.31 ^{**}	0.3 [*]	0.06	0.46 ^{**}	0.24	0.26	0.33 [*]

* Significant at p<0.05 level; ** significant at p<0.01 level

4.2.1 Qualitative Comparison between Stiffness and CECT Measurements

Maps of stiffness and CECT attenuation, overlaid on a top view of the samples, show the variation in these parameters across the cartilage surface (Figure 4.4 (a) to (f)). Although the samples did not exhibit gross morphological changes such as cartilage thickness defects, low values of CECT attenuation were evident in grade 1 testing locations, suggesting GAG depletion (e.g. Figure 4.4 (a) and (b)). These regions correspond to regions of reduced compressive stiffness in the stiffness maps.

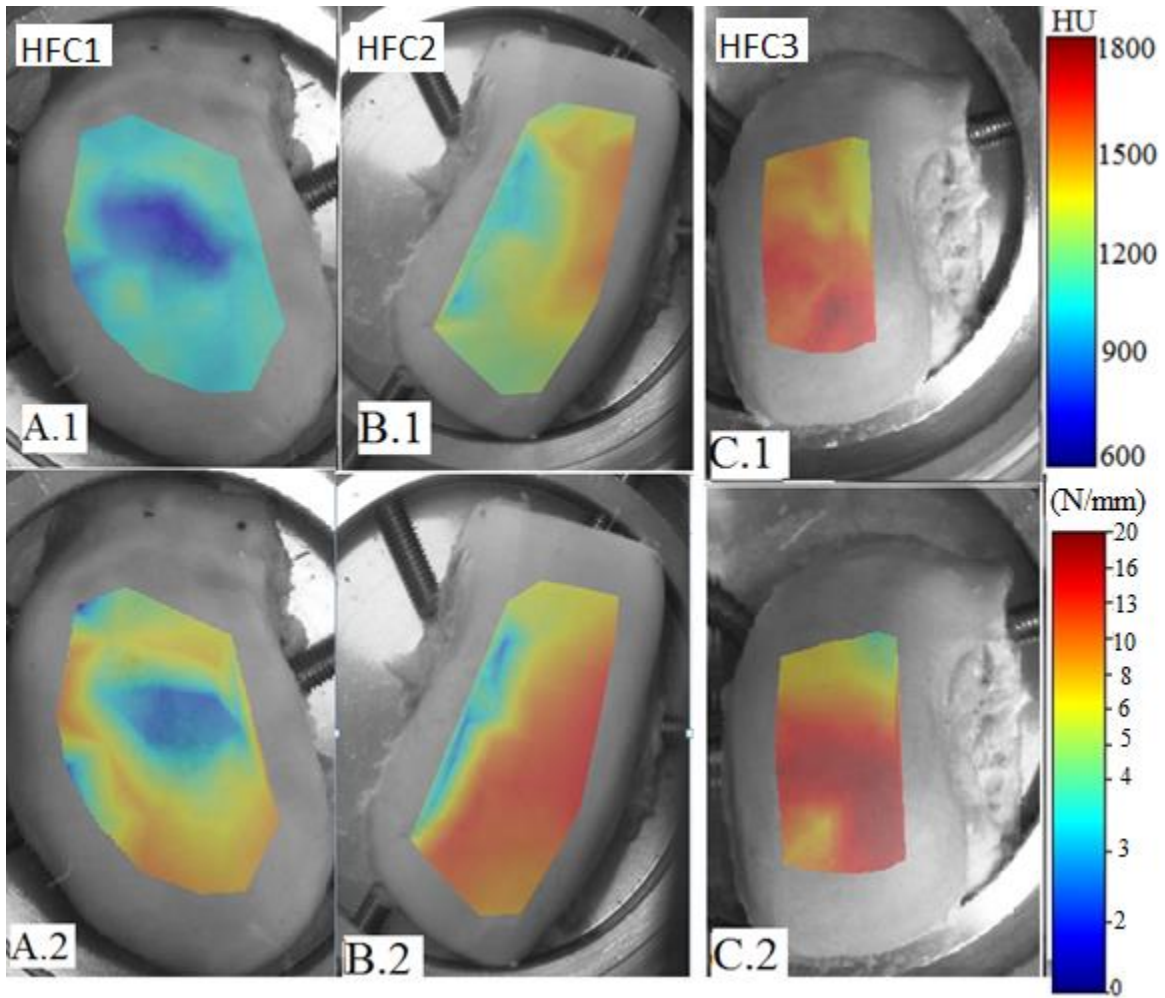


Figure 4.4 Maps of CECT attenuation and stiffness measurements.

CECT (A.1 - F.1) and stiffness (A.2 - F.2) maps of human femoral cartilage overlaid on regions that have been subjected to indentation tests. The topographic map of CECT represents average values of CECT attenuations over a depth of 0.6 mm. The CECT and stiffness maps exhibit generally similar spatial variations across the cartilage surface. Particularly, areas of reduced CECT attenuation, indicating depleted GAG (blue regions), correspond to areas in which softening of cartilage was measured.

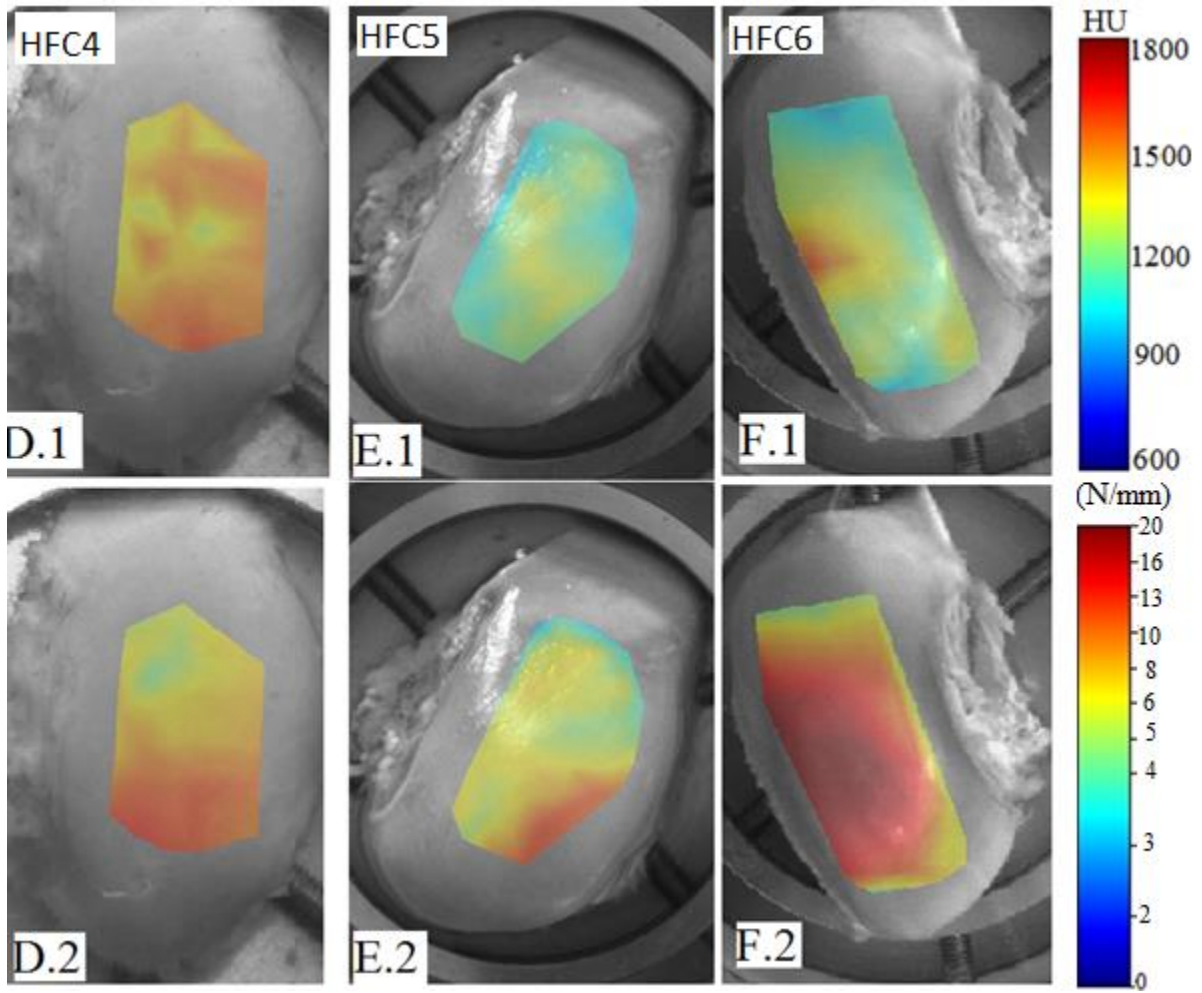


Figure 4.4 (continued)

4.2.2 Correlation Analysis between Stiffness and CECT Measurements

When CECT and stiffness measurements on each sample were pooled, a significant ($p < 0.01$) and positive correlation was found between the mean superficial CECT attenuation and stiffness for each of the six samples, with correlation coefficients ranging from $r = 0.41$ to 0.72 . A regression line was also fit for each sample to determine the relationship between CECT and stiffness (Figure 4.5). The slopes of the regression lines were not significantly different according to an ANCOVA analysis of the homogeneity of the slopes ($p = 0.116$), indicating same CECT-stiffness relationship across samples.

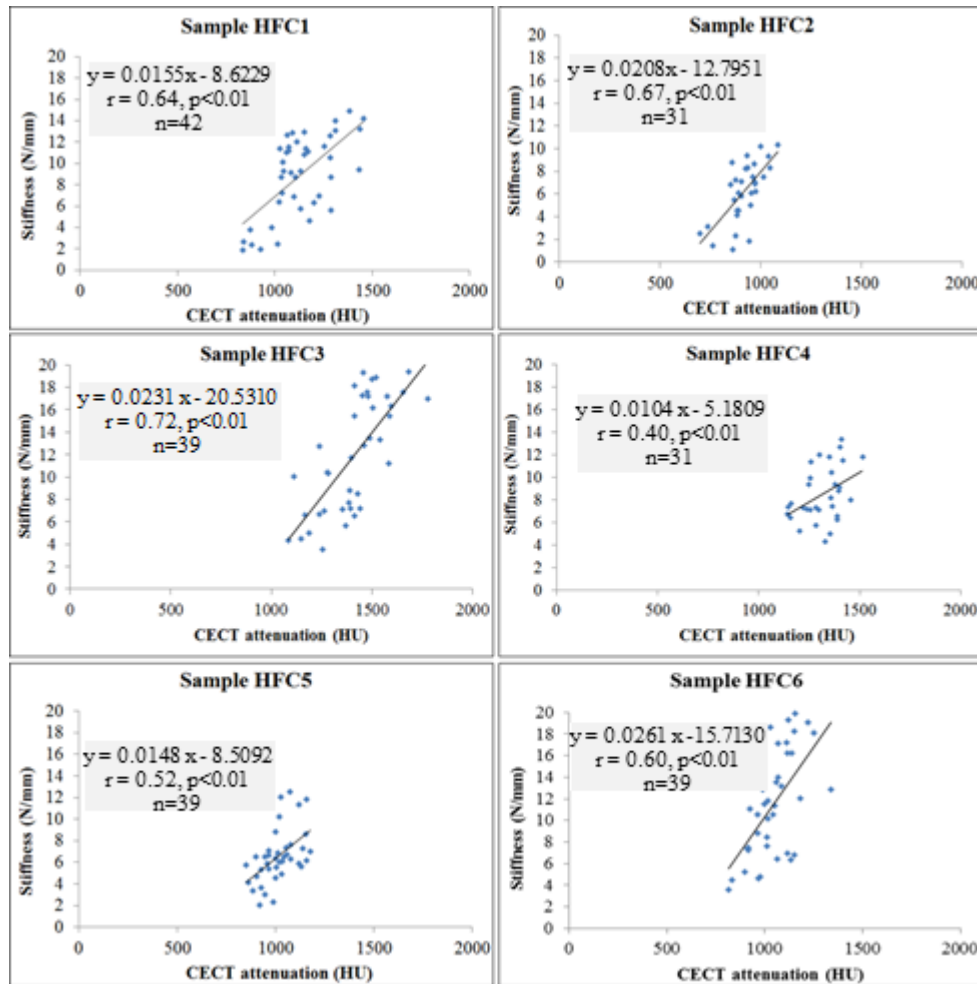


Figure 4.5 Scatterplots of stiffness vs. mean CECT attenuation (0.6 mm depth) in human cartilage samples. Regression line fits describing the relationship between stiffness and CECT attenuation in human femoral cartilage samples (HFC1-HFC6). The CECT attenuation is averaged over a cylindrical region of interest with 1 mm diameter and depth of 0.6 mm from cartilage surface in each testing locations. A significant positive correlation ($p < 0.01$) was observed in all plots.

When data across all samples was pooled, the correlation coefficient between superficial CECT and stiffness was $r=0.56$ ($p<0.01$) (Figure 4.6).

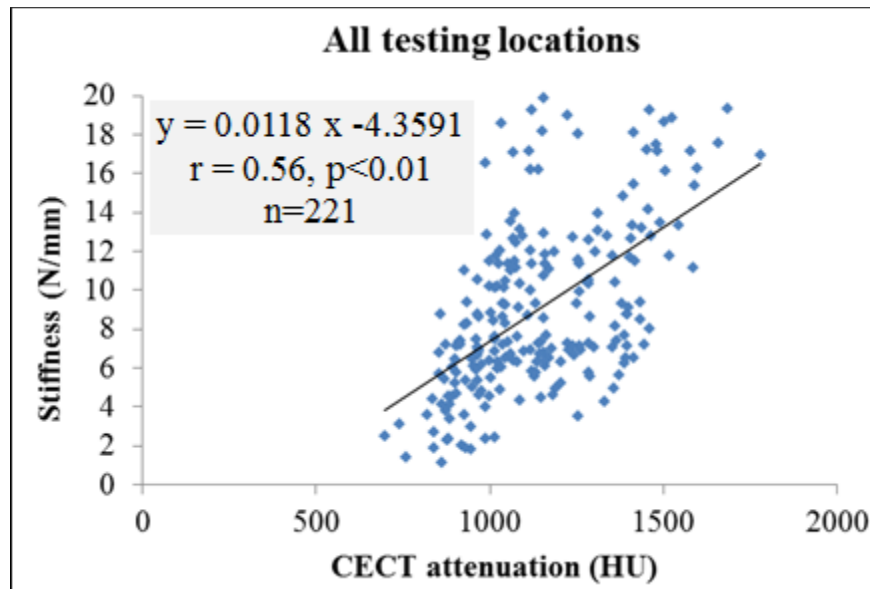


Figure 4.6 Scatterplot of pooled stiffness measurement vs. mean CECT attenuation (0.6 mm depth). Regression line fit describing the relationship between stiffness and CECT attenuation when all testing locations were combined together for the human samples. The CECT attenuation is averaged over a cylindrical region of interest with 1 mm diameter and depth of 0.6 mm from cartilage surface in each testing location. A significant positive correlation ($p<0.01$) was observed in the plot with a correlation coefficient $r=0.56$.

Weaker correlations were observed between stiffness measurements and CECT values averaged over the full depth of cartilage (Table 4.2). The highest correlation coefficient reported among samples was $r=0.47$. In three samples (HFC#2,4, and 5), the correlation between stiffness and mean CECT attenuation averaged over the full depth did not quite reach statistical significance ($p=0.73, 0.08,$ and 0.066 respectively). For the other three specimens (HFC#1,3, and 6), although reaching statistical significance ($p<0.05$) a weak to moderate correlation ($r=0.3, 0.47,$ and 0.33) was observed which was lower than the correlation values obtained from associating stiffness to superficial CECT attenuation.

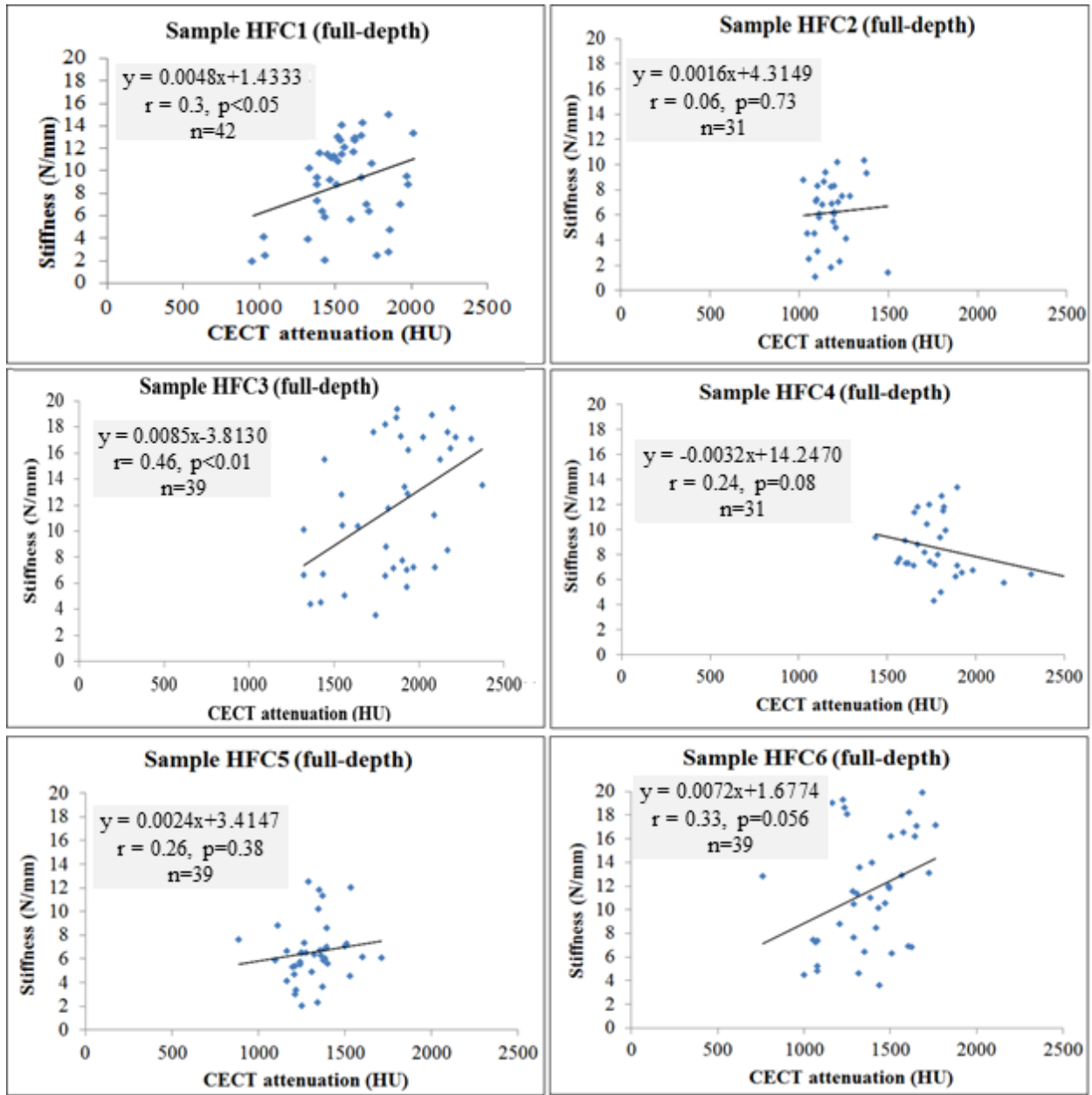


Figure 4.7 Scatterplots of stiffness vs. mean CECT attenuation (full-depth) in human cartilage samples. Regression line fits describing the relationship between stiffness and full-depth CECT attenuation in human femoral cartilage samples (HFC1-HFC6). The CECT attenuation is averaged over a cylindrical region of interest with 1 mm diameter and depth equal to cartilage thickness in each testing location. The stiffness-CECT curve in samples HFC1 and HFC3 showed significant correlation ($p < 0.05$ and $p < 0.01$ respectively, while other samples did not reach statistical significance ($p > 0.05$). This result suggests the minimal contribution of deep GAG content into instantaneous stiffness of cartilage.

4.2.3 Spatial Variation and Depth Dependence of CECT Measurements

CECT mapping revealed spatial variation of CECT attenuation (or CA⁴⁺ concentration) across surface for each sample (Figure 4.8).

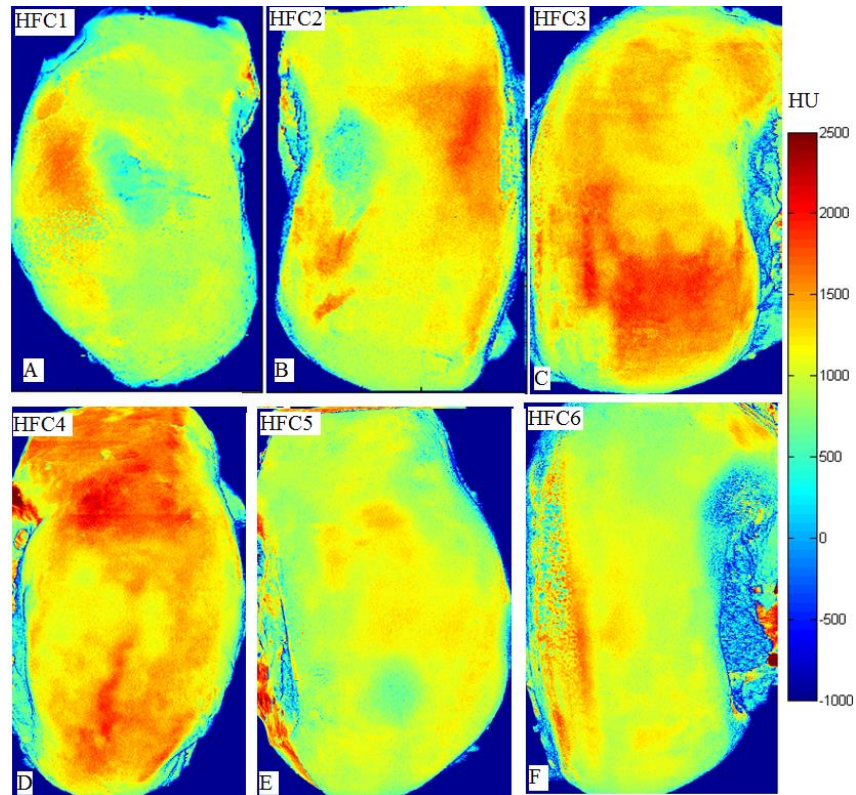


Figure 4.8 CECT maps of human cartilage surface.

Corresponding maps of CECT attenuation (A-F) are presented for cartilage samples (HFC1-HFC6). The CECT attenuations are averaged over a depth of 600 μ m and mapped into the cartilage surface. The regions with higher CECT attenuations indicate higher concentration of cationic contrast agent and thereby higher GAG concentration inside the tissue.

CECT attenuations increased from the superficial to the deep layer of cartilage (Figure 4.9) in all locations, as expected given the depth dependent variation of GAG concentration. The average CECT attenuation varied from 500 (superficial cartilage) to 3000 (deep cartilage) HU, corresponding to CA4+ concentration of 14-51 mg/ml. As noted before, the concentration of CA4+ contrast agent is proportional to the cartilage GAG concentration because of the electrostatic attraction between positively-charged CA4+ agents and negatively-charged GAG molecules. The zonal variation of GAG distribution along the cartilage thickness was visible in CECT scans.

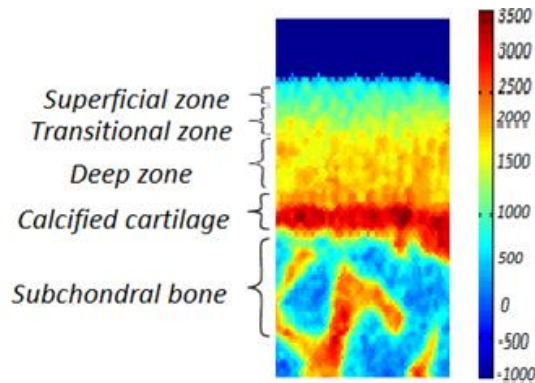


Figure 4.9 Variation of CECT attenuation along cartilage thickness.
CECT attenuations increase toward the deep zone of cartilage, reflecting zonal variations of GAG distribution .

4.2.3 Effect of Compartment (Medial/Lateral)

We compared associations for testing locations in medial and lateral compartments to determine whether the relationship between stiffness and superficial CECT attenuation is different between these regions (Figure 4.10 and 4.11). The difference in the slopes of the regression lines for medial (slope=0.0114) and lateral (slope=0.008) regions was not statistically significant ($p>0.01$) according to an ACNOVA analysis of the homogeneity of slopes. However, t-test analysis showed that testing locations in the medial compartment were stiffer in general (17 versus 7 N/mm, $p<0.01$) and showed higher CECT average values (1194 versus 1075 HU, $p<0.01$). When medial and lateral compartments from the same knee joint were compared (HFC1 versus HFC2, and HFC6 versus HFC5), similar regression slopes (slope=0.0155 vs. 0.0208, and slope=0.0261 vs. 0.0148) were found ($p>0.01$).

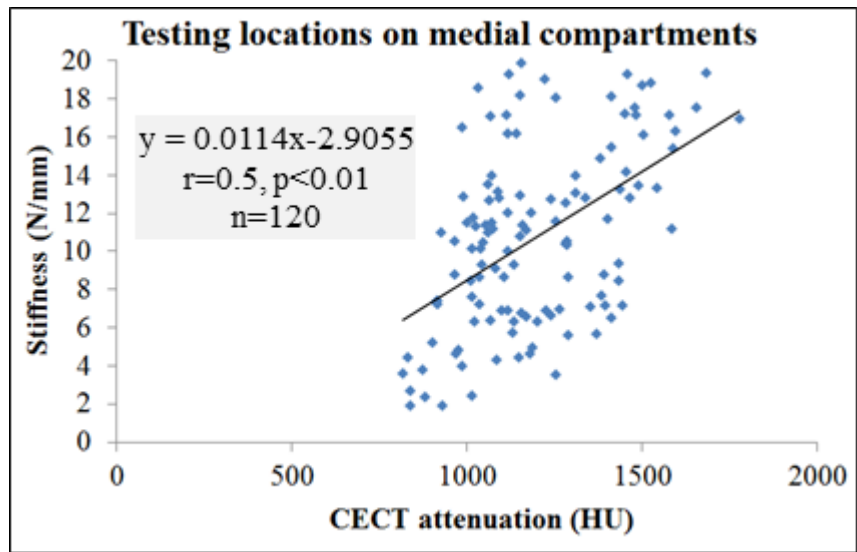


Figure 4.10 Scatterplots of stiffness vs. mean CECT attenuation (0.6 mm depth) in all medial cartilage compartments. Regression line fit describing the relationship between stiffness and CECT attenuation in medial human femoral cartilage samples (HFC2, HFC4, and HFC5). The CECT attenuation is averaged over a cylindrical region of interest with 1 mm diameter and depth of 0.6 mm from cartilage surface in each testing location. A significant positive correlation ($p < 0.01$) was observed in the plot with correlation coefficient of $r = 0.5$.

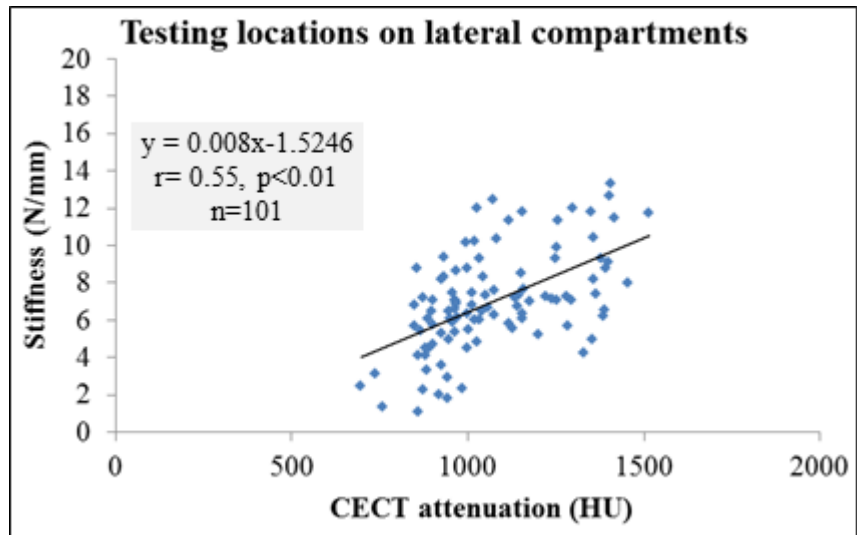


Figure 4.11 Scatterplots of stiffness vs. mean CECT attenuation (0.6 mm depth) in all lateral cartilage compartments. Regression line fit describing the relationship between stiffness and CECT attenuation in lateral human femoral cartilage samples (HFC1, HFC3, and HFC6). The CECT attenuation is averaged over a cylindrical region of interest with 1 mm diameter and depth of 0.6 mm from cartilage surface in each testing location. A significant positive correlation ($p < 0.01$) was observed in the plot with a correlation coefficient of $r = 0.55$.

4.2.4 Effect of Cartilage Grade

We compared stiffness, superficial CECT measurements and stiffness-CECT associations between testing locations in grade 0 cartilage and in grade 1 cartilage. Grade 1 cartilage was less stiff than Grade 0 cartilage (4.30 N/mm for Grade 1, 9.68 N/mm for Grade 0, ($p < 0.01$)). T-test analysis revealed that CECT attenuation (0.6 mm depth) in grade 1 cartilage was lower than Grade 0 cartilage (973 HU for Grade 1, 1165 HU for Grade 0, ($p < 0.01$)). However, the correlation coefficient ($r = 0.57$ for Grade 1, 0.57 for Grade 0) and slope of stiffness-CECT line (0.0067 N/mm.HU for Grade 1, 0.0102 for Grade 0) were not significantly different ($p > 0.01$) according to fisher r-to-z transformation and ANCOVA analyses (Figure 4.12).

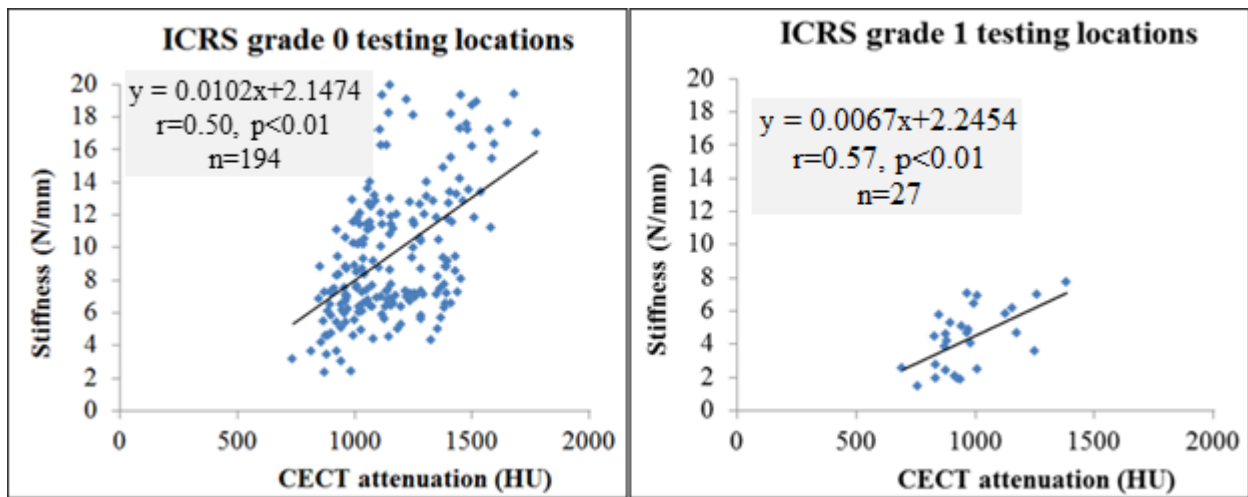


Figure 4.12 Scatterplots of stiffness versus mean CECT attenuation (0.6 mm depth) in grade 0 and 1 testing locations.

4.2.4 Effect of Thickness Variations on Stiffness Measurements

To ensure that the correlation between stiffness and GAG concentration is not affected by thickness variation, we assessed correlations between thickness and stiffness data in all testing locations (Table 4.3 and Figure 4.14). Across samples, thickness varies between 1.3 and 3.8 mm (Figure 4.13). In all specimens except 1 (HFC#3), the correlation between stiffness and thickness was not statistically significant (p values were higher than 0.01). When all data points from all specimens were included, no correlation was observed between stiffness and thickness (Figure 4.14). These findings suggest that cartilage thickness does not affect stiffness substantially.

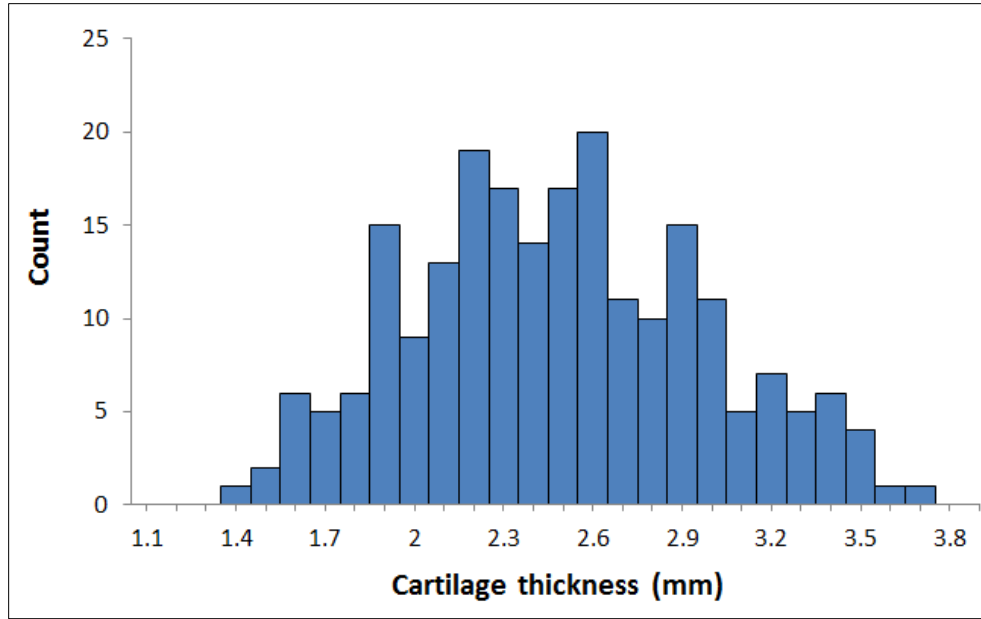


Figure 4.13 Distribution of articular cartilage thickness across samples. The thickness ranges from 1.3 mm to 3.8 mm with mean value of 2.43 mm.

Table 4.3 Correlation coefficients between stiffness and thickness data in human cartilage samples. Mean±SD values of thickness is presented in the second row.

	All	HFC#1	HFC#2	HFC#3	HFC#4	HFC#5	HFC#6
Thickness vs. stiffness correlation	-0.11	0.3	0.06	-0.47 ^{**}	-0.31	0.14	0.26
Thickness (mm)	2.43 ± 0.49	2.58 ± 0.35	2.51 ± 0.39	2.47 ± 0.61	2.3 ± 0.47	2.45 ± 0.37	2.18 ± 0.5

* Significant at p<0.05 level; ** significant at p<0.01 level.

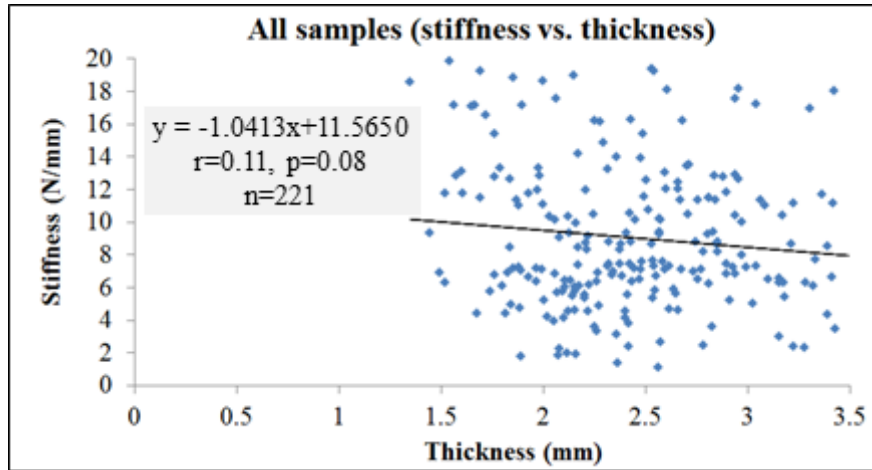


Figure 4.14 Scatterplot of stiffness vs. thickness in human cartilage samples.

The stiffness is plotted against thickness for human femoral cartilage samples to evaluate the effect of thickness as a confounding variable on stiffness measurements. The correlation was not significant ($p > 0.05$) suggesting a minimal effect of thickness on mechanical measurements.

We tested whether excluding the testing locations corresponding to thin regions of cartilage surface affected the CECT-stiffness relationship. This was motivated by results from a FEM model [106] suggested that the effect of thickness on stiffness measurement will be more pronounced in thinner areas of cartilage. We examined the relationship between stiffness-CECT measurements in two conditions; one considering all data points and the second including only thick areas of cartilage ($> 2\text{mm}$). The difference between the slopes (0.0118 vs. 0.0121) was not statistically significant ($p > 0.01$) (Figure 4.15).

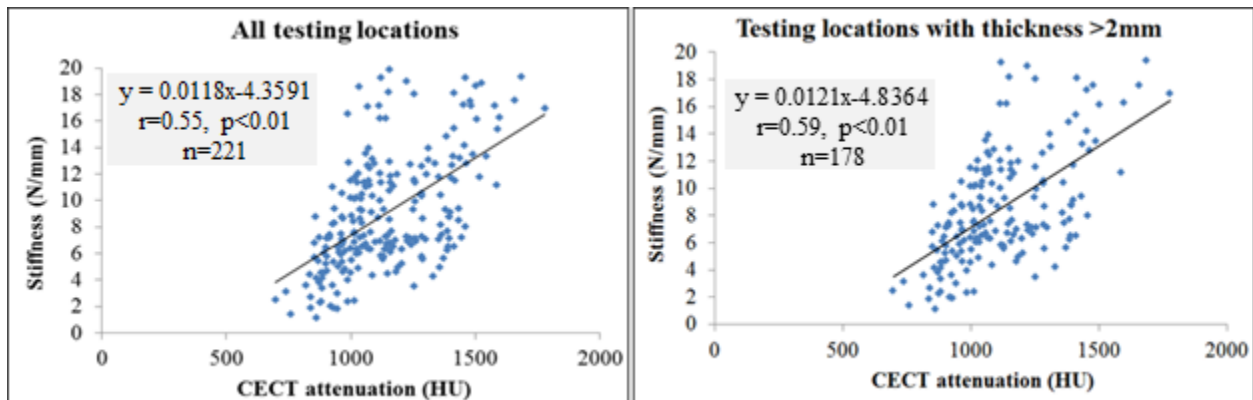


Figure 4.15 Scatterplots of stiffness vs. mean CECT attenuation (0.6 mm depth) in all testing locations and testing locations with thickness $> 2\text{mm}$.

Correlations between stiffness and CECT attenuations were reanalyzed after excluding testing locations with thickness $< 2\text{mm}$ (right).

5 Discussions

5.1 Motivation and Contributions

This study was undertaken to assess the link between stiffness and CECT attenuation measurements in intact human femoral articular cartilage. It was motivated by the need for a non-invasive method to assess cartilage mechanical function that had higher resolution and better visualization of cartilage than current methods. We found that CECT using a cationic contrast agent (CA4+) is correlated with stiffness assessed with indentation testing ($r = 0.55$, $p < 0.01$) if the appropriate region of interest is chosen for the CECT attenuation calculation. Since loss of cartilage stiffness is an early hallmark of osteoarthritis, this non-invasive imaging method has potential as a powerful research tool for osteoarthritis studies.

The main contributions of this study are:

- We have developed an experimental methodology for studying relationships between imaging and mechanical measurements in intact articular cartilage samples.
- We have applied this method in the first validation of CECT to indentation measurements in intact human cartilage samples.

5.2 Significance and Findings

5.2.1 Comparison of Indentation and CECT Results with Literature

Our stiffness findings were consistent with the results of previous work that assessed instantaneous stiffness of human femoral condyle cartilage using indentation techniques. Those studies used either a mechanical tester [112] (similar to our work) or an arthroscopy probe [106],[107] to perform indentation. We reported the instantaneous stiffness as the ratio of the measured peak load to the applied displacement normal to the cartilage surface. For comparison with other studies in literature, we calculated the corresponding contact pressure and instantaneous Young's modulus from our indentation measurements (Appendix G). The values of contact pressure found in our study were consistent with arthroscopic stiffness measurements in cadaver [107] and *in vivo* [106] investigations of femoral condyle cartilage. These two investigations used an arthroscopy probe with a plane-ended ($d=1$ mm) cylindrical indenter and measured the load response of cartilage to a 0.3 mm displacement.

The mean contact pressure in our measurements was 5.7 ± 2.74 MPa which is in the same range but lower than those reported in the cadaver (7.05 ± 3.84 MPa) and *in vivo* (6.53 ± 1.53 MPa) studies. The range of values for Young's modulus in our indentation tests (0.1-24 MPa) was on the same order as reported in a recent study [112] that used the same mechanical testing method to measure stiffness in human femoral condyle cartilage. However, the average values for Young's modulus in our samples (ranging between 5.75-13.6 MPa) were higher than those reported in that study (ranging between 3.61-6.87 MPa). We included a narrower, healthier range of cartilage health (ICRS=0 and 1) which likely explains the higher values (stiffer cartilage) obtained from our stiffness measurement.

Our finding that CECT attenuation is correlated with articular cartilage stiffness is consistent with many studies that linked non-invasive assessments of GAG with stiffness [13],[12],[108],[109],[81][102],[88]. Most similar to our work are two studies [12],[13] which associated measures of GAG concentration obtained from MR imaging to instantaneous stiffness of cartilage. Those studies reported correlations ranging from 0.64-0.94 between mechanical and GAG measurements, which are somewhat higher than our findings of correlation coefficients between 0.4 and 0.72. The difference between correlation coefficients can partly be explained by the difference in cartilage samples used in the studies. The two MR studies used human tibial plateaus; while in our study femoral condyle cartilage samples were examined. The composition and biomechanical properties are different in the tibial plateau than in the femoral condyle [110],[111],[112], which can lead to different load-bearing mechanisms in articulating surfaces of the knee joint. In addition, the tibial plateau can have more degeneration, yielding a broader range of properties that can yield higher correlations. A disadvantage of the experimental methodology used in the previous studies was that, due to the limitation of the indentation protocols used, measurements of cartilage properties were restricted to flat regions of the samples only.

5.2.2 Selecting the Wrong Region of Interest Confounds the Results

An important consideration in the studies examining the relationship between structure and function of cartilage is selecting the relevant region of interest for measuring the GAG content. In order to accurately correlate the mechanical and imaging measurements, GAG concentration should be computed in exactly the same region as the one used for indentation test. According to a FEM study [111], the deformed region in the cartilage due to the indentation forms a cylindrical volume with diameter and height equal to indenter size and indentation amplitude, respectively. Since in our study indentation was performed along a normal direction to the cartilage surface, the region of interest

was also segmented normal to the surface. A significant and positive correlation was observed between these two measurements in all samples. When the GAG concentration was measured in full-depth cartilage, however, the correlation coefficient was decreased and did not reach statistical significance in four specimens. This finding is not surprising, since it has been shown that the stress concentration drop by 50% at a depth twice the indentation amplitude during focal indentation [111]. In other words, the instantaneous load response of the tissue is mostly modulated by GAG components close to the cartilage surface, while deeper regions make minimal contributions.

Our results suggest that the poor correlation between GAG and indentation stiffness in some studies [114],[107] is likely due, in part, to the need to accurately match indentation location to imaging location. Comparing the instantaneous stiffness (using a handheld indentation probe) and GAG content (obtained from biochemical analysis), Bae et al.[114] found a weak correlation ($r=0.24$) and Franz et al. [107] found no correlation between stiffness and GAG concentration in human cartilage samples. These findings may be because the region in which GAG content was measured did not accurately represent the region which was loaded during indentation measurement. In these studies, the volume of the cartilage plug harvested for measurement of GAG content was at least one order of magnitude larger than the region which was actually influenced by indentation. Our findings, consistent with previous studies [13],[102], suggest the importance of selecting the right region of interest for having a valid comparison between mechanical and biochemical properties of articular cartilage. Both stiffness and GAG distribution exhibited high topographical variation across the cartilage surface, with significant variations over a short distance (e.g a 150% increase over a 5 mm displacement). With such a high spatial variation in cartilage biochemical and biomechanical properties, it would not be surprising that no correlation was found between indentation and GAG measurements when the regions examined for measuring GAG content did not closely match the region subjected to indentation compression.

5.2.3 Predictive Potential of CECT for Stiffness Measurement

A model based on a regression line fit to the data points is able to predict the stiffness with a standard error of 3.58 N/mm, or nearly 20% of the stiffness range (1-20 N/mm) seen for testing locations. Depending on the accuracy needed for measurement of stiffness, this level of estimation error might be acceptable. For instance, if the effects of a treatment or drug on cartilage stiffness are to be studied, this model can be used with an expected effect size to determine the feasibility of detecting changes with CECT. Using this mathematical model for prediction of absolute values for cartilage

stiffness is unlikely to be sufficiently accurate in many applications, due to the large inter-subject variability in mechanical and compositional properties. The method appears to be useful for detecting local stiffness changes that are characteristic of early cartilage degeneration. CECT predictions were able to differentiate between normal cartilage and regions undergoing softening in our samples. CECT can therefore non-invasively provide the same information obtained during arthroscopy, when the relative stiffness is measured with a probe to detect areas of degeneration.

5.2.4 Why Would We Not Expect $r=1$ between CECT and Stiffness Measurements?

Even with perfect stiffness and GAG measurement methods, we would not expect the correlation coefficient between indentation stiffness and GAG content of cartilage to equal $r=1$. This is because GAG is not the only component determining load response of cartilage. Collagen makes a large contribution to cartilage biomechanical behavior [25],[115]. When the cartilage surface is subjected to compressive loading, aside from compressive stress, it undergoes lateral deformation resulting in tensile stresses that are resisted by collagen in superficial cartilage. The collagen is oriented parallel to the cartilage surface in the superficial layer and generates a “trampoline effect” [116] which influences the response of cartilage to indentation.

5.2.4 CECT Advantages over MRI Methods

Quantitative MRI techniques have been widely used for evaluation of articular cartilage composition and structure. In particular, dGERMIC assesses GAG content and has been successfully used in several investigations [5],[9],[14],[117],[118]. dGERMIC relies on the fact that an anionic contrast agent distributes in cartilage in inverse proportion to the negatively-charged GAG molecules due to electrostatic repulsion. The concentration of contrast agent affects the relaxation time, and the mapped relaxation time therefore corresponds to the GAG concentration in cartilage. The high cost, low spatial resolution, and long acquisition time of MRI as well as the requirement for complicated pulse sequences and analysis limits the broader application of dGERMIC. In addition, dGERMIC images are sensitive to many competing factors due to factors such as collagen and water content of the cartilage, which makes the interpretation of the images challenging [2]. These limitations make CECT a viable alternative to dGERMIC for measuring cartilage GAG content. Furthermore, the potential of CECT for simultaneous imaging of bone and cartilage provides a unique opportunity for more comprehensive understanding of osteoarthritis initiation and progression as several studies have documented the possible role of subchondral bone in development of the disease [119],[121],[122].

5.2.5 Challenges to Implement CECT in Clinical Practice

For implementation of this method *in vivo*, several important issues must be taken into account. First, the interaction of the cationic contrast agent with live tissue is not yet known and its likely toxicity inside the body must be investigated. Second, the optimal dose of contrast agent and its injection route have to be determined. Finally, the required radiation dose and the potential risks associated with radiation exposure have to be studied carefully to determine whether the benefits of this method justify the risks to the patient.

5.2.6 CECT Offers an Alternative for Histology Assessment in Cartilage Repair Studies

Currently, the endpoint method for assessment of cartilage in osteoarthritis research is histological analysis [123] which is both destructive and time-consuming. Therefore, histology may not be very useful in the osteoarthritis studies where the effects of a new treatment or drug need to be monitored over a period of time and repeated measurements of cartilage properties are demanded. Having a reliable and non-invasive method for assessment of cartilage structure and quality is an essential requirement for further progress in this field. Such method can be useful for monitoring cartilage repair strategies and disease-modifying drugs in animal studies and preclinical trials. Based on present findings, CECT as a non-invasive and non-destructive imaging tool can be a promising alternative for histology.

5.3 Strengths

This study, to the best of our knowledge, is the first work validating the CECT method in presence of a cationic contrast agent against mechanical measurements in human cartilage samples. A key strength of this study is that we performed both imaging and mechanical testing in intact cartilage surface samples. Unlike many previous studies that used harvested cartilage plugs, the testing protocols used here more closely represent the *in vivo* condition and therefore more realistically reflect cartilage mechanical behavior. Indentation stiffness is a good representation of *in vivo* loading on the knee joint, since force is typically applied and removed rapidly in a loading scenario such as walking. Indentation in intact cartilage surfaces required less sample preparation than testing in cartilage plugs, and its non-destructive nature enables repetitive measurements on a sample. Indentation in intact cartilage also maintains its physiological environment. It has been shown that

the swelling pressure within the cartilage matrix results in non-zero stress fields in unloaded tissue [124],[125]. These non-zero stress fields, equivalent to residual stresses in engineering terms, keep the cartilage in a nearly zero-stress state when subjected to loading. However, as the cartilage plug is extracted from the sample, these residual stresses are released and its biomechanical behavior may be different from when it was part of a continuous surface.

A second strength of this study is that the data obtained from imaging was validated by making a comparison against a functional measure of articular cartilage. Many previous validation studies compared the results of imaging to histology[21],[85],[86],[89],[126]-[128]. Since the relationship between cartilage composition and function is complicated, the measures of cartilage composition may not fully describe cartilage function. Functional measures of cartilage are important, particularly if obtained using non-invasive imaging methods, because changes in function (e.g. softening) are known to occur during OA initiation and progression long before gross morphology changes become evident [119],[129],[130]. We were able to identify regions of reduced cartilage stiffness, indicating impaired function, using CECT. Our results reveal the potential of CECT for functional imaging of articular cartilage and providing a more sensitive measure for evaluation of cartilage degeneration.

A third strength of our study was that a relatively low concentration of contrast agent was used in our CECT protocol. We were able to visualize articular cartilage in CECT images using a lower dose of cationic contrast agent than is normally used in anionic contrast agent protocols (12 mg/ml vs 80 mg/ml) [19],[131],[99],[93]. This finding indicates the potential use of CA4+ for *in vivo* imaging, since the lower concentration of contrast agent is desirable for clinical practice. An excessive dose of contrast agent injected into the joint space is likely to cause temporary softening of the tissue, which could in turn cause cell death and cartilage damage due to the hyperosmolaric nature of the contrast agent [33].

A key strength of our indentation protocol is that our indenter size was optimized for the cartilage thickness. Thickness is known to affect the instantaneous load response of articular cartilage. Therefore, to be able to attribute the measurements only to the cartilage structure and its composition, the effect of thickness should be minimized. An FEM study of indentation [34] suggested that the effect of cartilage thickness on load measurements is negligible if the size of indenter is less than the sample thickness. The thinnest cartilage in our testing locations was 1.33 mm thick, which was still larger than the size of the spherical indenter ($d=1$ mm). For the indenter size and sample thicknesses of our study, cartilage thickness will account for no more than 10% variation in indentation

measurements [34]. Since the effect of thickness on load response of cartilage is more pronounced as the indenter size approaches the thickness, we also examined the relationship between stiffness and GAG measurements when only the results of testing sites with more than 2mm thickness were included. Excluding the thinner samples did not significantly alter the correlation coefficient and slope of the stiffness-GAG curve. Additionally, the stiffness measurement showed no correlation with thickness when the data for all testing location were pooled together.

5.4 Limitations

This study has specific limitations related to sample acquisition, testing protocols, and data processing. First, our cartilage samples were obtained from cadaver knee joints that had been used in another experiment in our group and were kept frozen at -20°C for a year. Several investigators reported that freezing does not influence load response of cartilage to indentation test [132],[133],[134], and revealed no detectable pattern of histology changes in cartilage following freezing [135]. However, being exposed to room temperature during the course of that experiment, the samples may have undergone non-physiologic degeneration and changes in tissue properties.

Another limitation of this study is that only femoral condyle cartilage was studied. Mechanical properties and cartilage composition are known to vary significantly between the patella, femoral condyle, and tibial plateau [110]. In a previous study [117], the strongest correlation between mechanical and biochemical properties was found when data from all of the articulating surfaces of the knee joint were considered altogether.

Our imaging protocol has some limitations that should be considered. In our CECT images, the boundary between the cartilage surface and air was easily detectable. In the *in vivo* condition, however, accurate segmentation of the articular surface is challenging because the attenuation in synovial fluid is close to that of cartilage following administration of contrast agent. Inaccurate delineation of the cartilage surface can result in subsequent errors in thickness measurement and mapping of GAG distribution. The resolution of CECT images in this study (41 μm) is smaller than the resolution typically used in clinical CT scanners. Whether CECT using a clinical scanner can measure the heterogeneous spatial distribution of GAG content must be investigated.

Another limitation is that we have assumed that contrast agent distribution is proportional to GAG concentration within the tissue following administration of the cationic contrast agent. However, the exact relationship between CECT attenuation, which reflects contrast agent concentration, and GAG

content of cartilage samples was not assessed in this study. The relationship between GAG content, obtained from histology, and CECT attenuation has been established in animal samples[20][21], but it has not been established in human cartilage.

A further limitation is that our mechanical and imaging measures do not account for the role of collagen in cartilage. The collagen network is the primary structure for transmitting tensile stress, and consequently plays an important role in the instantaneous load response of cartilage. The diffusion behavior of contrast agent is also affected by the collagen network orientation and distribution. Further studies for exploring the sensitivity of CECT to collagen are warranted to better assess the ability of CECT to measure GAG content and predict cartilage stiffness.

5.5 Future Directions

The correlation between CECT and stiffness should be investigated in a larger sample size, including all surfaces from all major joints and a full range of ages and both genders, to provide a complete understanding of the cartilage composition-function relationship. Of particular interest will be testing intact surfaces of human hip cartilage, since practical limitations such as the difficulty of performing indentation on the curved articulating surfaces of the hip have limited experimental work on this joint.

Histology assessments must be conducted to reveal the exact relationship between CECT measurement and GAG content in cartilage. In this study, we assumed that the correlation coefficient between CECT attenuation and GAG content is $r=1$, while in reality other factors might affect CECT measurements. In addition, the relationship between CECT attenuation and collagen architecture is not known yet and finding the association is a must for further application of CECT method.

The results of the present study can be applied for more accurate FEM modeling of articular cartilage. The distribution of GAG content and the resulting mechanical properties as well as cartilage morphology obtained from CECT measurements can be used to develop anisotropic and inhomogeneous models of cartilage (sample specific thickness, Young's modulus, and Poisson's ratio). More accurate FEM models of cartilage could then be used to investigate the effects of softening and focal cartilage loss on stress distribution within cartilage and therefore explain the role of mechanics in the initiation and progression of osteoarthritis.

CECT provides the opportunity to simultaneously image bone and cartilage with high resolution. CECT can be used to assess links between cartilage composition, cartilage function, bone density, and bone stiffness in studies of the role of subchondral bone in osteoarthritis initiation and progression.

The sensitivity of CECT as a diagnostic method for osteoarthritis needs to be investigated to determine whether this method can detect degenerative changes in cartilage. Cartilage degeneration can be induced either through mechanical injury or enzymatic degradation and the corresponding changes in CECT measurements can be assessed to determine the method's sensitivity.

The potential of this method for *in vivo* studies should be assessed, provided that the challenges associated with translating this method to clinical practice are addressed (eg approval of the contrast agent, assessment of radiation dose). For instance, it should be determined how sensitive the CECT method is to differences between normal participants and people with different stage of osteoarthritis.

5.6 Conclusion

Contrast-enhanced computed tomography (CECT) attenuation using the novel cationic contrast agent (CA4+) was significantly correlated with instantaneous cartilage stiffness assessed in intact cartilage surfaces, in human femora. This study demonstrates the potential of the CECT imaging method to assess cartilage function, making it a powerful research tool for deeper understanding of osteoarthritis initiation and progression.

References

- [1] M. Bhandari, J. Smith, L. E. Miller, and J. E. Block, "Clinical and economic burden of revision knee arthroplasty," *Clin. Med. Insights Arthritis Musculoskelet. Disord.*, vol. 5, pp. 89–94, 2012.
- [2] D. Burstein and M. L. Gray, "Is MRI fulfilling its promise for molecular imaging of cartilage in arthritis?," *Osteoarthr. Cartil.*, vol. 14, no. 11, pp. 1087–1090, 2006.
- [3] G. Blumenkrantz and S. Majumdar, "Quantitative magnetic resonance imaging of articular cartilage in osteoarthritis," *Eur. Cell. Mater.*, vol. 13, pp. 76–86, 2007.
- [4] V. Mlynárik, S. Trattnig, M. Huber, A. Zembsch, and H. Imhof, "The role of relaxation times in monitoring proteoglycan depletion in articular cartilage," *J. Magn. Reson. Imaging*, vol. 10, no. 4, pp. 497–502, 1999.
- [5] S. Trattnig, V. Mlynárik, M. Breitenseher, M. Huber, A. Zembsch, T. Rand, and H. Imhof, "MRI visualization of proteoglycan depletion in articular cartilage via intravenous administration of Gd-DTPA," *Magn. Reson. Imaging*, vol. 17, no. 4, pp. 577–583, 1999.
- [6] A. Bashir, M. L. Gray, and D. Burstein, "Gd-DTPA²⁻ as a measure of cartilage degradation," *Magn. Reson. Med.*, vol. 36, pp. 665–673, 1996.
- [7] Y.-J. Kim, D. Jaramillo, M. B. Millis, M. L. Gray, and D. Burstein, "Assessment of early osteoarthritis in hip dysplasia with delayed gadolinium-enhanced magnetic resonance imaging of cartilage," *J. Bone Joint Surg. Am.*, vol. 85-A, no. 10, pp. 1987–1992, 2003.
- [8] C. J. Tiderius, R. Jessel, Y. J. Kim, and D. Burstein, "Hip dGEMRIC in asymptomatic volunteers and patients with early osteoarthritis: The influence of timing after contrast injection," *Magn. Reson. Med.*, vol. 57, no. 4, pp. 803–805, 2007.
- [9] T. C. B. Pollard, E. G. McNally, D. C. Wilson, D. R. Wilson, B. Mädler, M. Watson, H. S. Gill, and a J. Carr, "Localized cartilage assessment with three-dimensional dGEMRIC in asymptomatic hips with normal morphology and cam deformity," *J. Bone Joint Surg. Am.*, vol. 92, no. 15, pp. 2557–69, Nov. 2010.
- [10] A. Bashir, M. L. Gray, J. Hartke, and D. Burstein, "Nondestructive imaging of human cartilage glycosaminoglycan concentration by MRI," *Magn. Reson. Med.*, vol. 41, pp. 857–865, 1999.
- [11] A. Williams, R. A. Oppenheimer, M. L. Gray, and D. Burstein, "Differential recovery of glycosaminoglycan after IL-1-induced degradation of bovine articular cartilage depends on degree of degradation," *Arthritis Res. Ther.*, vol. 5, no. 2, pp. R97–R105, 2003.
- [12] J. T. Samosky, D. Burstein, W. E. Grimson, R. Howe, S. Martin, and M. L. Gray, "Spatially-localized correlation of dGEMRIC-measured GAG distribution and mechanical stiffness in the human tibial plateau," *J. Orthop. Res.*, vol. 23, pp. 93–101, 2005.
- [13] M. Baldassarri, J. S. L. Goodwin, M. L. Farley, B. E. Bierbaum, S. R. Goldring, M. B. Goldring, D. Burstein, and M. L. Gray, "Relationship between cartilage stiffness and dGEMRIC index: correlation and prediction," *J. Orthop. Res.*, vol. 25, pp. 904–912, 2007.
- [14] M. J. Nissi, J. Tyyryläinen, M. S. Laasanen, J. Rieppo, S. Saarakkala, R. Lappalainen, J. S. Jurvelin, and M. T. Nieminen, "Proteoglycan and collagen sensitive MRI evaluation of normal and degenerated articular cartilage," *J. Orthop. Res.*, vol. 22, pp. 557–564, 2004.

- [15] D. Burstein, J. Velyvis, K. T. Scott, K. W. Stock, Y. J. Kim, D. Jaramillo, R. D. Boutin, and M. L. Gray, "Protocol issues for delayed Gd(DTPA)₂-enhanced MRI (dGEMRIC) for clinical evaluation of articular cartilage," *Magn. Reson. Med.*, vol. 45, no. 1, pp. 36–41, 2001.
- [16] A. Gillis, M. Gray, and D. Burstein, "Relaxivity and diffusion of gadolinium agents in cartilage," *Magn. Reson. Med.*, vol. 48, no. 6, pp. 1068–1071, 2002.
- [17] N. S. Joshi, P. N. Bansal, R. C. Stewart, B. D. Snyder, and M. W. Grinstaff, "Effect of contrast agent charge on visualization of articular cartilage using computed tomography: Exploiting electrostatic interactions for improved sensitivity," *J. Am. Chem. Soc.*, vol. 131, pp. 13234–13235, 2009.
- [18] P. N. Bansal, N. S. Joshi, V. Entezari, B. C. Malone, R. C. Stewart, B. D. Snyder, and M. W. Grinstaff, "Cationic contrast agents improve quantification of glycosaminoglycan (GAG) content by contrast enhanced CT imaging of cartilage," *J. Orthop. Res.*, vol. 29, pp. 704–709, 2011.
- [19] R. C. Stewart, P. N. Bansal, V. Entezari, H. Lusic, R. M. Nazarian, B. D. Snyder, and M. W. Grinstaff, "Contrast-enhanced CT with a high-affinity cationic contrast agent for imaging ex vivo bovine, intact ex vivo rabbit, and in vivo rabbit cartilage," *Radiology*, vol. 266, pp. 141–50, 2013.
- [20] B. A. Lakin, D. J. Grasso, S. S. Shah, R. C. Stewart, P. N. Bansal, J. D. Freedman, M. W. Grinstaff, and B. D. Snyder, "Cationic agent contrast-enhanced computed tomography imaging of cartilage correlates with the compressive modulus and coefficient of friction," *Osteoarthr. Cartil.*, vol. 21, pp. 60–68, 2013.
- [21] P. N. Bansal, R. C. Stewart, V. Entezari, B. D. Snyder, and M. W. Grinstaff, "Contrast agent electrostatic attraction rather than repulsion to glycosaminoglycans affords a greater contrast uptake ratio and improved quantitative CT imaging in cartilage," *Osteoarthr. Cartil.*, vol. 19, pp. 970–976, 2011.
- [22] B. a. Lakin, H. Patel, K. S. Stok, B. D. Snyder, and M. W. Grinstaff, "Contrast-enhanced computed tomography imaging using a cationic contrast agent correlates with the equilibrium modulus of mouse tibial plateau cartilage," *Osteoarthr. Cartil.*, vol. 22, no. 2014, pp. S345–S346, 2014.
- [23] V. C. Mow, A. Ratcliffe, and A. R. Poole, "Cartilage and diarthrodial joints as paradigms for hierarchical materials and structures," *Biomaterials*, vol. 13, no. 2, pp. 67–97, 1992.
- [24] M. Huber, S. Trattng, and F. Lintner, "Anatomy, biochemistry, and physiology of articular cartilage," *Invest. Radiol.*, vol. 35, no. 10, pp. 573–580, 2000.
- [25] X. L. Lu and V. C. Mow, "Biomechanics of articular cartilage and determination of material properties," *Med. Sci. Sports Exerc.*, vol. 40, no. 2, pp. 193–9, Feb. 2008.
- [26] J. M. Mansour and D. Ph, "Biomechanics of Cartilage," pp. 66–79.
- [27] V. C. Mow and W. M. Lai, "Recent Developments in Synovial Joint Biomechanics," *SIAM Review*, vol. 22, no. 3, pp. 275–317, 1980.
- [28] G. E. Kempson, H. Muir, S. A. Swanson, and M. A. Freeman, "Correlations between stiffness and the chemical constituents of cartilage on the human femoral head," *Biochim. Biophys. Acta*, vol. 215, no. 1, pp. 70–77, 1970.
- [29] J. A. Buckwalter and H. J. Mankin, "Articular cartilage: tissue design and chondrocyte-matrix interactions," *Instr. Course Lect.*, vol. 47, pp. 477–486, 1998.

- [30] D. Burstein, A. Bashir, and M. L. Gray, "MRI techniques in early stages of cartilage disease.," *Invest. Radiol.*, vol. 35, no. 10, pp. 622–638, 2000.
- [31] L. T. Brody, "Knee Osteoarthritis: Clinical Connections to Articular Cartilage Structure and Function," *Phys. Ther. Sport*, 2014.
- [32] W. C. Hayes, L. M. Keer, G. Herrmann, and L. F. Mockros, "A mathematical analysis for indentation tests of articular cartilage.," *J. Biomech.*, vol. 5, pp. 541–551, 1972.
- [33] M. J. Turunen, J. Töyräs, M. J. Lammi, J. S. Jurvelin, and R. K. Korhonen, "Hyperosmolaric contrast agents in cartilage tomography may expose cartilage to overload-induced cell death," *J. Biomech.*, vol. 45, no. 3, pp. 497–503, 2012.
- [34] T. Lyyra-Laitinen, M. Niinimäki, J. Töyräs, R. Lindgren, I. Kiviranta, and J. S. Jurvelin, "Optimization of the arthroscopic indentation instrument for the measurement of thin cartilage stiffness.," *Phys. Med. Biol.*, vol. 44, pp. 2511–2524, 1999.
- [35] S. Knecht, B. Vanwanseele, and E. Stüssi, "A review on the mechanical quality of articular cartilage - Implications for the diagnosis of osteoarthritis," *Clin. Biomech.*, vol. 21, no. 10, pp. 999–1012, 2006.
- [36] V. C. Mow, S. C. Kuei, W. M. Lai, and C. G. Armstrong, "Biphasic creep and stress relaxation of articular cartilage in compression? Theory and experiments.," *J. Biomech. Eng.*, vol. 102, pp. 73–84, 1980.
- [37] B. Cohen, W. M. Lai, and V. C. Mow, "A transversely isotropic biphasic model for unconfined compression of growth plate and chondroepiphysis.," *J. Biomech. Eng.*, vol. 120, pp. 491–496, 1998.
- [38] J. Soulhat, M. D. Buschmann, and A. Shirazi-Adl, "A fibril-network-reinforced biphasic model of cartilage in unconfined compression.," *J. Biomech. Eng.*, vol. 121, pp. 340–347, 1999.
- [39] W. M. Lai, J. S. Hou, and V. C. Mow, "A triphasic theory for the swelling and deformation behaviors of articular cartilage.," *J. Biomech. Eng.*, vol. 113, pp. 245–258, 1991.
- [40] R. C. Lawrence, C. G. Helmick, F. C. Arnett, R. A. Deyo, D. T. Felson, E. H. Giannini, S. P. Heyse, R. Hirsch, M. C. Hochberg, G. G. Hunder, M. H. Liang, S. R. Pillemer, V. D. Steen, and F. Wolfe, "Estimates of the prevalence of arthritis and selected musculoskeletal disorders in the United States," *Arthritis Rheum.*, vol. 41, pp. 778–799, 1998.
- [41] J. A. Buckwalter and H. J. Mankin, "Articular cartilage: degeneration and osteoarthritis, repair, regeneration, and transplantation.," *Instr. Course Lect.*, vol. 47, pp. 487–504, 1998.
- [42] H. Lorenz and W. Richter, "Osteoarthritis: Cellular and molecular changes in degenerating cartilage," *Prog. Histochem. Cytochem.*, vol. 40, pp. 135–163, 2006.
- [43] J. A. Buckwalter and L. C. Rosenberg, "Electron microscopic studies of cartilage proteoglycans.," *Electron Microsc. Rev.*, vol. 1, pp. 87–112, 1988.
- [44] K. D. Brandt, P. Dieppe, and E. Radin, "Etiopathogenesis of Osteoarthritis," *Medical Clinics of North America*, vol. 93, pp. 1–24, 2009.
- [45] D. R. Wilson, E. J. McWalter, and J. D. Johnston, "The Measurement of Joint Mechanics and Their Role in Osteoarthritis Genesis and Progression," *Rheumatic Disease Clinics of North America*, vol. 39, pp. 21–44, 2013.

- [46] A. Heijink, A. H. Gomoll, H. Madry, M. Drobnič, G. Filardo, J. Espregueira-Mendes, and C. N. van Dijk, "Biomechanical considerations in the pathogenesis of osteoarthritis of the knee," *Knee Surgery, Sports Traumatology, Arthroscopy*, vol. 20, pp. 423–435, 2012.
- [47] D. T. Felson, "Osteoarthritis as a disease of mechanics," *Osteoarthr. Cartil.*, vol. 21, no. 1, pp. 10–15, 2013.
- [48] M. B. Goldring and S. R. Goldring, "Osteoarthritis," *Journal of Cellular Physiology*, vol. 213, no. 3, pp. 626–634, 2007.
- [49] D. T. Felson, S. McLaughlin, J. Goggins, M. P. LaValley, M. E. Gale, S. Totterman, W. Li, C. Hill, and D. Gale, "Bone Marrow Edema and Its Relation to Progression of Knee Osteoarthritis," *Ann. Intern. Med.*, vol. 139, pp. 330–336+I33, 2003.
- [50] L. Sharma, J. Song, D. T. Felson, S. Cahue, E. Shamiyeh, and D. D. Dunlop, "The role of knee alignment in disease progression and functional decline in knee osteoarthritis.," *JAMA*, vol. 286, pp. 188–195, 2001.
- [51] D. T. Felson, "Weight and osteoarthritis," in *Journal of Rheumatology*, 1995, vol. 22, pp. 7–9.
- [52] D. T. Felson and C. E. Chaisson, "Understanding the relationship between body weight and osteoarthritis.," *Baillieres. Clin. Rheumatol.*, vol. 11, pp. 671–81, 1997.
- [53] J. A. Buckwalter and T. D. Brown, "Joint injury, repair, and remodeling: roles in post-traumatic osteoarthritis.," *Clin. Orthop. Relat. Res.*, pp. 7–16, 2004.
- [54] T. J. Wang, B. Belza, F. Elaine Thompson, J. D. Whitney, and K. Bennett, "Effects of aquatic exercise on flexibility, strength and aerobic fitness in adults with osteoarthritis of the hip or knee," *J. Adv. Nurs.*, vol. 57, pp. 141–152, 2007.
- [55] K. H. Pridie, "A method of resurfacing osteoarthritic knee joints," *J. Bone Jt. Surg.*, vol. 41, pp. 618–619, 1959.
- [56] M. Brittberg, A. Lindahl, A. Nilsson, C. Ohlsson, O. Isaksson, and L. Peterson, "Treatment of deep cartilage defects in the knee with autologous chondrocyte transplantation.," *N. Engl. J. Med.*, vol. 331, pp. 889–895, 1994.
- [57] L. Hangody and P. Füles, "Autologous osteochondral mosaicplasty for the treatment of full-thickness defects of weight-bearing joints: ten years of experimental and clinical experience.," *J. Bone Joint Surg. Am.*, vol. 85-A Suppl, pp. 25–32, 2003.
- [58] J. Kellgren and J. Lawrence, "Radiological assessment of osteoarthritis," *Ann. Rheum. Dis.*, vol. 16, p. 494, 1957.
- [59] S. A. Mazzuca, K. D. Brandt, K. A. Lane, and B. P. Katz, "Knee pain reduces joint space width in conventional standing anteroposterior radiographs of osteoarthritic knees," *Arthritis Rheum.*, vol. 46, pp. 1223–1227, 2002.
- [60] W. P. Chan, P. Lang, M. P. Stevens, K. Sack, S. Majumdar, D. W. Stoller, C. Basch, and H. K. Genant, "Osteoarthritis of the knee: Comparison of radiography, CT, and MR imaging to assess extent and severity," *Am. J. Roentgenol.*, vol. 157, pp. 799–806, 1991.
- [61] E. B. Y. The and O. Of, "Histological Assessment of Cartilage Repair," 2014.

- [62] G. Spahn, H. M. Klinger, and G. O. Hofmann, "How valid is the arthroscopic diagnosis of cartilage lesions? Results of an opinion survey among highly experienced arthroscopic surgeons," *Arch. Orthop. Trauma Surg.*, vol. 129, pp. 1117–1121, 2009.
- [63] G. Spahn, H. M. Klinger, M. Baums, U. Pinkepank, and G. O. Hofmann, "Reliability in arthroscopic grading of cartilage lesions: Results of a prospective blinded study for evaluation of inter-observer reliability," *Arch. Orthop. Trauma Surg.*, vol. 131, pp. 377–381, 2011.
- [64] D. T. Felson, J. Lynch, A. Guermazi, F. W. Roemer, J. Niu, T. McAlindon, and M. C. Nevitt, "Comparison of BLOKS and WOMBS scoring systems part II. Longitudinal assessment of knee MRIs for osteoarthritis and suggested approach based on their performance: Data from the Osteoarthritis Initiative," *Osteoarthr. Cartil.*, vol. 18, no. 11, pp. 1402–1407, 2010.
- [65] A. Guermazi, F. W. Roemer, I. K. Haugen, M. D. Crema, and D. Hayashi, "MRI-based semiquantitative scoring of joint pathology in osteoarthritis," *Nat. Rev. Rheumatol.*, vol. 9, no. 4, pp. 236–51, 2013.
- [66] D. J. Hunter, G. H. Lo, D. Gale, a J. Grainger, a Guermazi, and P. G. Conaghan, "The reliability of a new scoring system for knee osteoarthritis MRI and the validity of bone marrow lesion assessment: BLOKS (Boston Leeds Osteoarthritis Knee Score)," *Ann. Rheum. Dis.*, vol. 67, no. 2, pp. 206–211, 2008.
- [67] D. Burstein and M. Gray, "New MRI techniques for imaging cartilage," *J. Bone Joint Surg. Am.*, vol. 85-A Suppl 2, pp. 70–77, 2003.
- [68] T. C. Dunn, Y. Lu, H. Jin, M. D. Ries, and S. Majumdar, "Radiology T2 Relaxation Time of Cartilage at MR Imaging :," no. 7, 2004.
- [69] T. C. Mamisch, T. Hughes, T. J. Mosher, C. Mueller, S. Trattng, C. Boesch, and G. H. Welsch, "T2 star relaxation times for assessment of articular cartilage at 3 T: a feasibility study," *Skeletal Radiol.*, vol. 41, no. 3, pp. 287–92, Mar. 2012.
- [70] Z. V. Maizlin, J. J. Clement, W. B. Patola, D. M. Fenton, J. H. Gillies, P. M. Vos, and J. a. Jacobson, "T2 mapping of articular cartilage of glenohumeral joint with routine MRI correlation--initial experience," *HSS J.*, vol. 5, no. 1, pp. 61–6, Feb. 2009.
- [71] L. M. White, M. S. Sussman, M. Hurtig, L. Probyn, and G. Tomlinson, "Cartilage T2 Assessment : Differentiation of Normal Hyaline Cartilage and Reparative Tissue after Arthroscopic Cartilage Repair in Equine Methods : Results : Conclusion :," vol. 241, no. 2, pp. 407–414, 2006.
- [72] R. R. Regatte, S. V. S. Akella, J. H. Lonner, J. B. Kneeland, and R. Reddy, "T1?? mapping in human osteoarthritis (OA) cartilage: Comparison of T1?? with T2," *J. Magn. Reson. Imaging*, vol. 23, no. 4, pp. 547–553, 2006.
- [73] R. Stahl, A. Luke, X. Li, J. Carballido-Gamio, C. B. Ma, S. Majumdar, and T. M. Link, "T1rho, T2 and focal knee cartilage abnormalities in physically active and sedentary healthy subjects versus early OA patients--a 3.0-Tesla MRI study," *Eur. Radiol.*, vol. 19, no. 1, pp. 132–43, Jan. 2009.
- [74] L. Wang, G. Chang, J. Xu, R. L. R. Vieira, S. Krasnokutsky, S. Abramson, and R. R. Regatte, "T1rho MRI of menisci and cartilage in patients with osteoarthritis at 3T," *Eur. J. Radiol.*, vol. 81, no. 9, pp. 2329–2336, 2012.
- [75] A. Bashir, M. L. Gray, J. Hartke, and D. Burstein, "Nondestructive imaging of human cartilage glycosaminoglycan concentration by MRI," *Magn. Reson. Med.*, vol. 41, pp. 857–865, 1999.

- [76] E. M. Shapiro, A. Borthakur, A. Gougoutas, and R. Reddy, "23Na MRI accurately measures fixed charge density in articular cartilage," *Magn. Reson. Med.*, vol. 47, no. 2, pp. 284–291, 2002.
- [77] A. Borthakur, E. M. Shapiro, J. Beers, S. Kudchodkar, J. B. Kneeland, and R. Reddy, "Sensitivity of MRI to proteoglycan depletion in cartilage: Comparison of sodium and proton MRI," *Osteoarthr. Cartil.*, vol. 8, no. 4, pp. 288–293, 2000.
- [78] M. T. Nieminen, J. Rieppo, J. Silvennoinen, J. Töyräs, J. M. Hakumäki, M. M. Hyttinen, H. J. Helminen, and J. S. Jurvelin, "Spatial assessment of articular cartilage proteoglycans with Gd-DTPA-enhanced T1 imaging," *Magn. Reson. Med.*, vol. 48, pp. 640–648, 2002.
- [79] R. G. Allen, D. Burstein, and M. L. Gray, "Monitoring glycosaminoglycan replenishment in cartilage explants with gadolinium-enhanced magnetic resonance imaging," *J. Orthop. Res.*, vol. 17, no. 3, pp. 430–436, 1999.
- [80] E. Lammentausta, P. Kiviranta, M. J. Nissi, M. S. Laasanen, I. Kiviranta, M. T. Nieminen, and J. S. Jurvelin, "Estimation of mechanical properties of articular cartilage with MRI and dGEMRIC, T2 and T1 imaging in different species with variable stages of maturation," no. March, pp. 366–374, 2006.
- [81] M. J. Nissi, J. Rieppo, J. Töyräs, M. S. Laasanen, I. Kiviranta, M. T. Nieminen, and J. S. Jurvelin, "Estimation of mechanical properties of articular cartilage with MRI and dGEMRIC, T2 and T1 imaging in different species with variable stages of maturation," *Osteoarthritis Cartilage*, vol. 15, no. 10, pp. 1141–8, Oct. 2007.
- [82] M. De Filippo, A. Bertellini, F. Pogliacomi, N. Sverzellati, D. Corradi, G. Garlaschi, and M. Zompatori, "Multidetector computed tomography arthrography of the knee: Diagnostic accuracy and indications," *Eur. J. Radiol.*, vol. 70, no. 2, pp. 342–351, 2009.
- [83] J. A. Gagliardi, E. M. Chung, V. P. Chandnani, K. L. Kesling, K. P. Christensen, R. N. Null, M. G. Radvany, and M. F. Hansen, "Detection and staging of chondromalacia patellae: Relative efficacies of conventional MR imaging, MR arthrography, and CT arthrography," *Am. J. Roentgenol.*, vol. 163, no. 3, pp. 629–636, 1994.
- [84] F. E. Lecouvet, B. Dorzée, J. E. Dubuc, B. C. Vande Berg, J. Jamart, and J. Malghem, "Cartilage lesions of the glenohumeral joint: Diagnostic effectiveness of multidetector spiral CT arthrography and comparison with arthroscopy," *Eur. Radiol.*, vol. 17, no. 7, pp. 1763–1771, 2007.
- [85] M. D. Cockman, C. a Blanton, P. a Chmielewski, L. Dong, T. E. Dufresne, E. B. Hookfin, M. J. Karb, S. Liu, and K. R. Wehmeyer, "Quantitative imaging of proteoglycan in cartilage using a gadolinium probe and microCT," *Osteoarthritis Cartilage*, vol. 14, no. 3, pp. 210–4, Mar. 2006.
- [86] A. W. Palmer, R. E. Gulberg, and M. E. Levenston, "Analysis of cartilage matrix fixed charge density and three-dimensional morphology via contrast-enhanced microcomputed tomography," *Proc. Natl. Acad. Sci. U. S. A.*, vol. 103, pp. 19255–19260, 2006.
- [87] H. O. Stolberg and B. L. McClennan, "Ionic versus nonionic contrast use," *Current Problems in Diagnostic Radiology*, vol. 20, p. 49, 1991.
- [88] P. N. Bansal, N. S. Joshi, V. Entezari, M. W. Grinstaff, and B. D. Snyder, "Contrast Enhanced Computed Tomography can predict the glycosaminoglycan content and biomechanical properties of articular cartilage," *Osteoarthr. Cartil.*, vol. 18, pp. 184–191, 2010.

- [89] A. S. Kallioniemi, J. S. Jurvelin, M. T. Nieminen, M. J. Lammi, and J. Töyräs, “Contrast agent enhanced pQCT of articular cartilage,” *Phys. Med. Biol.*, vol. 52, pp. 1209–1219, 2007.
- [90] T. S. Silvast, J. S. Jurvelin, A. S. Aula, M. J. Lammi, and J. Töyräs, “Contrast agent-enhanced computed tomography of articular cartilage: association with tissue composition and properties,” *Acta radiol.*, vol. 50, pp. 78–85, 2009.
- [91] L. Xie, A. S. P. Lin, R. E. Guldborg, and M. E. Levenston, “Nondestructive assessment of sGAG content and distribution in normal and degraded rat articular cartilage via EPIC-CT,” *Osteoarthr. Cartil.*, vol. 18, pp. 65–72, 2010.
- [92] T. S. Silvast, J. S. Jurvelin, M. J. Lammi, and J. Töyräs, “pQCT study on diffusion and equilibrium distribution of iodinated anionic contrast agent in human articular cartilage--associations to matrix composition and integrity,” *Osteoarthritis Cartilage*, vol. 17, pp. 26–32, 2009.
- [93] H. T. Kokkonen, J. S. Jurvelin, V. Tiitu, and J. Töyräs, “Detection of mechanical injury of articular cartilage using contrast enhanced computed tomography,” *Osteoarthritis Cartilage*, vol. 19, pp. 295–301, 2011.
- [94] T. M. Piscaer, G. J. V. M. van Osch, J. A. N. Verhaar, and H. Weinans, “Imaging of experimental osteoarthritis in small animal models,” *Biorheology*, vol. 45, pp. 355–364, 2008.
- [95] M. Siebelt, J. H. Waarsing, N. Kops, T. M. Piscaer, J. A. N. Verhaar, E. H. G. Oei, and H. Weinans, “Quantifying osteoarthritic cartilage changes accurately using in vivo microCT arthrography in three etiologically distinct rat models,” *J. Orthop. Res.*, vol. 29, pp. 1788–1794, 2011.
- [96] T. M. Piscaer, J. H. Waarsing, N. Kops, P. Pavljasevic, J. A. N. Verhaar, G. J. V. M. van Osch, and H. Weinans, “In vivo imaging of cartilage degeneration using microCT-arthrography,” *Osteoarthritis Cartilage*, vol. 16, pp. 1011–1017, 2008.
- [97] J. Van Tiel, M. Siebelt, J. H. Waarsing, T. M. Piscaer, M. Van Straten, R. Booij, M. L. Dijkshoorn, G. J. Kleinrensink, J. A. N. Verhaar, G. P. Krestin, H. Weinans, and E. H. G. Oei, “CT arthrography of the human knee to measure cartilage quality with low radiation dose,” *Osteoarthr. Cartil.*, vol. 20, pp. 678–685, 2012.
- [98] M. Siebelt, J. van Tiel, J. H. Waarsing, T. M. Piscaer, M. van Straten, R. Booij, M. L. Dijkshoorn, G. J. Kleinrensink, J. A. N. Verhaar, G. P. Krestin, H. Weinans, and E. H. G. Oei, “Clinically applied CT arthrography to measure the sulphated glycosaminoglycan content of cartilage,” *Osteoarthr. Cartil.*, vol. 19, pp. 1183–1189, 2011.
- [99] H. T. Kokkonen, J.-S. Suomalainen, A. Joukainen, H. Kröger, J. Sirola, J. S. Jurvelin, J. Salo, and J. Töyräs, “In vivo diagnostics of human knee cartilage lesions using delayed CBCT arthrography,” *J. Orthop. Res.*, vol. 32, pp. 403–412, 2014.
- [100] P. N. Bansal, N. S. Joshi, V. Entezari, B. C. Malone, R. C. Stewart, B. D. Snyder, and M. W. Grinstaff, “Cationic contrast agents improve quantification of glycosaminoglycan (GAG) content by contrast enhanced CT imaging of cartilage,” *J. Orthop. Res.*, vol. 29, pp. 704–709, 2011.
- [101] A. S. Aula, J. S. Jurvelin, and J. Töyräs, “Simultaneous computed tomography of articular cartilage and subchondral bone,” *Osteoarthr. Cartil.*, vol. 17, pp. 1583–1588, 2009.
- [102] B. a Lakin, D. J. Grasso, S. S. Shah, R. C. Stewart, P. N. Bansal, J. D. Freedman, M. W. Grinstaff, and B. D. Snyder, “Cationic agent contrast-enhanced computed tomography imaging of cartilage correlates with the compressive modulus and coefficient of friction,” *Osteoarthritis Cartilage*, vol. 21, no. 1, pp. 60–68, Jan. 2013.

- [103] K. M. Clements, Z. C. Bee, G. V. Crossingham, M. A. Adams, and M. Sharif, "How severe must repetitive loading be to kill chondrocytes in articular cartilage?," *Osteoarthr. Cartil.*, vol. 9, no. 5, pp. 499–507, 2001.
- [104] A. Thambyah, J. C. H. Goh, and S. Das De, "Contact stresses in the knee joint in deep flexion," *Med. Eng. Phys.*, vol. 27, no. 4, pp. 329–335, 2005.
- [105] S. Umeyama, "Least-squares estimation of transformation parameters between two point patterns," *IEEE Trans. Pattern Anal. Mach. Intell.*, vol. 13, no. 4, pp. 376–380, 1991.
- [106] T. Lyyra, I. Kiviranta, U. Väättäinen, H. J. Helminen, and J. S. Jurvelin, "In vivo characterization of indentation stiffness of articular cartilage in the normal human knee," *J. Biomed. Mater. Res.*, vol. 48, no. 4, pp. 482–487, 1999.
- [107] T. Franz, E. M. Hasler, R. Hagg, C. Weiler, R. P. Jakob, and P. Mainil-Varlet, "In situ compressive stiffness, biochemical composition, and structural integrity of articular cartilage of the human knee joint," *Osteoarthr. Cartil.*, vol. 9, pp. 582–592, 2001.
- [108] E. Lammentausta, P. Kiviranta, M. J. Nissi, M. S. Laasanen, I. Kiviranta, M. T. Nieminen, and J. S. Jurvelin, "T2 relaxation time and delayed gadolinium-enhanced MRI of cartilage (dGEMRIC) of human patellar cartilage at 1.5 T and 9.4 T: Relationships with tissue mechanical properties," *J. Orthop. Res.*, vol. 24, pp. 366–374, 2006.
- [109] M. T. Nieminen, J. Töyräs, M. S. Laasanen, J. Silvennoinen, H. J. Helminen, and J. S. Jurvelin, "Prediction of biomechanical properties of articular cartilage with quantitative magnetic resonance imaging," *J. Biomech.*, vol. 37, no. 3, pp. 321–328, Mar. 2004.
- [110] M. I. Froimson, A. Ratcliffe, T. R. Gardner, and V. C. Mow, "Differences in patellofemoral joint cartilage material properties and their significance to the etiology of cartilage surface fibrillation.," *Osteoarthritis Cartilage*, vol. 5, no. 6, pp. 377–386, 1997.
- [111] J. E. Kurkijarvi, M. J. Nissi, I. Kiviranta, J. S. Jurvelin, and M. T. Nieminen, "Delayed gadolinium-enhanced MRI of cartilage (dGEMRIC) and T2 characteristics of human knee articular cartilage: Topographical variation and relationships to mechanical properties," *Magn. Reson. Med.*, vol. 52, pp. 41–46, 2004.
- [112] M. T. Nieminen, N. M. Menezes, A. Williams, and D. Burstein, "T2 of articular cartilage in the presence of Gd-DTPA2-," *Magn. Reson. Med.*, vol. 51, no. 6, pp. 1147–1152, 2004.
- [113] J. T. Samosky, "Spatially-Localized Correlation of MRI and Mechanical Stiffness To Assess Cartilage Integrity in the Human Tibial Plateau," p. 226, 2002.
- [114] W. C. Bae, M. M. Temple, D. Amiel, R. D. Coutts, G. G. Niederauer, and R. L. Sah, "Indentation Testing of Human Cartilage: Sensitivity to Articular Surface Degeneration," *Arthritis Rheum.*, vol. 48, no. 12, pp. 3382–3394, 2003.
- [115] F. Boschetti, G. Pennati, F. Gervaso, G. M. Peretti, and G. Dubini, "Biomechanical properties of human articular cartilage under compressive loads.," *Biorheology*, vol. 41, no. 3–4, pp. 159–66, Jan. 2004.
- [116] P. S. Donzelli, R. L. Spilker, G. A. Ateshian, and V. C. Mow, "Contact analysis of biphasic transversely isotropic cartilage layers and correlations with tissue failure," *J. Biomech.*, vol. 32, no. 10, pp. 1037–1047, 1999.

- [117] A. Watanabe, Y. Wada, T. Obata, T. Ueda, M. Tamura, H. Ikehira, and H. Moriya, "Delayed gadolinium-enhanced MR to determine glycosaminoglycan concentration in reparative cartilage after autologous chondrocyte implantation: preliminary results.," *Radiology*, vol. 239, pp. 201–208, 2006.
- [118] A. Williams, L. Sharma, C. a McKenzie, P. V Prasad, and D. Burstein, "Delayed gadolinium-enhanced magnetic resonance imaging of cartilage in knee osteoarthritis: findings at different radiographic stages of disease and relationship to malalignment.," *Arthritis Rheum.*, vol. 52, no. 11, pp. 3528–35, Nov. 2005.
- [119] J. D. Johnston, B. A. Masri, and D. R. Wilson, "Computed tomography topographic mapping of subchondral density (CT-TOMASD) in osteoarthritic and normal knees: methodological development and preliminary findings," *Osteoarthr. Cartil.*, vol. 17, pp. 1319–1326, 2009.
- [120] K. D. Brandt, E. L. Radin, and P. A. Dieppe, "Yet more evidence that osteoarthritis is not a cartilage disease."
- [121] C. Hulet, J. P. Sabatier, D. Souquet, B. Locker, C. Marcelli, and C. Vielpeau, "Distribution of bone mineral density at the proximal tibia in knee osteoarthritis," *Calcif. Tissue Int.*, vol. 71, no. 4, pp. 315–322, 2002.
- [122] M. Wada, Y. Maezawa, H. Baba, S. Shimada, S. Sasaki, and Y. Nose, "Relationships among bone mineral densities, static alignment and dynamic load in patients with medial compartment knee osteoarthritis.," *Rheumatology (Oxford)*, vol. 40, no. 5, pp. 499–505, 2001.
- [123] C. Hoemann, R. Kandel, S. Roberts, D. B. F. Saris, L. Creemers, P. Mainil-Varlet, S. Methot, A. P. Hollander, and M. D. Buschmann, "International Cartilage Repair Society (ICRS) Recommended Guidelines for Histological Endpoints for Cartilage Repair Studies in Animal Models and Clinical Trials," *Cartilage*, vol. 2, no. 2, pp. 153–172, 2011.
- [124] D. A. Narmoneva, J. Y. Wang, and L. A. Setton, "Nonuniform swelling-induced residual strains in articular cartilage," *J. Biomech.*, vol. 32, no. 4, pp. 401–408, 1999.
- [125] L. Setton, W. ~Y. Gu, W. ~M. Lai, and V. ~C. Mow, "Predictions of the swelling induced pre-stress in articular cartilage," *Mech. Poroelastic Media*, pp. 299–322, 1995.
- [126] X. Li, J. Cheng, K. Lin, E. Saadat, R. I. Bolbos, B. Jobke, M. D. Ries, A. Horvai, T. M. Link, and S. Majumdar, "Quantitative MRI using T1 ρ and T2 in human osteoarthritic cartilage specimens: Correlation with biochemical measurements and histology," *Magn. Reson. Imaging*, vol. 29, no. 3, pp. 324–334, 2011.
- [127] M. T. Nieminen, J. Rieppo, J. Töyräs, J. M. Hakumäki, J. Silvennoinen, M. M. Hyttinen, H. J. Helminen, and J. S. Jurvelin, "T2 relaxation reveals spatial collagen architecture in articular cartilage: A comparative quantitative MRI and polarized light microscopic study," *Magn. Reson. Med.*, vol. 46, no. 3, pp. 487–493, 2001.
- [128] M. Uhl, C. Ihling, K. H. Allmann, J. Laubenberger, U. Tauer, C. P. Adler, and M. Langer, "Human articular cartilage: in vitro correlation of MRI and histologic findings.," *Eur. Radiol.*, vol. 8, no. 7, pp. 1123–1129, 1998.
- [129] O. S. Schindler, "Current concepts of articular cartilage repair," *Acta Orthopaedica Belgica*, vol. 77, no. 6, pp. 709–726, 2011.
- [130] L. Sharma, "Local factors in osteoarthritis.," *Curr. Opin. Rheumatol.*, vol. 13, no. 5, pp. 441–446, 2001.

- [131] V. Entezari, P. N. Bansal, R. C. Stewart, B. a Lakin, M. W. Grinstaff, and B. D. Snyder, "Effect of mechanical convection on the partitioning of an anionic iodinated contrast agent in intact patellar cartilage," *J. Orthop. Res.*, vol. 32, no. October, pp. 1333–1340, 2014.
- [132] K. A. Athanasiou, M. P. Rosenwasser, J. A. Buckwalter, T. I. Malinin, and V. C. Mow, "Interspecies comparisons of in situ intrinsic mechanical properties of distal femoral cartilage," *J. Orthop. Res.*, vol. 9, pp. 330–340, 1991.
- [133] G. E. Kempson, C. J. Spivey, S. A. Swanson, and M. A. Freeman, "Patterns of cartilage stiffness on normal and degenerate human femoral heads.," *J. Biomech.*, vol. 4, pp. 597–609, 1971.
- [134] S. Elmore and L. Sokoloff, "Nature of 'imperfect' elasticity of articular cartilage," *J. Appl. ...*, vol. 18, no. 2, pp. 393–396, 1963.
- [135] A. Changoor, L. Fereydoonzad, A. Yaroshinsky, and M. D. Buschmann, "Effects of refrigeration and freezing on the electromechanical and biomechanical properties of articular cartilage.," *J. Biomech. Eng.*, vol. 132, p. 064502, 2010.
- [136] S. Knecht, B. Vanwanseele, and E. Stüssi, "A review on the mechanical quality of articular cartilage - Implications for the diagnosis of osteoarthritis," *Clin. Biomech.*, vol. 21, no. 10, pp. 999–1012, 2006.

Appendices

Appendix A: Validation of the Time Required for CA4+ Cationic Contrast agent to Reach Equilibrium the Cartilage Layer of an Intact Human Distal Femur Joint Surface

A-1- Introduction

The objective of the present study was to explore the diffusion behavior of a novel cationic agent (CA4+) in intact human femoral cartilage. The immersion time required for complete diffusion of contrast agent in cartilage varies with the type (size, geometry) of cartilage and the testing regimen (type of contrast agent, loading, temperature). Previous studies investigated the diffusion behavior of contrast agents in cartilage plugs [1],[2],[3], in which the diffusion into the cartilage is possible through joint surfaces and the cut sides of the cartilage. This is not directly applicable in intact joints because contrast agents can diffuse only through the articular surface. Our specific aims were to determine: 1) The required time for the cationic contrast agent to fully diffuse into the superficial and deep cartilage, 2) Changes in the distribution profile of the contrast agent across the surface and along the cartilage thickness with respect to time, and 3) Whether incomplete diffusion of contrast agent could be used to infer information regarding the relative distribution of the GAG and detect GAG-depleted areas.

A-2- Methods

A human cadaver right knee joint was disarticulated and the medial femoral condyle cartilage of this sample was used in this experiment. The sample exhibited articular surface without any evident cartilage disruption. Sequential images of the sample in the sagittal plane were taken using an XtremeCT (HR-pQCT) imaging system with an isotropic voxel size of 41 μm , 300 μAmp , and 120 kVp voltage. A baseline image was captured before the exposure of the sample to the contrast agent solution. The sample was then immersed in 60 ml of 12 mg/ml CA4+ solution, in which protease inhibitors were added to prevent degeneration during the course of the experiment. The sample was scanned at 3, 15, 22, 36, 42, 56, and 66 hours following immersion. Time of immersion is reported as the immersion time and the scanning time is not included.

Cartilage was segmented from the surrounding tissue in each image by using the image processing algorithm described in section 3.1. For qualitative analysis of diffusion, CECT attenuations were averaged in the superficial (0.6 mm from the surface) cartilage region and for the full depth of cartilage. The mean attenuation (in Hounsfield units) was then mapped to the articular surface (this procedure was described in section 3.1) to provide a GAG distribution map. 36 cylindrical regions of interest were defined in the specimen (Figure A.1). To study the contrast agent concentration in superficial cartilage, the diameter of the cylinders was 1mm and the depth was 0.6 mm. The depth was equal to cartilage thickness, and the diameter of the cylinders was 1mm, when the concentration of agents at full thickness was measured. The regions of interest can be considered as virtual cartilage plugs.

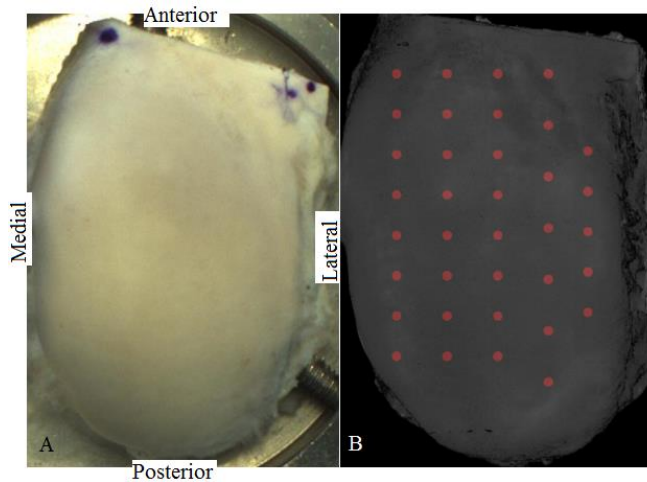


Figure A.1 Top view of the sample used for the diffusion experiment

(A) 36 cylindrical regions of interest (diameter= 1mm) were defined on the articular surface in the image. (B) The depth (starting from articular surface toward deep cartilage) was 0.6 mm when measuring contrast agent for superficial cartilage.

A-3- Results

The results of this experiment show that CECT attenuation changed for both superficial and full thickness cartilage with an exponential pattern (Figures A.2 and A.3 show the average attenuation in all regions of interest). This finding is consistent with the physics behind the diffusion behavior of ions (e.g contrast agent) in a semi-permeable environment (e.g cartilage [4]). Once exposed to the cartilage, contrast agent diffuses into the cartilage until a balance between ion concentration gradient and electrical gradient is reached and the net flow becomes zero (equilibrium state). The plateau phase of the exponential curve corresponds to this equilibrium state. We defined full equilibration as the state in which the mean CECT attenuation had reached 95% of the maximum mean CECT

attenuation (80-90% has been defined as the near-equilibrium state [5]). The data were modeled with the following equation:

$$\text{CECT attenuation (t)} = a \cdot (1 - \exp(-t/b))$$

(Equation 4 : CECT attenuation as a function of time during diffusion)

Where a is the maximum mean CECT attenuation, t is the immersion time, and b is the time constant (that) that is equal to the time required for reaching the 63% of full diffusion CECT attenuation.

Full equilibration of contrast agent into superficial and full-thickness cartilage took 16 and 44 hours, respectively.

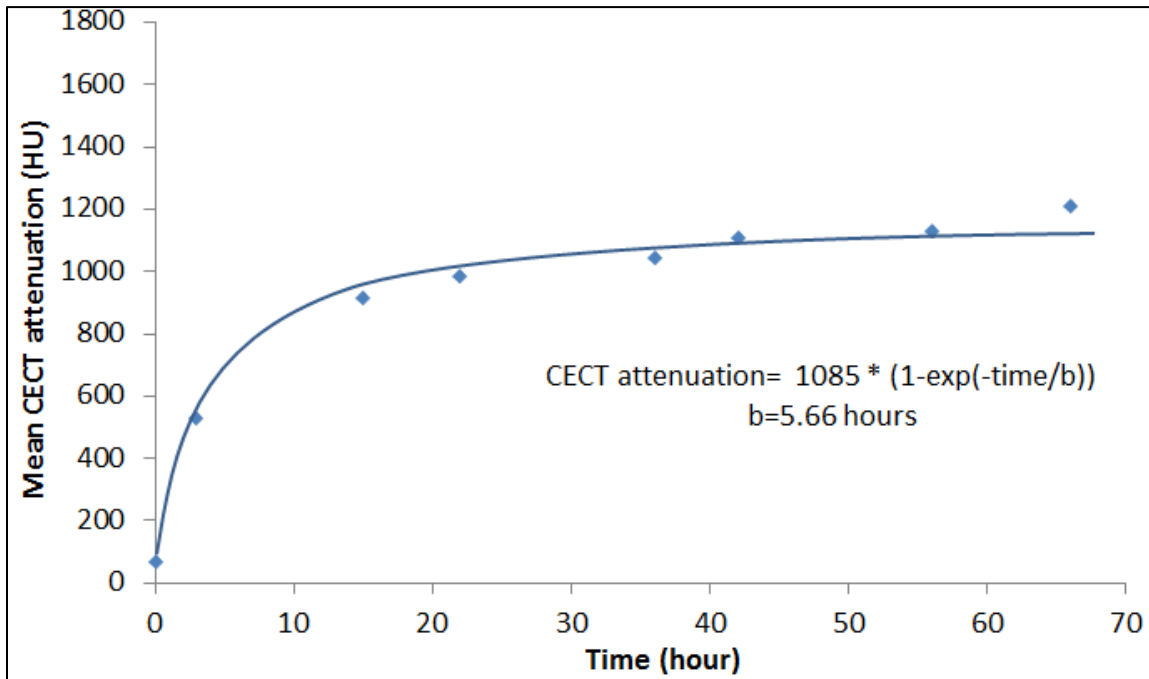


Figure A.2 Diffusion behavior of the cationic contrast agent (CA4+) into superficial human femoral cartilage.
The mean CECT attenuation in all regions of interest, reflecting the contrast agent concentration, in superficial cartilage (h=0.6mm) is plotted as a function of immersion time. The curve is fit by an exponential function in form of $a \cdot (1 - \exp(-t/b))$, where a is maximum attenuation, and b is time constant.

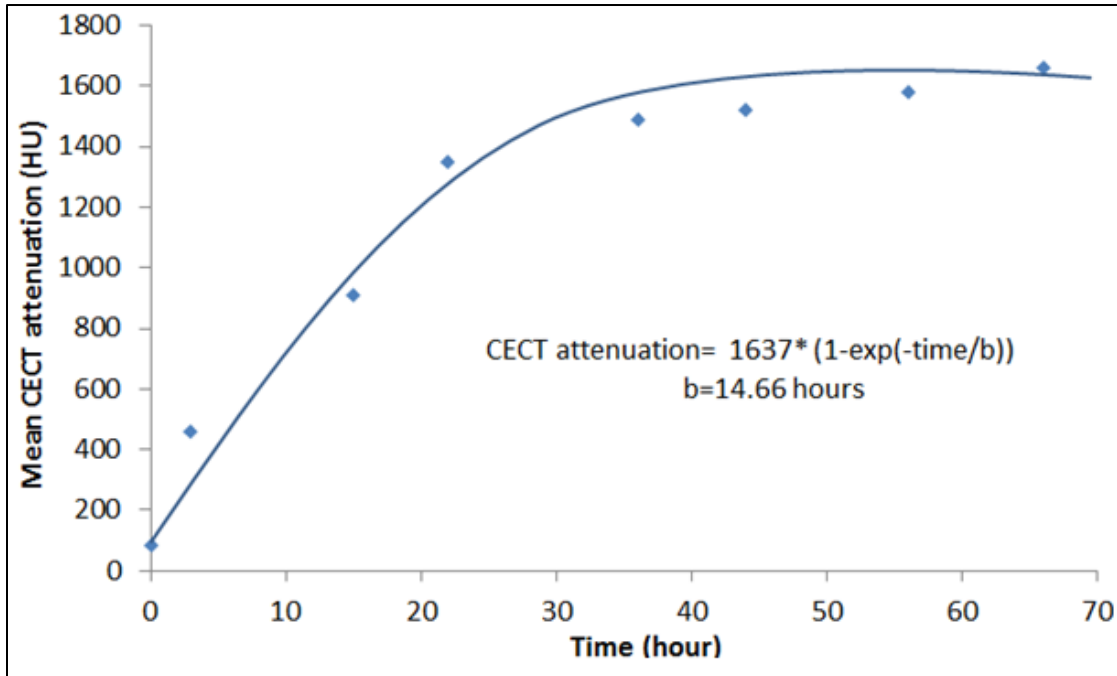


Figure A.3 Diffusion behavior of the cationic contrast agent (CA4+) into full-thickness human femoral cartilage.
The mean CECT attenuation in all regions of interest, reflecting the contrast agent concentration, in full depth cartilage is plotted as a function of immersion time. The curve is fit by an exponential function in form of $a(1-\exp(-\text{time}/b))$, where a is maximum attenuation, and b is time constant.*

In the superficial cartilage, the general pattern of attenuation was apparent before full equilibrium was reached (Figure A.4). After 3 hours of immersion, the topographical variation of contrast agent concentration in superficial cartilage had a relatively similar pattern to the equilibrium state. Except for the pre-contrast state, a general similarity in superficial contrast agent distribution maps could be seen at all time points.

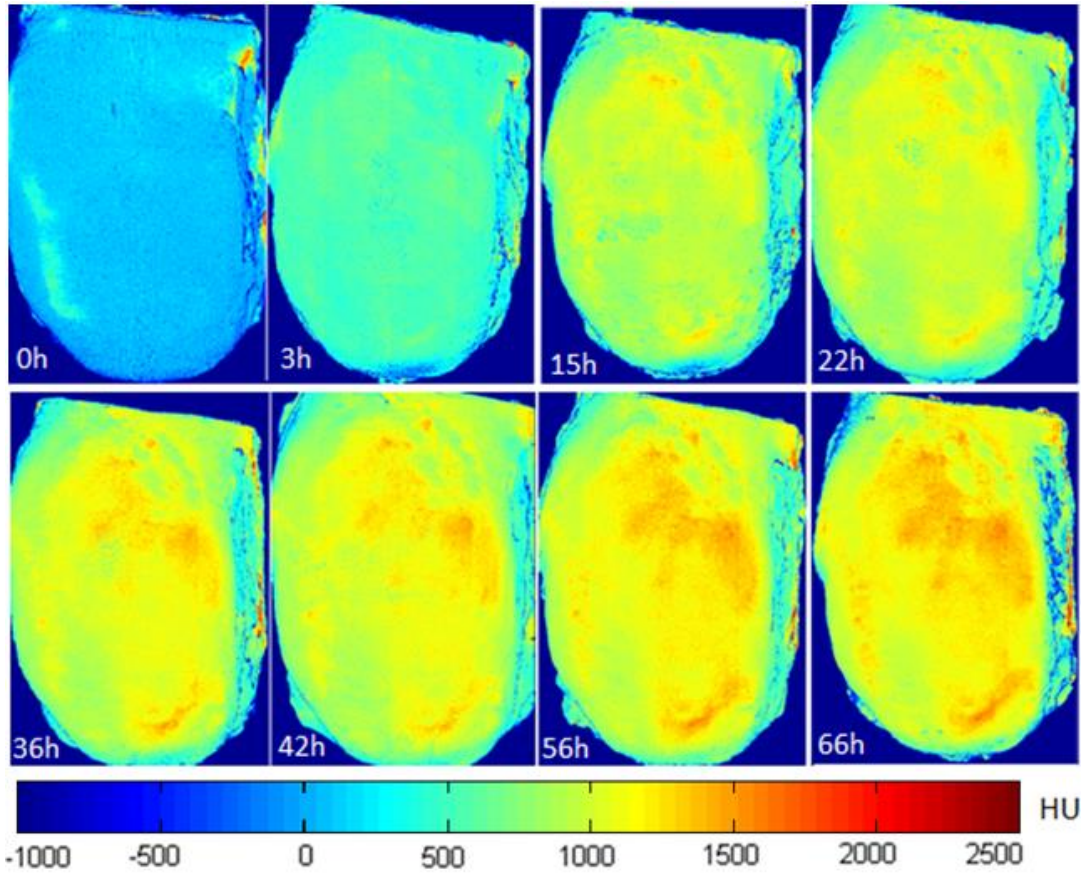


Figure A.4 Topographical maps of CECT attenuation, reflecting contrast agent concentration in superficial cartilage. The CECT attenuation is averaged over a depth of 0.6 mm relative to cartilage surface. The mean CECT attenuation for each sampled region is mapped into its corresponding location on the articular surface. Similar patterns of the contrast agent distribution profile were seen in all maps (except the map obtained in 0h).

In the full-depth cartilage maps, however, the general pattern of attenuation was only apparent after 22 hours of immersion (Figure A.5).

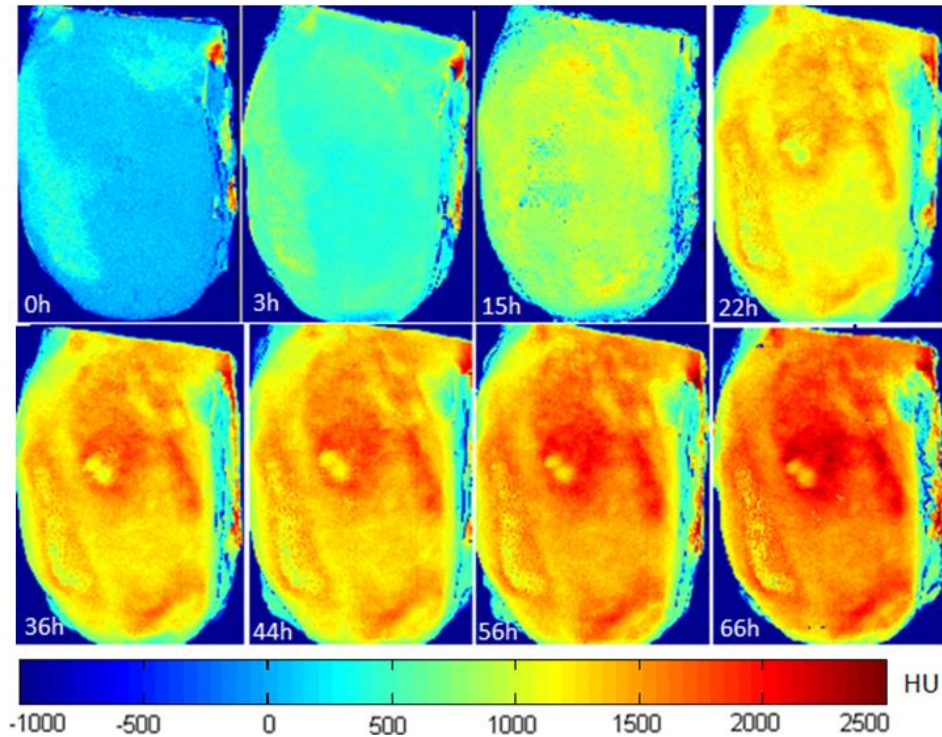


Figure A.5 Topographical maps of contrast agent concentration in full-depth cartilage. *The CECT attenuation is averaged over the articular cartilage thickness. The mean CECT attenuation for each sampled region is mapped into its corresponding location on the articular surface. Following 22 hours of immersion, similar patterns of contrast agent distribution profile were detectable.*

Quantitative analysis of the superficial contrast agent concentrations in 36 regions of interest showed a significant correlation ($p < 0.01$) with the equilibrium state for every time point after 3 hours of immersion (Table A.1, Figure A.6).

CECT attenuations were converted to contrast agent concentration using the mathematical model which was obtained from the phantom study. Figure 8 shows the concentration of the contrast agent in the cartilage as a function of the immersion time. The uptake of the contrast agent in the cartilage was more than 200% of the concentration in the immersion solution (12 mg/ml).

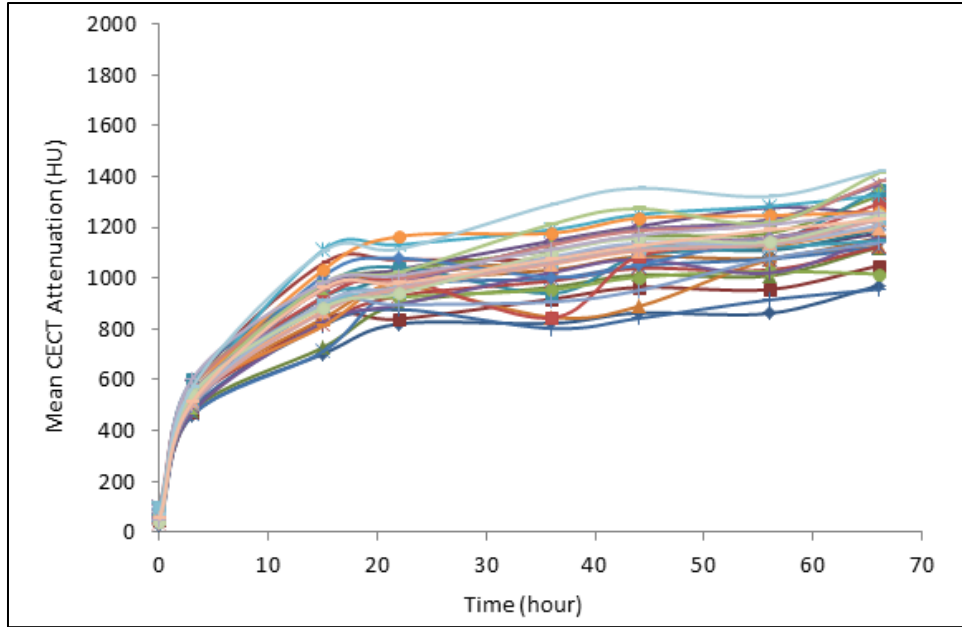


Figure A.6 Mean CECT attenuation of superficial cartilage in each region of interest plotted as a function of immersion time. Each line represents one region of interest. The curves follow similar trends.

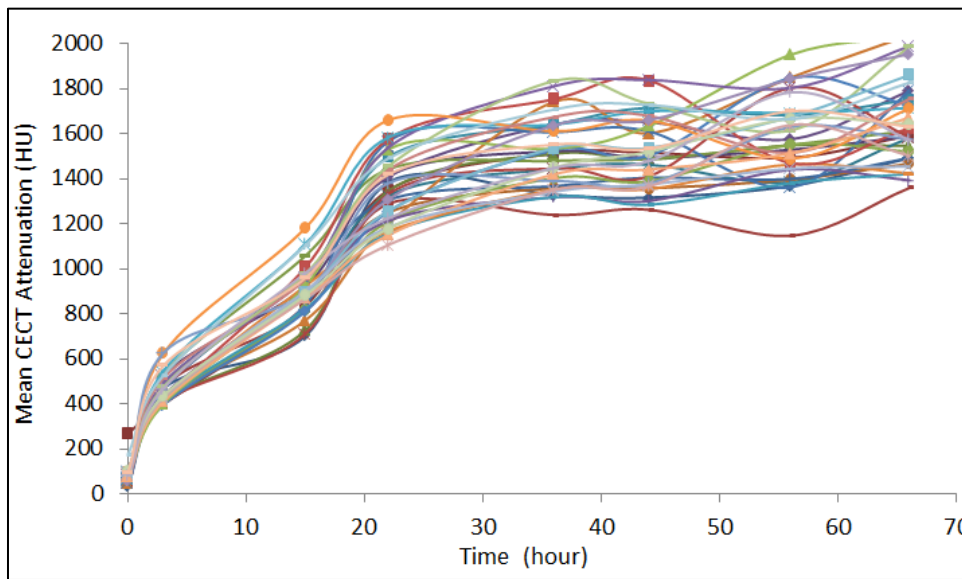


Figure A.7 Mean CECT attenuation of full-depth cartilage in each region of interest plotted as a function of immersion time. Each line represents one region of interest. The curves follow similar trends.

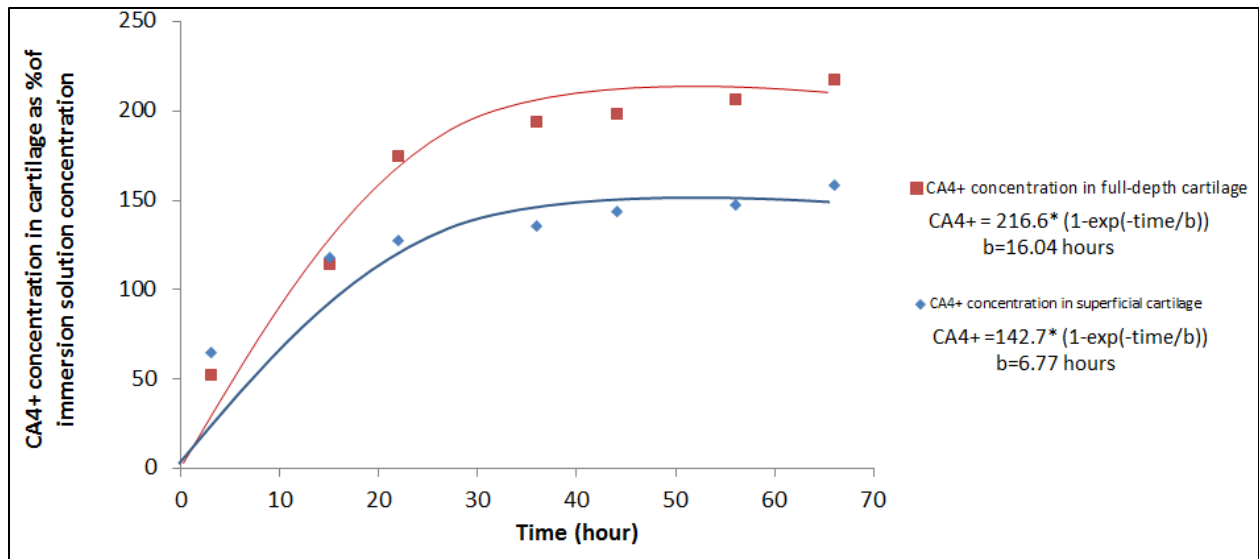


Figure A.8 CA4+ concentration in articular cartilage as a percentage of the immersion solution concentration, plotted as a function of immersion time.

The values of CA4+ attenuation are acquired by subtracting the CECT image from the baseline image at each time point. CA4+ attenuation was converted into CA4+ concentration using the linear model obtained from the phantom study. CA4+ concentration in cartilage reaches 216% and 142% of the immersion solution concentration in full-depth and superficial tissue, respectively.

Table A.1 The correlation coefficient between the pattern of GAG distribution at measured time points and the equilibrium state.

Immersion Time (hour)	0	3	15	22	36	44	56	66
Correlation of contrast agent distribution and the final post-contrast scan-66h(Comparison of mean CECT attenuations in superficial cartilage)	0.29	0.59	0.68	0.7	0.74	0.86	0.88	1
Correlation of contrast agent distribution and the final post-contrast scan (Comparison of mean CECT attenuations in full-depth cartilage)	0.09	0.05	0.24	0.45	0.83	0.79	0.68	1

In the baseline (unenhanced image), an increase in attenuation with depth from the surface could be seen, which reflects denser cartilage matrix in the deep zone (Figure A.9). In the second scan (3 hours of immersion), however, an opposite trend was observed and attenuation was highest in the superficial zone. An increasing trend of higher CECT attenuation in the deep cartilage was seen in the images after 15 hours of immersion (Figure A.9). The pattern of attenuation with depth from the

surface changed markedly with contrast enhancement (Figure A.10 represents the average of attenuation in all regions of interest with respect to depth).

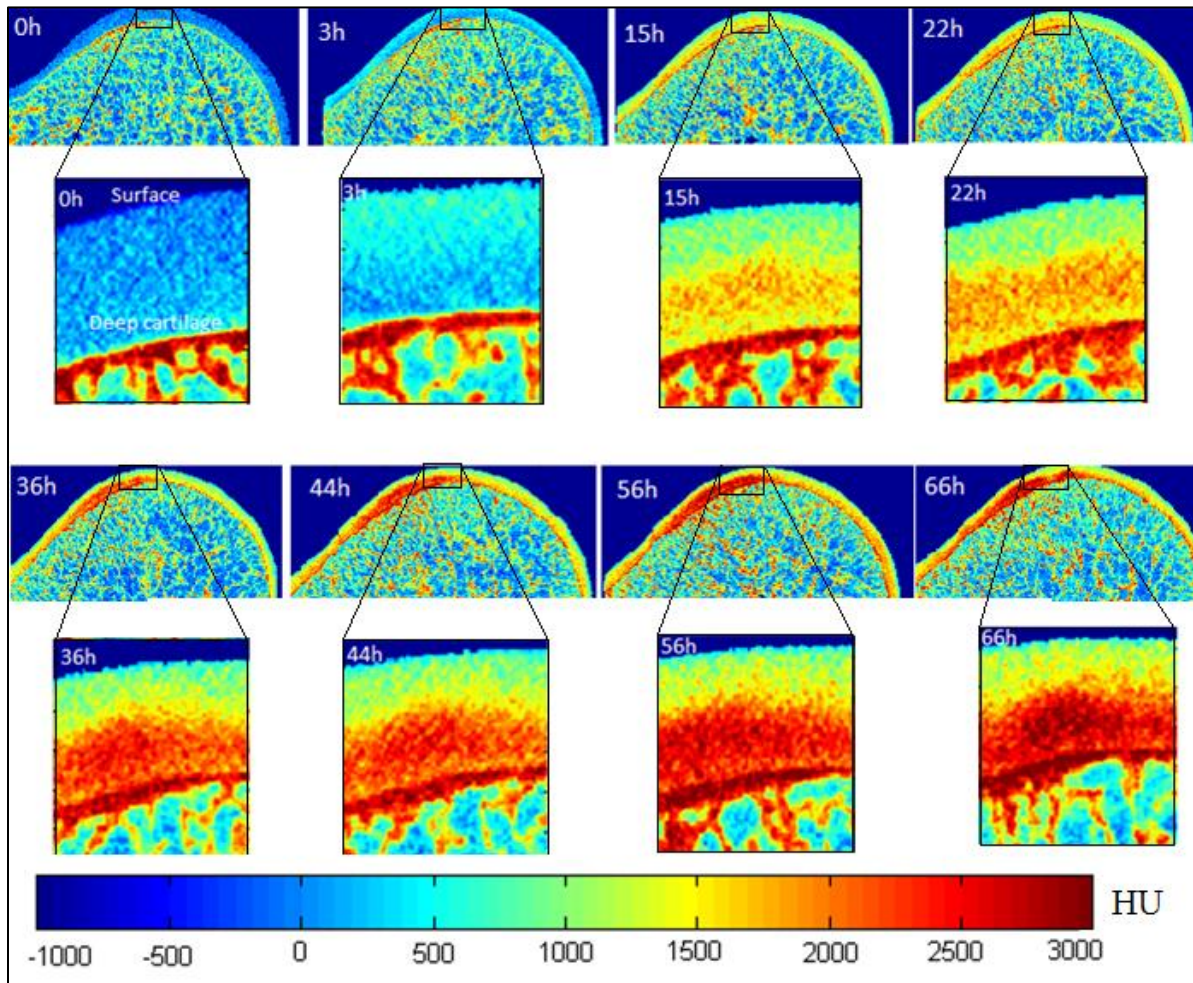


Figure A.9 Cross-sectional (sagittal plane) CECT images of the human medial femoral cartilage at different time points. Areas with higher attenuation (red) represent higher concentration of contrast agent and thus higher GAG content. The expected zonal variations in GAG concentration along cartilage thickness were observed in images taken after 15 hours of immersion

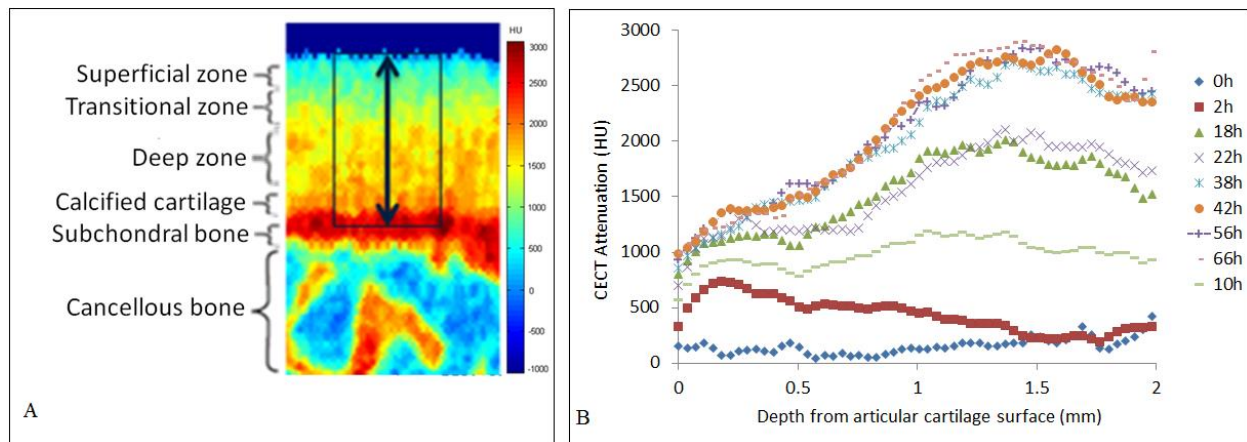


Figure A.10 Spatial contrast agent profiles along cartilage thickness as a function of immersion time (B). The Depth-wise GAG concentration (A) could be seen in CECT images.

A-4- Discussion

In this experiment the diffusion behavior and equilibrium distribution of a cationic contrast agent (CA4+) in human articular cartilage was investigated. The complete diffusion (95% equilibrium) of the cationic agent into the superficial and deep layers of the cartilage took 16 and 44 hours, respectively. The pattern of attenuation in the superficial cartilage was generally consistent with the equilibrium state at every time point after 3 hours of immersion. For full thickness cartilage, the pattern of attenuation was generally consistent with the equilibrium state at every time point after 22 hours of immersion. A depth-dependent profile of attenuation, consistent with the expected zonal variation of cartilage structure, was apparent at all scans (except the second scan (2h)).

The equilibration time we observed is consistent with previous findings suggesting that full equilibration in thick cartilage (2-4 mm) takes over 12 hours [1],[6]. It is difficult to compare our diffusion times directly to those found in previous studies because we tested an intact cartilage sample and the contrast agent diffusion was therefore only permitted through the cartilage surface, while cartilage plugs have been used in most diffusion studies. In cartilage plugs, diffusion occurs from all directions and may not be a representative of the *in vivo* situation. The rate of contrast agent diffusion in our experiment was comparable with that reported in a similar study [5], whereby diffusion of commercially available anionic contrast agents was investigated in bovine patellar cartilage plugs. In that study penetration was only allowed through cartilage surface using a custom-built sample holder, and reaching the near-equilibrium state took over 29 hours. It is noteworthy that a lower concentration of contrast agent was used in the present study (12 versus 26 mgI/ml), indicating that the use of a cationic contrast agent (e.g. CA4+) enables CECT imaging of the

cartilage at relatively lower concentration than use of an anionic contrast agent. Our finding of an uptake cationic contrast agent concentration in the cartilage that was approximately 250% of the concentration in the immersion solution is in the same range as the uptake ratio reported in CECT experiments using the same contrast agent [3].

We found that even incomplete diffusion of contrast agent can show the spatial variation of GAG distribution (as reflected in CECT attenuation) in cartilage. The GAG concentration profile across the cartilage surface in the first post-contrast image (3 hours) was significantly correlated ($r=0.64$ and $p<0.01$) with the profile in the final post-contrast image (66 hours). This suggests that even after a short immersion time, the relative distribution of contrast agent in the superficial layer reflects the regional variation of GAG and potentially detects regions with GAG depletion. This is consistent with the finding from the first in vivo CECT experiment [7], which showed that using an anionic contrast agent (Hexabrix320) with CECT imaging could improve the detection of cartilage surface lesions and surrounding areas with inferior quality a short time (5 and 45 minutes) after contrast agent was injected.

Our results show that CECT using CA4+ can image the depth-dependent properties of articular cartilage, but that sufficient time for contrast agent diffusion is essential. CECT attenuation increased with depth from the cartilage surface, which is in line with the known zonal structure of the articular cartilage (higher GAG concentration in deep cartilage). To observe the zonal variations the contrast agents need to diffuse into full depth of cartilage. The increase in the profile of CECT attenuation toward deep cartilage was not seen till 15 hours of immersion. In the first post-contrast scan (3 hours), the opposite profile was seen along the cartilage thickness as the contrast agents did not have enough time to diffuse into the deep cartilage and mostly accumulated in the superficial cartilage.

To the best of our knowledge, this is the first study that examined the diffusion behavior of a CT contrast agent in human cartilage samples. A key strength of this experiment is that we tested an intact surface of cartilage (as opposed to cartilage plugs). Our methods more closely resemble the in vivo situation, where the contrast agent is injected into to the joint space and diffusion happens through the articular surface. Another key strength of this experiment was that the use of the cationic contrast agent (CA4+) enabled us to enhance cartilage visualization with a relatively lower concentration of contrast agent compared to the range of concentration commonly used in CECT studies with anionic contrast agents (12 mgI/ml vs. 80-320 mgI/ml). CA4+ also had a faster rate of diffusion compared to its anionic counterparts, which makes it a potential candidate for application in

clinical settings where a shorter equilibrium time is desirable. A key limitation of this experiment was that only one sample was tested. Investigation in a larger sample size is warranted for a complete understanding of the diffusion behavior of CA4+ contrast agent and its potential application for *in vivo* studies.

A-References

- [1] T. S. Silvast, J. S. Jurvelin, M. J. Lammi, and J. Töyräs, “pQCT study on diffusion and equilibrium distribution of iodinated anionic contrast agent in human articular cartilage--associations to matrix composition and integrity.,” *Osteoarthritis Cartilage*, vol. 17, pp. 26–32, 2009.
- [2] P. N. Bansal, N. S. Joshi, V. Entezari, B. C. Malone, R. C. Stewart, B. D. Snyder, and M. W. Grinstaff, “Cationic contrast agents improve quantification of glycosaminoglycan (GAG) content by contrast enhanced CT imaging of cartilage,” *J. Orthop. Res.*, vol. 29, pp. 704–709, 2011.
- [3] R. C. Stewart, P. N. Bansal, V. Entezari, H. Lusic, R. M. Nazarian, B. D. Snyder, and M. W. Grinstaff, “Contrast-enhanced CT with a high-affinity cationic contrast agent for imaging ex vivo bovine, intact ex vivo rabbit, and in vivo rabbit cartilage.,” *Radiology*, vol. 266, pp. 141–50, 2013.
- [4] K. Nissinen, “Diffusion of X-ray contrast agents in intact and repaired articular cartilage”, PhD Thesis, University of Eastern Finland, 2013.
- [5] T. S. Silvast, H. T. Kokkonen, J. S. Jurvelin, T. M. Quinn, M. T. Nieminen, and J. Töyräs, “Diffusion and near-equilibrium distribution of MRI and CT contrast agents in articular cartilage.,” *Phys. Med. Biol.*, vol. 54, pp. 6823–6836, 2009.
- [6] A. S. Kallioniemi, J. S. Jurvelin, M. T. Nieminen, M. J. Lammi, and J. Töyräs, “Contrast agent enhanced pQCT of articular cartilage.,” *Phys. Med. Biol.*, vol. 52, pp. 1209–1219, 2007.
- [7] H. T. Kokkonen, J.-S. Suomalainen, A. Joukainen, H. Kröger, J. Sirola, J. S. Jurvelin, J. Salo, and J. Töyräs, “In vivo diagnostics of human knee cartilage lesions using delayed CBCT arthrography.,” *J. Orthop. Res.*, vol. 32, pp. 403–12, 2014.

Appendix B: Variation of Mean X-ray Attenuation with Changes in Contrast Agent Concentration

B-1-Introduction

In contrast-enhanced computed tomography of cartilage using CA4+, the positively-charged contrast agent molecules are attracted to negatively-charged GAG content within cartilage structure. At equilibrium, the concentration of CA4+ agents should provide a measure of the GAG content in the cartilage. Theoretically, due to the radiopaque properties of CA4+, changes in CA4+ concentration will change x-ray attenuation. However, the exact relationship between the concentration of CA4+ and the resulting x-ray attenuation must be established to ensure the accuracy with which GAG content is estimated from CECT images in our study. The objective of this experiment was to assess the variation of x-ray attenuation with changes in CA4+ concentration.

B-2-Method

A contrast phantom was made using 9 concentrations of CA4+ contrast agent diluted by Phosphate buffered saline (PBS). The contrast agent concentrations ranged from 0 to 40 mgI/mL. The phantom was scanned at an isotropic voxel resolution of 41 μm , 300 μAmp tube current, and 120 kVp voltage in an XtremeCT (HR-pQCT) imaging system (Figure B.1). A threshold-based segmentation method was used to segment the regions of interest corresponding to contrast agent solution. The mean x-ray attenuation value in Hounsfield unit (HU), was then measured for each tube.

B-3-Result

There was a strong and positive correlation between contrast agent concentration and CECT attenuations ($r^2=0.97$, $p<0.001$) (Figure B.2).

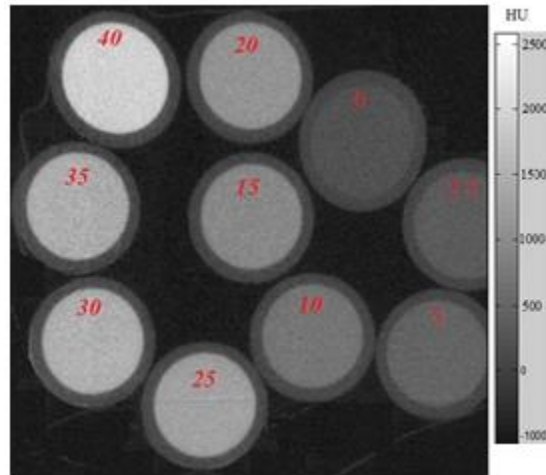


Figure B.1 Xtreme-CT image of phantom tubes with different levels of CA4+ concentration.
The red number indicates the concentration of contrast agent in the tube. The x-ray attenuation is reported in Hounsfield Units (HU).

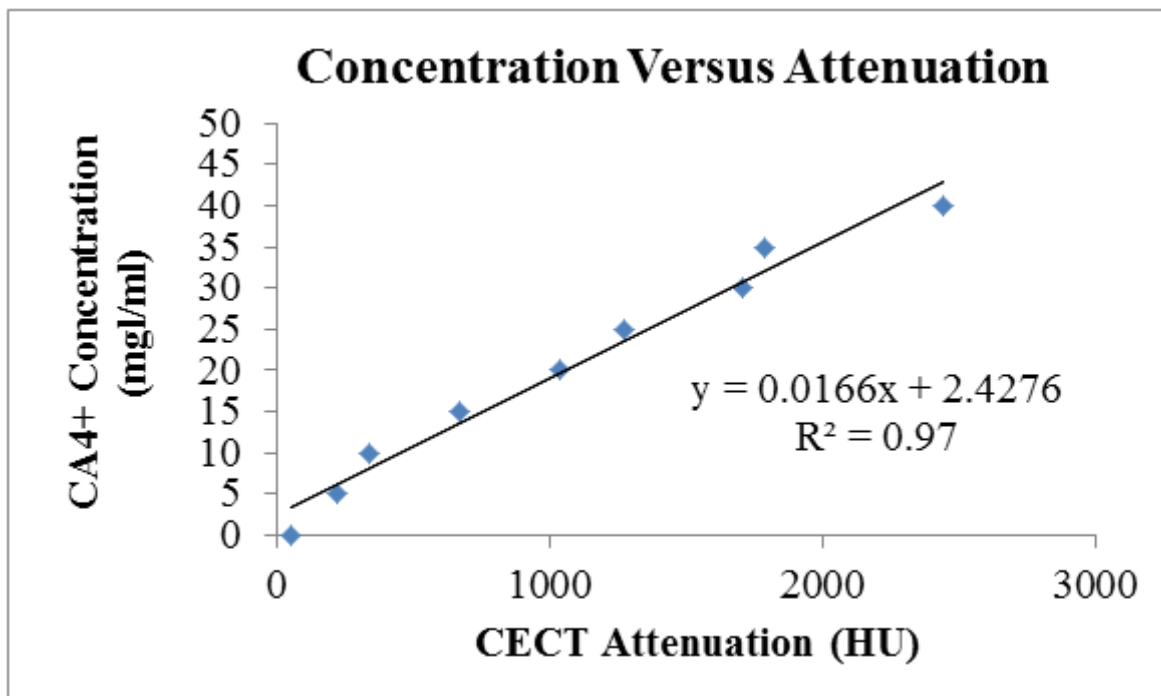


Figure B.2 Linear correlation between CA4+ concentration and observed x-ray attenuation in CECT scans. ($r=0.98$, $p<0.01$).

B-4-Discussion

It is helpful that the correlation between CA4+ concentration and x-ray attenuation is so strong because it permits estimation of contrast agent concentration (and thus GAG content) in cartilage directly from x-ray attenuations. In addition, knowing the relationship between CA4+ concentration

and x-ray attenuation is essential for determining the optimal concentration of CA4+ for enhancement of cartilage visualization. For instance, segmentation of cartilage from bone and synovial fluid is difficult, if the attenuation of bone and synovial fluid is close to the attenuation of cartilage. The positive correlation observed in our phantom study was expected, given that CA4+ contains Iodine which is a radiopaque material that absorbs x-ray. Therefore, higher concentrations of CA4+ contrast agent result in higher attenuation of x-ray and brighter regions in the image.

Appendix C: Repeatability of Instantaneous Stiffness Measures from Indentation Tests in Intact Human Distal Femur Cartilage

C-1-Introduction

Indentation testing is the method of choice for assessing cartilage stiffness. It is non-destructive and also can be done on intact joint surfaces. The repeatability of measured stiffness serves as an implicit confirmation of the repeatability of indenter positioning, normal surface detection, and the displacements of the stages as well as the load measurements. The objective of this experiment was to determine the repeatability of the indentation testing protocol used in this study.

C-2-Method

A human knee joint was disarticulated and all soft tissues except cartilage were carefully removed. The lateral femoral cartilage surface of the dissected joint was selected for testing because it exhibited areas with minimal cartilage disruption. A horizontal cut was made approximately 30 mm below the cartilage surface; a sagittal cut was then made to divide the distal femur into medial and lateral compartments. 16 testing locations were defined on the surface of the lateral compartment. Indentation testing to assess cartilage stiffness was then done as described in chapter 3. The measurements were repeated 6 times at each testing location; 3 measurements on the first day and 3 measurements on the second day. The inter-trial interval between measurements on the same day was about 1 hour. The sample was refrigerated at 4°C in a humid chamber between measurements to limit degeneration over the course of the experiment. The repeatability of indentation measurements was determined by computing the root mean square (RMS) average of the coefficient of variation (CV) in percentage.

C-3-Result

The coefficient of variation (CV) of the stiffness measurements ranged between 3% to 17%. The RMS average of the coefficients of variation was found to be nearly 8%. The details of the stiffness measurements in testing locations are illustrated in Table C.1 and Figure C.1.

Table C.1 Mean, SD, and CV of stiffness measurement for each testing location.

Testing location #	Mean (N/mm)	SD (N/mm)	CV (%)
1	18.94	0.61	3.23
2	10.47	0.47	4.53
3	6.18	0.51	8.30
4	5.66	0.46	8.21
5	7.49	0.38	5.16
6	4.10	0.28	6.86
7	3.79	0.39	10.33
8	4.78	0.46	9.79
9	17.98	0.78	4.37
10	14.74	0.94	6.42
11	11.64	0.67	5.81
12	5.53	0.97	17.55
13	3.69	0.40	11.05
14	5.38	0.46	8.57
15	5.14	0.27	5.41
16	5.51	0.41	7.51

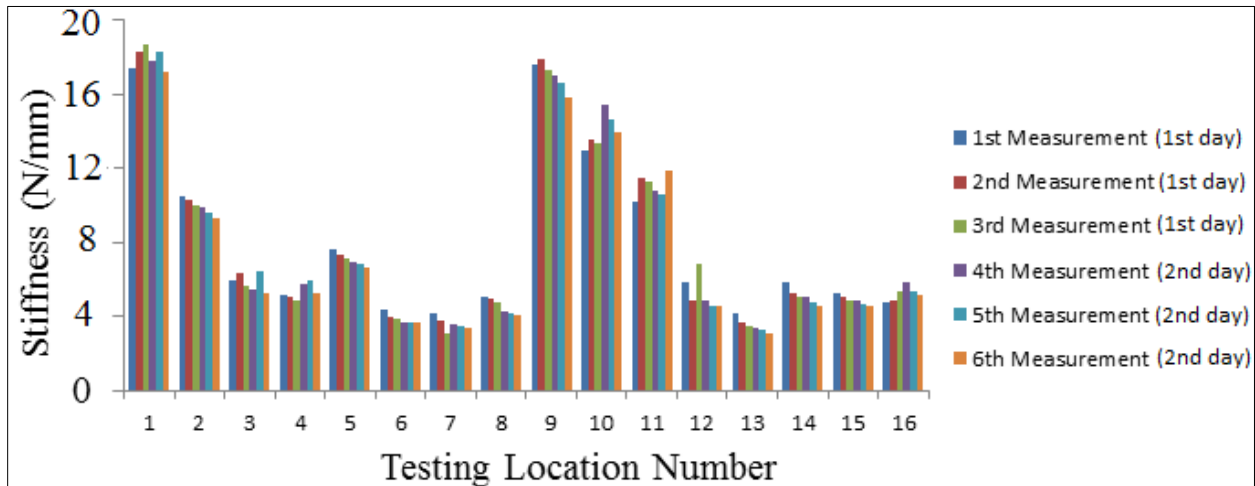


Figure C.1 Repeatability of stiffness measurements for a series of 16 testing locations on one lateral femoral cartilage compartment.

C-4-Discussion

Our finding of an 8% coefficient of variation for repeated stiffness measurements demonstrated the high inter-trial repeatability of the indentation protocol. Most of the testing locations experienced lower values for stiffness in the last measurements, which could be due to the alteration of cartilage properties in the course of two days. Similar variation across testing locations was observed among measurements. When stiffness data was compared among measurements, correlation coefficient was found to be more than $r=0.97$. This error (8%) was much smaller than the observed stiffness difference (54%) between grade 0 and 1 cartilage. However, testing more samples would result in a more accurate estimation of our indentation protocol repeatability.

Appendix D: Validation of Articular Cartilage Thickness Measurement using CECT

D-1-Introduction

The objective of the present work was to investigate the accuracy of using CECT to measure cartilage thickness in intact sheep femora and tibiae. Measurements of cartilage thickness were needed in our study to examine the possible confounding effect of thickness variation on our stiffness measurements.

D-2- Method

A subset of sheep samples (aged 12-20 months), previously scanned and tested, was randomly selected for this experiment (one femoral condyle and one tibial plateau). Thickness was measured in CECT images using the thickness measurement method described in chapter 3. A needle indentation test was then used to measure cartilage thickness and serve as the reference for our thickness measurements (Figure D.1). To do this, the spherical indenter of the mechanical tester (Mach-1) was replaced by a needle probe. Starting from above the cartilage surface, the needle was lowered at a constant speed while recording the force in the vertical direction. Contact with the cartilage surface was defined as the position where the vertical force deviated from zero. The bone-cartilage interface was defined as the position where the force-displacement curve changed abruptly. The distance between the cartilage surface and the bone-cartilage interface defined the vertical thickness. The cartilage thickness was determined from the vertical distance and the surface orientation. Thickness measurements from the indentation method were compared against thickness measurements from CECT scans at about 40 testing locations in each sample.

D-3-Results

Significant correlations ($R^2=0.91$ and 0.87 , $p<0.001$) were observed between the needle indentation and CECT measurements of thickness (Figure D.2). The mean thickness error was 0.057 and 0.11 mm for the sheep femoral condyle and tibial plateau, respectively, corresponding to 6% and 8% error of the mean thickness values.

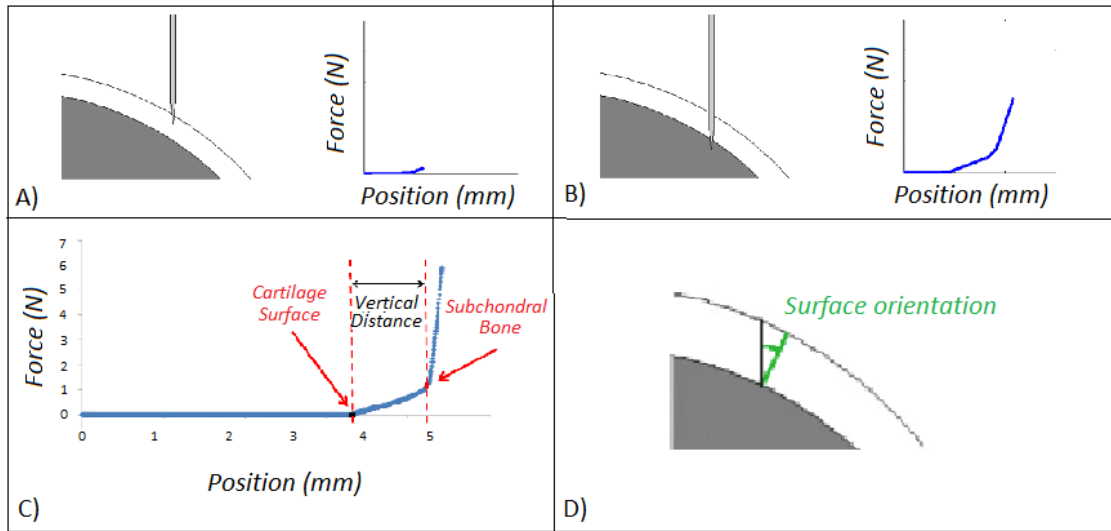


Figure D.1 Needle indentation technique for physical measurement of cartilage thickness.

A) As the tip of the needle reaches the cartilage surface, a small increase in load is observed. B) As the needle penetrates the cartilage and reaches the subchondral bone, there is a significant increase in load. C) Typical load-displacement curve in needle indentation technique. The vertical distance of cartilage surface from subchondral bone is determined from the curve. D) Cartilage thickness is determined using vertical distance and surface orientation. ©Reproduced with permission from Biomomentum Inc.

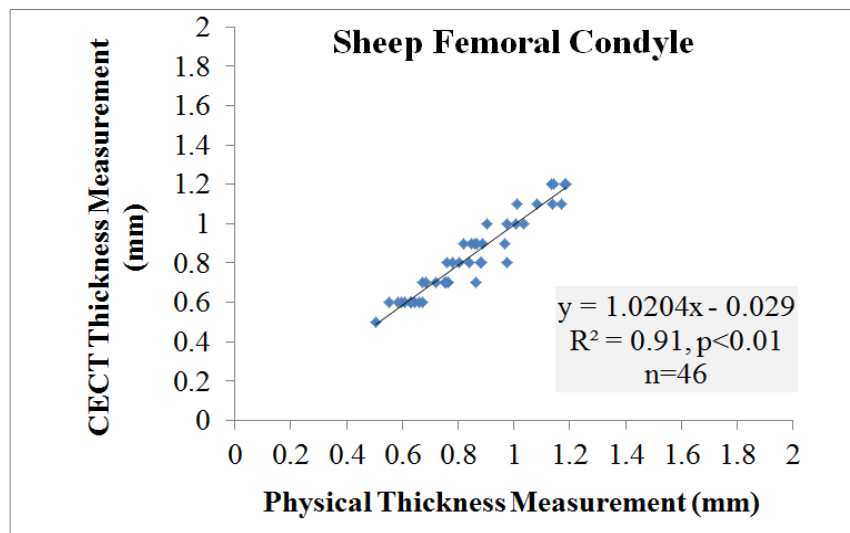


Figure D.2 Thickness measurements from needle indentation method versus CECT method (Sheep femoral condyle).

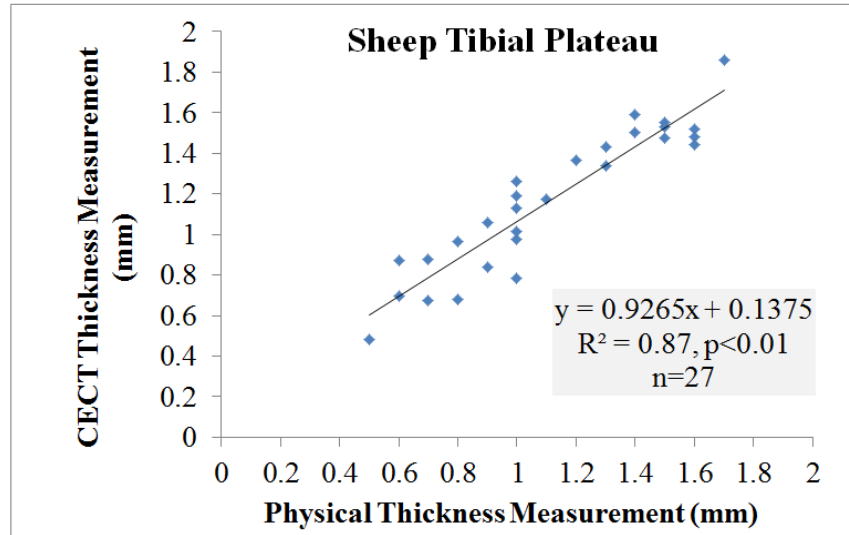


Figure D.3 Thickness measurements from needle indentation method versus CECT method.

D-4-Discussion

The results of this experiment show that CECT measures cartilage thickness with an error less than 0.12 mm. A key strength of this method is that both needle indentation and CECT measurements of thickness were performed in intact joint surfaces, which more closely represents the in vivo situation in which thickness measurements will be required than the widely-used cartilage plugs. Plug harvest procedures could lead to a difference between the preharvest thickness measurement obtained from imaging and the postharvest physical thickness measurements due to the tendency of the cartilage to change in shape and dimension following harvest.

Appendix E: Registration Accuracy

E-1-Introduction

A key step required to compare cartilage stiffness measurements to CECT attenuation was registration of these data. The details of the registration procedure were discussed in the thesis (chapter 3). The objective of this experiment was to quantify errors associated with this registration procedure.

E-2-Method

To quantify the cumulative error associated with the registration procedure, 10 markers were inserted into one sheep femoral cartilage surface. Two of them (markers #1 and #2 in Figure E.1) were used as references and the rest were targets to be localized in image space. Using the registration procedure described in chapter 3, the locations of the other 8 markers were determined in image space based on the coordinates of the two reference markers.

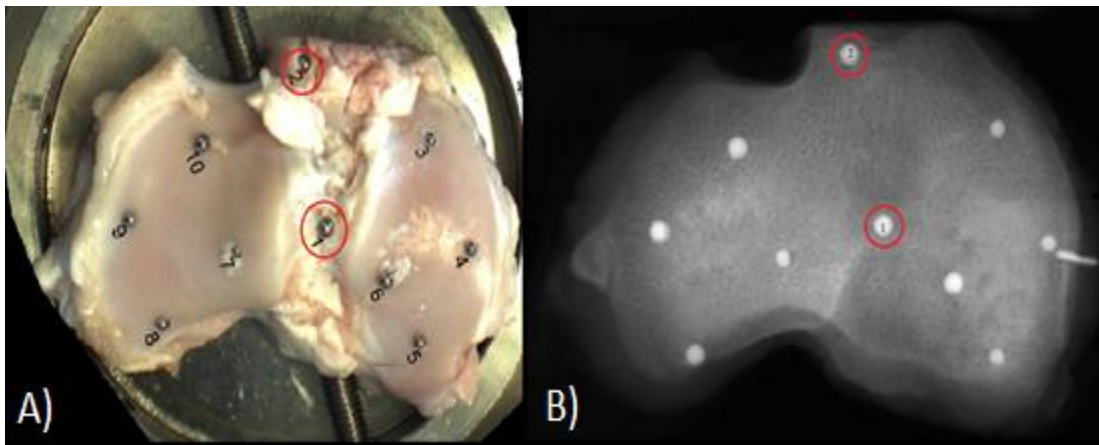


Figure E.1 The metal markers in physical space (A), and image space (B).
The first and second markers were used as references for registration between physical and image coordinate systems.

E-3-Result

Errors in finding the location of the target markers ranged from 3.74 to 7.34 voxels, or 0.15 to 0.3 mm (Table E.1).

Table E.1 Estimation error for determination of coordinates in image space.

Testing location #	Coordinates in image space			Estimated coordinates in image space			Error (Voxel)
	Slice#	Colum#	Row#	Slice#	Colum#	Row#	
3	134	172	256	129	173	255	5.19
4	271	103	232	264	104	230	7.34
5	402	172	243	396	171	241	6.4
6	316	230	167	315	228	162	5.47
7	289	458	172	292	459	174	3.74
8	399	577	263	396	572	264	5.91
9	260	624	170	261	625	175	5.19
10	154	518	273	156	520	270	4.12

E-4-Discussion

The highest value of the difference between the position of markers in image space and the predicted position was reported as the worst-case error of registration. The registration algorithm could predict the position of markers with less than 250 μm accuracy which was less than 8 voxels. The registration method thus enabled us to closely register and relate measurements from indentation to CECT method.

Appendix F: Repeatability of CECT Measurements

F-1-Introduction

CECT is a non-invasive imaging method for measuring the GAG content of articular cartilage. The objective of this experiment was to examine the repeatability of CECT measurements of attenuation in human articular cartilage.

F-2-Method

The details of the CECT imaging protocol were described in chapter 3 of the thesis. We randomly selected one of the human cartilage samples and scanned it a second time to investigate the repeatability of the CECT measurements. Following the first scan, the selected sample (HFC1) was equilibrated in PBS for 24 hours which is sufficient for the contrast agent to diffuse out of the cartilage[19]. The cartilage was then immersed in a 12 mgI/ml CA4+ contrast agent solution for another 48 hours and scanned for a second time. Using the image processing algorithms described in chapter 3, the average CECT attenuation in superficial cartilage was determined at 38 locations. The difference between CECT measurements between the first and the second scan was determined and the repeatability was reported as the root mean square (RMS) average of the coefficient of variation (CV) in percentage.

F-3-Results

The coefficient of variation (CV) of the CECT measurements ranged between 1% and 32%. The RMS average of the coefficients of variation was found to be nearly 15%. The details of the stiffness measurements in testing locations are illustrated in Table F.1 and Figure F.1.

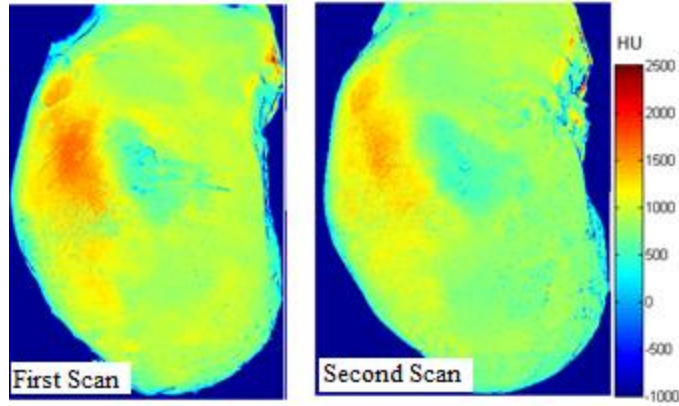


Figure F.1 Mapping of CECT attenuation (averaged over 0.6mm) in two scans representing two complete equilibration and imaging cycles in one specimen.

Table F.1 Mean, SD, and CV of CECT measurement for each testing location.

Testing Location #	Mean (HU)	SD (HU)	CV (%)	Testing Location #	Mean (HU)	SD (HU)	CV (%)
1	855	9	1	20	582	110	19
2	1,082	65	6	21	494	157	32
3	1,421	232	16	22	725	216	30
4	1,334	177	13	23	891	110	12
5	913	43	5	24	826	78	9
6	890	152	17	25	907	94	10
7	761	133	17	26	926	123	13
8	805	120	15	27	899	154	17
9	855	68	8	28	737	143	19
10	809	101	12	29	716	27	4
11	874	32	4	30	778	127	16
12	983	87	9	31	858	157	18
13	915	26	3	32	846	123	14
14	827	106	13	33	843	131	16
15	828	64	8	34	901	103	11
16	780	205	26	35	874	98	11
17	862	149	17	36	856	145	17
18	821	97	12	37	873	138	16
19	851	136	16	38	893	83	9

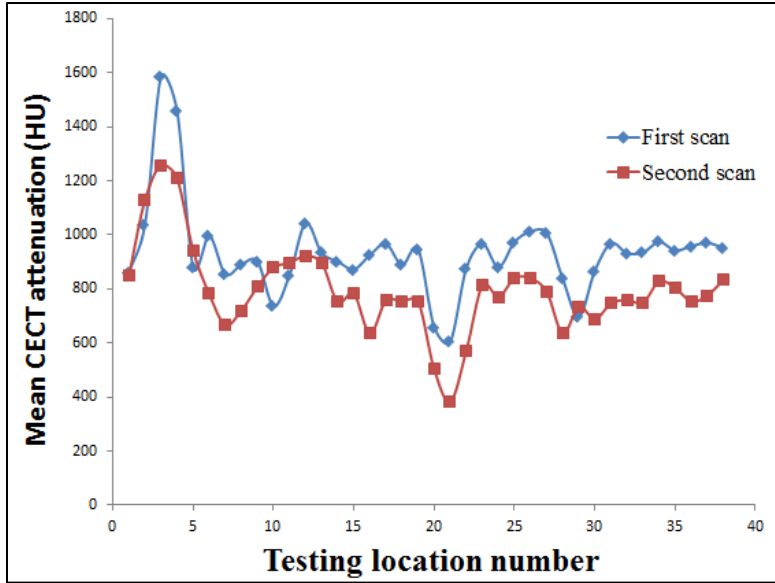


Figure F.2 Repeatability of CECT measurements for a series of 38 testing locations in one lateral femoral compartment.
Correlation coefficient between the CECT attenuation data in the first and the second scan was 0.81.

F-4-Discussion

A 15% coefficient of variation for the two CECT measurements represents good inter-trial repeatability for the CECT imaging protocol. Same spatial variation across testing locations is observed between the two measurements resulting in a correlation coefficient of $r=0.81$ ($p<0.01$). This finding suggests the repeatability of CECT measurement for revealing spatial variation of GAG content across cartilage surface. Depending on the required accuracy, this error might be acceptable for calculation of absolute values of GAG content. The range of precision error reported here is comparable with those reported for repeatability assessment of quantitative MRI methods [1][2][3]. In those studies, dGERMIC [3], sodium MRI [2], and T2 mapping [1] exhibited precision errors ranging between 9.3-15.2%, 7.5-13.6%, and 8-13%, respectively. Most of the testing locations had lower CECT values in the second measurement, which could be due to changing cartilage properties in the course of the experiment (4 days at room temperature).

F- References

- [1] Williams, Y. Qian, and C. R. Chu, “UTE-T2* mapping of human articular cartilage in vivo: a repeatability assessment.,” *Osteoarthritis Cartilage*, vol. 19, no. 1, pp. 84–8, Jan. 2011.
- [2] G. Madelin, J. S. Babb, D. Xia, G. Chang, A. Jerschow, and R. R. Regatte, “Reproducibility and repeatability of quantitative sodium magnetic resonance imaging in vivo in articular cartilage at 3 T and 7 T,” *Magn. Reson. Med.*, vol. 68, no. 3, pp. 841–849, 2012.
- [3] C. Siversson, C. J. Tiderius, P. Neuman, L. Dahlberg, and J. Svensson, “Repeatability of T1-quantification in dGEMRIC for three different acquisition techniques: Two-dimensional inversion recovery, three-dimensional look locker, and three-dimensional variable flip angle,” *J. Magn. Reson. Imaging*, vol. 31, no. 5, pp. 1203–1209, 2010

Appendix G: Estimation of the Young's Modulus of Cartilage using Indentation and CECT Measurement of Thickness

In this study, cartilage stiffness was reported as the ratio of peak load to indentation amplitude. For comparison to other studies, we calculated the corresponding values for Young's modulus. This appendix describes the mathematical procedure used to determine Young's modulus from the results of the indentation test combined with CECT measurement of tissue thickness.

The details of the indentation protocol and CECT measurement of thickness were described in chapter 3. An elastic model [1] of indentation of cartilage was used to find Young's modulus. This model is based on the indentation of an elastic, isotropic, and incompressible (Poisson's ratio=0.5) layer of cartilage attached to a rigid infinite half-space (bone). Young's modulus (E) can be calculated from the following equation:

$$E = \frac{F(1-\nu^2)}{2awk}$$

(Equation 5 : Relationship between indentation load and Young's modulus)

Where F is the peak normal load, ν is the Poisson's ratio, a is the contact radius between indenter and cartilage, w is the indentation amplitude, and k is a factor obtained from theoretical formulas. Assuming $\nu=0.5$, and with a given a, and a given w, E is related to F through k which is dependent on the aspect ratio (a/h, h is cartilage thickness) and ν . Values of k for indentation using a spherical indenter were calculated and tabulated [1].

G-References

[1] W. C. Hayes, L. M. Keer, G. Herrmann, and L. F. Mockros, "A mathematical analysis for indentation tests of articular cartilage.," J. Biomech., vol. 5, pp. 541-551, 1972.

Appendix H: Comparison between Different Measures of Cartilage Stiffness (Instantaneous, Equilibrium, and Dynamic stiffness)

H-1- Introduction

Articular cartilage behaves as a viscoelastic material and thus the effective stiffness of the tissue depends on the rate of application of displacement. Instantaneous (or immediate) stiffness of cartilage can be assessed as the load response of the tissue to a rapidly applied displacement whereby there is insufficient time for fluid motion and cartilage exhibits nearly elastic behavior. In contrast, if enough time elapses the fluid exudes through the cartilage matrix till reaching an equilibrium state and the resulting load response determines the equilibrium stiffness of cartilage. Dynamic stiffness of cartilage is defined as the load response of the tissue to cyclic displacement (e.g. sinusoid displacement). The objective of the present experiment was to determine if there are substantial differences between different measures of cartilage stiffness (instantaneous, equilibrium, and dynamic) in intact surface of sheep cartilage samples.

H-2- Method

One femoral condyle of a sheep (aged 12-20 months) knee joint was selected for this experiment. Using the mechanical testing system (Mach-1) and a spherical indenter ($d=1$ mm) described in chapter 3, a series of displacement protocols were applied to the intact surface of the cartilage samples. Due to practical limitations of the tester, we performed displacement protocols in one direction (z direction of the tester) and thus testing locations were limited to flat regions of the samples (12 testing sites per sample). At each testing location, the displacement protocol (Figure H-1) consisted of:

- An $80\mu\text{m}$ amplitude pulse test: peak load (immediate response) and equilibrium load (response after 5 min) were measured.
- A second $80\mu\text{m}$ amplitude pulse test: peak load (immediate response) and equilibrium load (response after 5 min) were measured.
- Two sinusoidal displacements (indentation amplitude= $10\mu\text{m}$) at two frequencies (1 Hz and 0.1 Hz): amplitude of load response was measured.
- The displacement protocol was the same across all testing locations and thus the corresponding load responses were directly reflective of stiffness.

The displacement protocol was the same across all testing locations and thus the corresponding load responses were directly reflective of stiffness. The measured peak load, equilibrium load, and load amplitude in sinusoidal displacement were reported as measures of cartilage instantaneous stiffness, equilibrium stiffness, and dynamic stiffness, respectively.

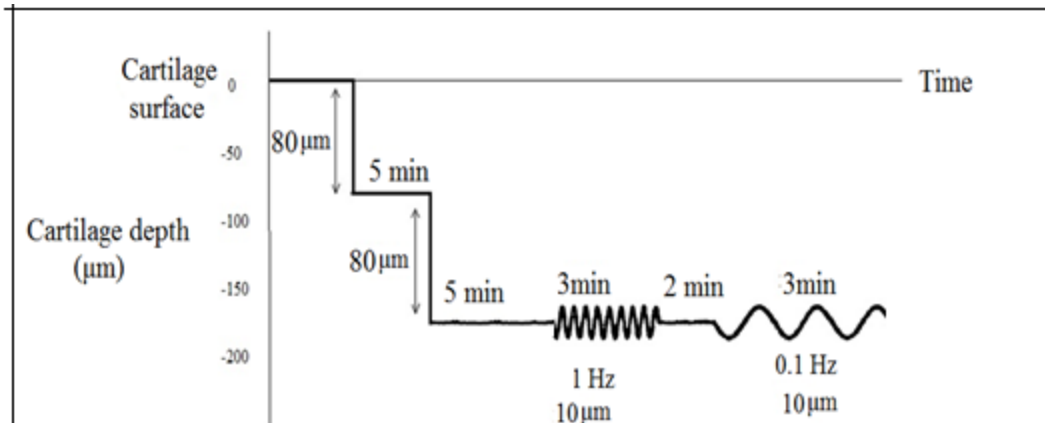


Figure H-6 : Displacement protocol used for inferring different measures of cartilage stiffness.

H-3- Result

Figure H-2 represents a schematic load response of cartilage to the displacement protocol applied using indentation. Peak load responses (point A and C) assess the instantaneous (or immediate) stiffness, while equilibrium load responses (point B and D) assess the equilibrium stiffness. The resulting load amplitudes in the last cycle of sinusoidal displacements (point E and F) assess the dynamic stiffness of cartilage.

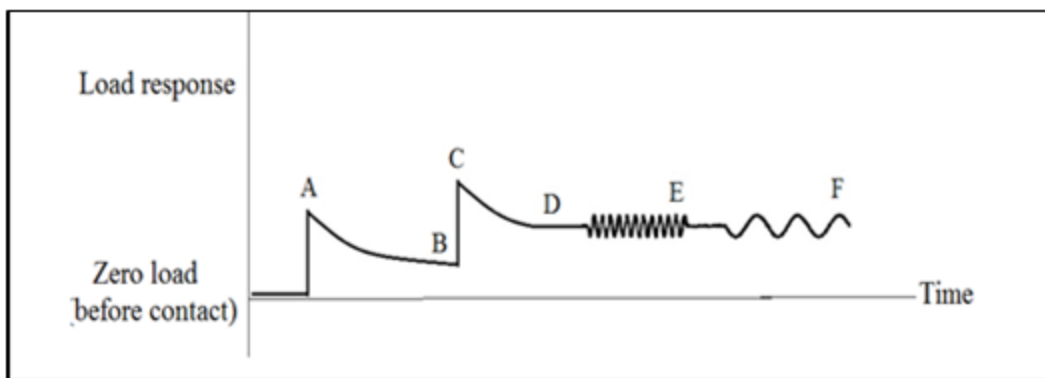


Figure H-2 : Schematic representation of cartilage load response to the multi-functional displacement protocol.

A general similarity between different measures of cartilage stiffness was found across samples (Figure H-3).

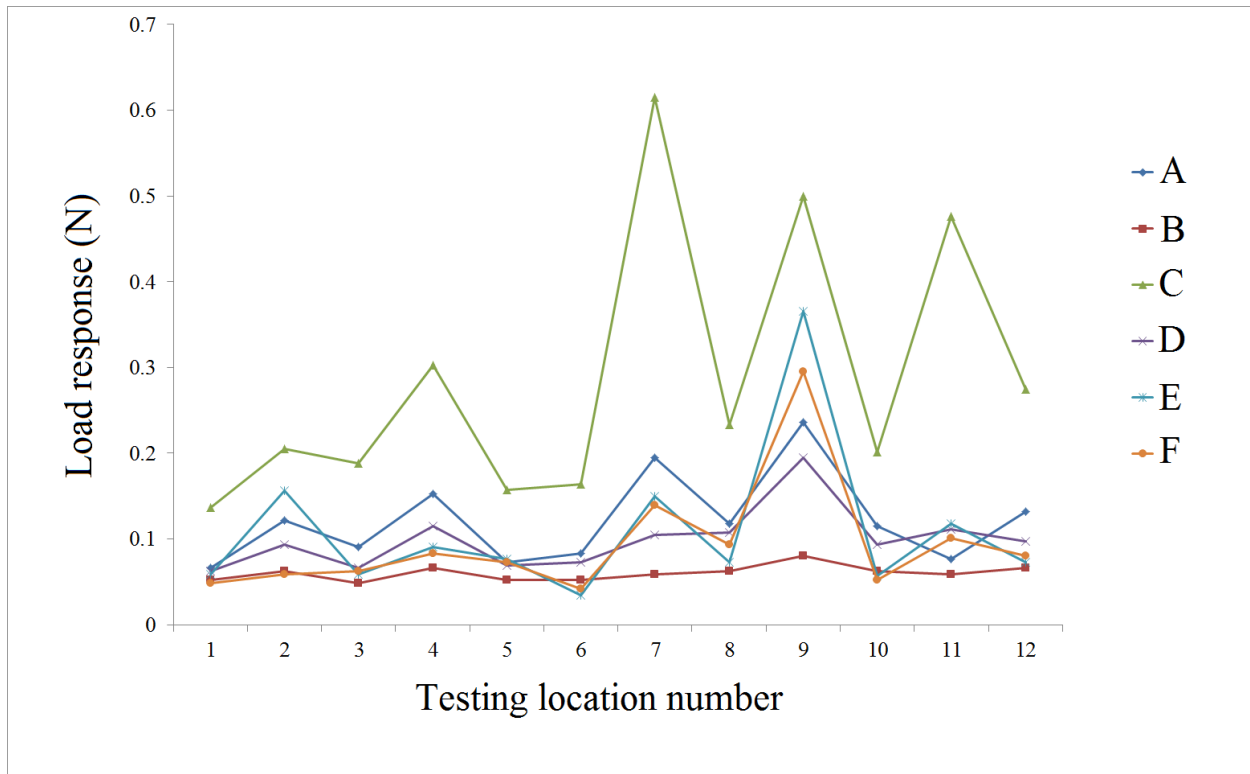


Figure H-3 : Comparison of different 6 load response profiles across 12 locations on one femoral condyle cartilage.

For quantitative comparison, the correlation coefficient between the load response at point A and the load response of other points (B-F) was calculated for all testing locations (Table H-1):

Table H-1 : Correlation analysis among different measures of cartilage stiffness.

Correlation coefficient (r), p<0.01	B	C	D	E	F
A	0.82	0.71	0.84	0.79	0.82

The immediate stiffness of cartilage (load response at A) was significantly correlated ($r=0.75-0.94$) with all measures of cartilage stiffness: equilibrium stiffness (load responses at B and D), immediate stiffness with a pre-strain (load response at C), and dynamic stiffness (load responses at E and F).

H-4- Discussion

Instantaneous, equilibrium, and dynamic load responses of cartilage to the multi-functional displacement protocol used in this experiment served as measures of instantaneous, equilibrium, and dynamic stiffness of the tissue, respectively. Instantaneous load response (stiffness) of cartilage showed similar variations across a series of testing locations compared to equilibrium and dynamic load response (stiffness) of the tissue. Instantaneous stiffness of cartilage can therefore provide a reliable measure for the overall stiffness and the integrity of the tissue. Since instantaneous stiffness is measured quickly compared to other measures of cartilage stiffness (less than 1 minute versus 10-minute duration for measurement of equilibrium/dynamic stiffness), this quantity is of particular interest for mapping of stiffness across surface of cartilage.

Appendix I: Accuracy Assessment of the Normal Displacement in the Indentation Protocol

I-1- Introduction

A practical challenge of the indentation technique is that the tip of the indenter has to be displaced normal to the cartilage surface. The indentation protocol employed in this thesis (as described in chapter 3) automatically detects surface orientation at each testing location and then moves the indenter normal to the surface. The accuracy of normal displacement in the indentation protocol should be quantified to ensure that indentation occurs along the correct direction. The objective of the present study is to compare the normal displacement of the indenter in our protocol to the normal axis calculated from the surface orientation.

I-2- Methods

A series of 20 testing locations were randomly selected from the data of indentation tests on human cartilage samples. Figure I-1 illustrates typical displacement-time curves during normal indentation in the X, Y, and Z directions, respectively (X, Y, and Z directions correspond to the axes of the mechanical tester stages). The displacement for each axis was calculated as the difference between the final and initial position (equation I-1) and the net displacement vector was obtained from the three displacements (equation I-2):

$$\text{Displacement in X direction} = \text{Final position X (t=0.85)} - \text{initial position X (t=0.25)}$$

$$\text{Displacement in Y direction} = \text{Final position Y (t=0.85)} - \text{initial position Y (t=0.25)}$$

$$\text{Displacement in Z direction} = \text{Final position Z (t=0.85)} - \text{initial position Z (t=0.25)}$$

(equation I-1: calculation of displacement in X, Y, and Z direction)

$$\text{Net displacement vector} = (\text{displacement in X direction}, \text{displacement in Y direction}, \text{displacement in X direction})$$

(equation I-2: calculation of the net displacement vector)

The angle between the net displacement vector and the surface normal (obtained from the surface orientation determination method in section 3.2.3.2) was calculated at each testing location.

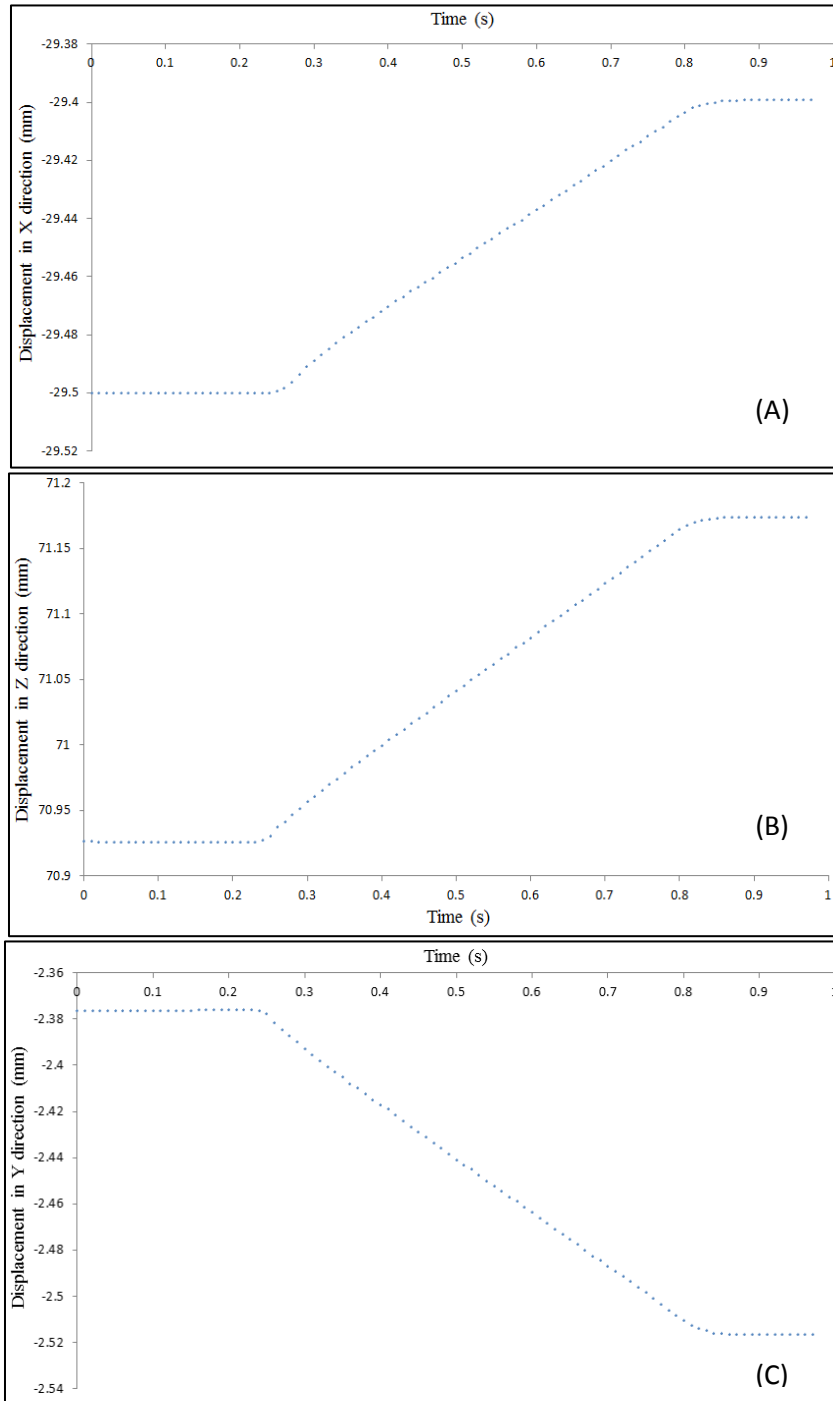


Figure I-1: Displacement versus time curves in X, Y, and Z directions (Plots A, B, and C, respectively) for the stages of the Mach 1 system during a typical cartilage indentation test.

I-3- Results

The X, Y, and Z components of the surface normal vector and the net displacement vector as well as the difference between them are summarized in table I-1. The maximum error for normal displacement of the indenter was 1.17° .

Table I.1 : Comparison between the surface normal vector and the net displacement vector.

testing site #	Surfae normal (unit vector)			Displacement vector (mm)			Difference (degrees)
	X	Y	Z	X	Y	Z	
1	0.2975	0.603	0.7402	0.0855	0.171	0.2055	0.71
2	0.0661	0.5009	0.863	0.019	0.14	0.238	0.36
3	-0.2949	0.2682	0.9171	-0.0845	0.078	0.253	0.96
4	0.0552	-0.5938	0.8027	0.016	-0.1575	0.214	0.31
5	0.1605	0.2646	0.9509	0.046	0.076	0.2615	0.73
6	-0.2403	0.3942	0.887	-0.068	0.1145	0.244	1.17
7	-0.1859	0.7122	0.6769	-0.054	0.196	0.1905	0.78
8	0.0417	0.1983	0.9793	0.012	0.057	0.27	0.48
9	-0.0633	0.0087	0.998	-0.0185	0.0015	0.275	0.28
10	0.0873	-0.3311	0.9396	0.025	-0.096	0.2595	0.9
11	0.2674	-0.462	0.8456	0.077	-0.1285	0.2325	0.7
12	0.5482	-0.7489	0.3723	0.1515	-0.206	0.1065	0.76
13	-0.18	-0.5281	0.8299	-0.052	-0.146	0.2305	0.43
14	0.439	-0.677	0.5907	0.124	-0.186	0.167	0.8
15	0.7199	-0.4438	0.5336	0.1985	-0.1215	0.1525	0.99
16	0.4561	0.2497	0.8542	0.128	0.071	0.236	0.5
17	0.5142	-0.3581	0.7793	0.144	-0.1035	0.215	0.88
18	0.2807	0.1052	0.954	0.08	0.03	0.2635	0.52
19	0.4573	0.463	0.7593	0.122	0.1235	0.202	0.07
20	-0.0524	0.1397	0.9888	-0.015	0.041	0.272	0.54

I-4- Discussion

The indentation protocol employed in this thesis was able to move the indenter in a direction perpendicular to the surface of cartilage with high accuracy (with less than 1.2° deviation from normal axis).

Appendix J: Calibration Certificate for the Load-Cell and the Control Report for all Stages

J-1: Load-cell certificate



Detailed Certificate of Calibration

Equipment Calibrated		Customer Information
Description:	Six-Axis Force/Torque Sensor	Mr. Antoine Larouche
Manufacturer:	ATI Industrial Automation	Biomomentum Inc.
Serial Number:	FT13299	970, rue Michelin (suite 200)
Model:	Nano17	2nd Floor
Calibration:	SI-50-0.5	Laval, QC H7L 5C1
Electronics:	DAQ	CANADA
Output Range:	±10V	larouche@biomomentum.com
Gain Multiplier:	100%	

Equipment Condition and Notes: Factory new.

Calibration Results: Passed
 Offset: Normal
 Gain: Normal

Calibrated Ranges (±):

Fx	Fy	Fz	Tx	Ty	Tz
50 N	50 N	70 N	500 N-mm	500 N-mm	500 N-mm

Measurement Uncertainty (95% confidence level, percent of full-scale load):

Fx	Fy	Fz	Tx	Ty	Tz
1.50%	1.50%	1.50%	1.50%	1.50%	1.75%

The above Measurement Uncertainty values are the maximum amount of error for each axis expressed as a percentage of its full-scale load.

Calibration Temperature: 22.2±1.1° C (72±2° F)
 Temperature Compensation: hardware
 Calibration Method: WI-FTP-026, DAQ Calibration Instructions

Date of Calibration: 24 Jan 2013

Certificate Date: 24 Jan 2013
 Calibrated by: J Parker, Calibration Technician



This calibration is traceable to the National Institute of Standards and Technology (NIST). Calibration standards (not all of the listed standards are used for this calibration):

Calibration Equipment	
Description	Identification
Calibration Tool	FTT-1908
DAQ, 200KS/S, 16-BIT, 16 AN	CNTRLR-2002-1
DAQ, 200KS/S, 16-BIT, 16 AN	CNTRLR-2015-3
DAQ, 200KS/S, 16-BIT, 16 AN	CNTRLR-2025-2
3X STND-ALN CONTROLLER	CNTRLR-2040
3X STND-ALN CONTROLLER	CNTRLR-2042
3X STND-ALN CONTROLLER	CNTRLR-2050
PCI-6034E	CNTRLR-2060-4
30K LOAD CELL	FTT-1990
9105-NETB BOX #2	FTT-1999
SS Hook Weights	WHT-1700
Weights Type II	WHT-1706
SS Set of 13 Weights	WHT-1707
SS Set of 13 Weights	WHT-1708
Brass Set of 13 Weights	WHT-1709
SS Set of 13 Weights	WHT-1720
SS Set of 13 Weights	WHT-1730

ATI Industrial Automation (ATI) certifies that the above product was calibrated in accordance with applicable ATI procedures. These procedures are compliant with the ISO 9001 standard to ensure that the above product is within ATI specifications. To meet this level of accuracy any loads must be correctly aligned to the transducer origin and the transducer must be mounted to a sufficiently strong surface.

To ensure the transducer measurement uncertainties listed on page 1 are met, more-conservative limits are used as calibration targets during the calibration process. If any of the calibration targets are exceeded the calibration will not pass. It is possible for a transducer to exceed these calibration targets while meeting the page 1 measurement uncertainties. The following calibration targets were used for this transducer: $F_x=1.25\%$, $F_y=1.25\%$, $F_z=1.25\%$, $T_x=1.25\%$, $T_y=1.25\%$, and $T_z=1.50\%$.

Note: If this is a recalibration of a legacy transducer that does not have precision locating features (such as dowel holes), there could be additional error in T_x and T_y due to inexact mounting location. Precision locating features are highly recommended for best accuracy and can be added by ATI.

This certificate shall not be reproduced except in full without written approval from ATI. This certificate only applies to the items listed and does not include unlisted ancillary items such as data acquisition equipment.

For questions or comments, please contact your ATI representative.



Calibration Accuracy Section
Sensor System FT13299, Nano17/SI-50-0.5
Force units: N; Torque units: N-mm

Calibrated Ranges (±)					
Fx	Fy	Fz	Tx	Ty	Tz
50	50	70	500	500	500

Applied Loads						
	Fx	Fy	Fz	Tx	Ty	Tz
1	0.000	9.452	0.000	-359.419	0.000	0.000
2	-9.452	0.000	0.000	0.000	-359.419	0.000
3	0.000	-9.452	0.000	359.419	0.000	0.000
4	9.452	0.000	0.000	0.000	359.419	0.000
5	0.000	40.034	0.000	65.588	0.000	0.000
6	-40.034	0.000	0.000	0.000	65.588	0.000
7	0.000	-40.034	0.000	-65.588	0.000	0.000
8	40.034	0.000	0.000	0.000	-65.588	0.000
9	0.000	11.121	0.000	67.791	0.000	-423.580
10	0.000	11.121	0.000	67.791	0.000	423.269
11	-11.121	0.000	0.000	0.000	67.791	-423.439
12	-11.121	0.000	0.000	0.000	67.791	424.145
13	0.000	-11.121	0.000	-67.791	0.000	-423.269
14	0.000	-11.121	0.000	-67.791	0.000	423.580
15	11.121	0.000	0.000	0.000	-67.791	-424.145
16	11.121	0.000	0.000	0.000	-67.791	423.439
17	0.000	0.000	15.569	-414.745	0.000	0.000
18	0.000	0.000	15.569	0.000	-414.310	0.000
19	0.000	0.000	15.569	415.417	0.000	0.000
20	0.000	0.000	15.569	0.000	414.824	0.000
21	0.000	0.000	53.379	0.000	0.000	0.000
22	0.000	0.000	-53.379	0.000	0.000	0.000
23	0.000	0.000	-15.569	414.745	0.000	0.000
24	0.000	0.000	-15.569	0.000	414.310	0.000
25	0.000	0.000	-15.569	-415.417	0.000	0.000
26	0.000	0.000	-15.569	0.000	-414.824	0.000

Refer to page 6 for important information on regarding this report.



Full-Scale Error						
	Fx	Fy	Fz	Tx	Ty	Tz
1	0.00%	0.06%	0.17%	-0.14%	-0.04%	0.19%
2	-0.16%	0.08%	0.19%	0.28%	-0.16%	0.05%
3	0.02%	0.02%	0.18%	0.24%	0.04%	-0.04%
4	-0.07%	0.07%	0.25%	-0.17%	0.18%	0.03%
5	0.08%	0.12%	0.15%	0.11%	-0.02%	-0.11%
6	-0.39%	0.04%	0.19%	0.03%	0.18%	0.00%
7	0.09%	-0.27%	0.15%	-0.03%	-0.04%	0.02%
8	-0.01%	0.06%	0.14%	0.08%	0.06%	0.06%
9	-0.03%	-0.34%	0.02%	-0.09%	0.30%	-0.05%
10	-0.10%	-0.60%	0.04%	0.02%	-0.24%	-0.06%
11	0.24%	-0.06%	-0.02%	-0.22%	0.04%	-0.04%
12	0.32%	-0.12%	-0.02%	0.00%	0.09%	-0.07%
13	-0.12%	0.25%	0.02%	0.04%	-0.14%	-0.21%
14	-0.04%	0.29%	0.02%	0.09%	0.20%	-0.18%
15	-0.43%	-0.26%	0.05%	0.17%	0.06%	-0.16%
16	-0.52%	0.01%	0.04%	-0.19%	0.22%	-0.14%
17	0.05%	-0.02%	-0.07%	0.07%	-0.07%	-0.03%
18	-0.02%	0.10%	-0.02%	-0.09%	0.26%	0.13%
19	0.01%	0.11%	-0.07%	-0.16%	0.04%	0.03%
20	-0.17%	0.11%	-0.04%	-0.04%	0.16%	-0.24%
21	0.02%	0.24%	0.28%	0.26%	-0.11%	0.01%
22	-0.01%	0.22%	-0.21%	-0.07%	-0.11%	-0.02%
23	0.06%	0.13%	0.36%	0.09%	0.06%	0.11%
24	-0.13%	0.10%	0.38%	0.51%	-0.04%	0.13%
25	0.04%	0.04%	0.37%	0.19%	0.25%	0.00%
26	-0.02%	0.12%	0.40%	0.12%	0.15%	-0.24%

Refer to page 6 for important information on regarding this report.

Offset Report						
	Fx	Fy	Fz	Tx	Ty	Tz
F/T Offset	-0.0602	0.3027	-0.3247	0.7184	-0.2017	-0.7430
	SG0	SG1	SG2	SG3	SG4	SG5
SG Offset	0.0074	0.0170	0.0296	0.0188	0.0033	0.0262
±SG Limit	0.4883	0.4883	0.4883	0.4883	0.4883	0.4883

Offsets are measured in a unique configuration not available to the user.
Refer to page 6 for important information on regarding this report.



Gain-Check Report						
	SG0	SG1	SG2	SG3	SG4	SG5
Lower Limit	0.5000	0.5000	0.5000	0.5000	0.5000	0.5000
Lower Output	0.7695	0.7599	0.7241	0.7365	0.7475	0.7595
Upper Output	0.7715	0.7600	0.7330	0.7389	0.7655	0.7682
Upper Limit	1.0000	1.0000	1.0000	1.0000	1.0000	1.0000

*Gain readings are measured in a unique loading configuration.
Refer to page 6 for important information on regarding this report.*

Engineered Products for Robotic Productivity



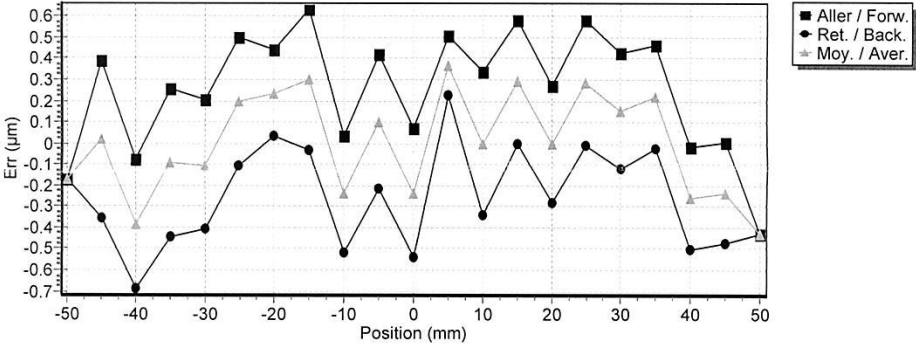
As part of our commitment to quality, each ATI force/torque transducer undergoes rigorous accuracy testing. This process, which involves applying and verifying a rich set of loading cases designed to cover the transducer's entire six-axis calibrated range, is designed to ensure that your transducer meets the measurement uncertainties listed in this Certificate of Calibration.

Our transducers often exceed our quality standards for accuracy. Often, transducers perform exceptionally well in certain loading situations. This report summarizes the performance of your ATI F/T transducer in our factory tests. It can be thought of as a 'best-case scenario' snapshot of your transducer's performance under laboratory conditions, in a variety of loading situations. You can expect the accuracy of your transducer measurements to fall somewhere between its performance during testing and the measurement uncertainties listed on its calibration certificate.

The *Calibration Accuracy Section* contains several tables of data. The *Calibrated Ranges (\pm)* table lists the transducer's rated range for each axis. The *Applied Loads* table lists the loads applied during calibration and testing. The *Full-Scale Error* table shows the sensor system's measurement error as a percentage of full scale for each axis in each loading case. The *Offset Report* table shows transducer readings during offset adjustment and associated control limits. And the *Gain-Check Report* table shows verification of the transducer's sensitivity and associated control limits. If included, the *Before and After Report* table shows a loading case relating the transducer's performance as received to its performance after recalibration.

For best accuracy, be sure to use your transducer's precision location features, and mount your transducer to a stiff surface. If an ongoing guarantee of sensor accuracy is important to you, we recommend that your sensor be tested annually. Contact your ATI Industrial Automation distributor to schedule recalibrations.

J-2: Control report for stage 1 (X axis)

 MICRO-CONTROLE une marque du groupe Newport	Rapport de controle <i>Control report</i>	12/12/2012	 INDEXATION une division du groupe Newport
Informations / Data			
Nom du produit <i>Product name</i>	<input type="text" value="ILS@ILS100"/>	Nom de l'opérateur <i>Operator name</i>	<input type="text" value="D MERLET"/>
Nom du fichier <i>File name</i>	<input type="text" value="12_9179_I2.mes"/>	Instrument <i>Measure tool</i>	<input type="text" value="Interféromètre Renishaw"/>
N° de série <i>Serial Number</i>	<input type="text" value="12_9179"/>	Identifiant <i>Identifier</i>	<input type="text" value="B6 40029"/>
			
Incrément vrai <i>True increment</i>	<input type="text" value="0.0005000317"/>	Unité <i>Unit</i>	<input type="text" value="µm"/>
Répétabilité <i>Repeatability</i>	<input type="text" value="0.493"/>		
Précision dans l'axe <i>On axis accuracy</i>	<input type="text" value="0.796"/>		
Précision absolue <i>Absolute accuracy</i>	<input type="text" value="6.188"/>		
Moyenne hystérésis <i>Average hysteresis</i>	<input type="text" value="0.516"/>		
Commentaires <i>Reviewed by:</i> <i>nt 12 Jan 2013</i>			

LACET / TANGAGE Spectra-Physics
une division du groupe Newport

Informations / Data

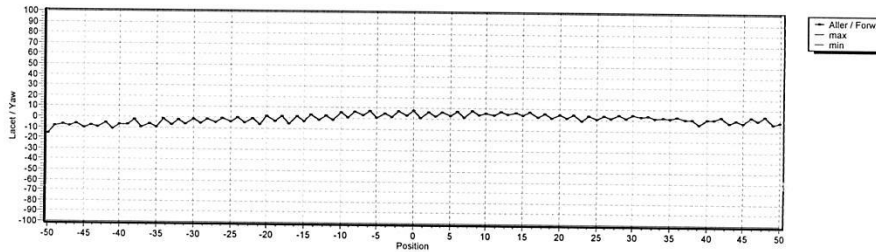
Nom du produit Product name	ILS@ILS100	Nom de l'opérateur Operator name	D MERLET
Nom du fichier File name	12_9179_L1.mes	Instrument Measurement tool	LDS
N° de série Serial Number	12_9179	Identifiant Identifier	B4 41 030

Lacet / Yaw

Critère acceptation catalogue
Catalogue acceptance criterium

Unité / Unit

Max (A / F)

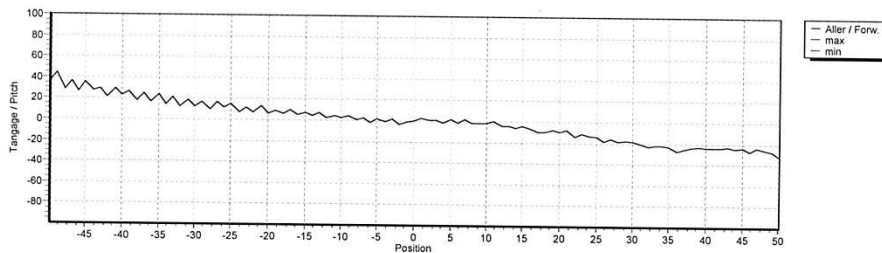


Tangage / Pitch

Critère acceptation catalogue
Catalogue acceptance criterium

Unité / Unit

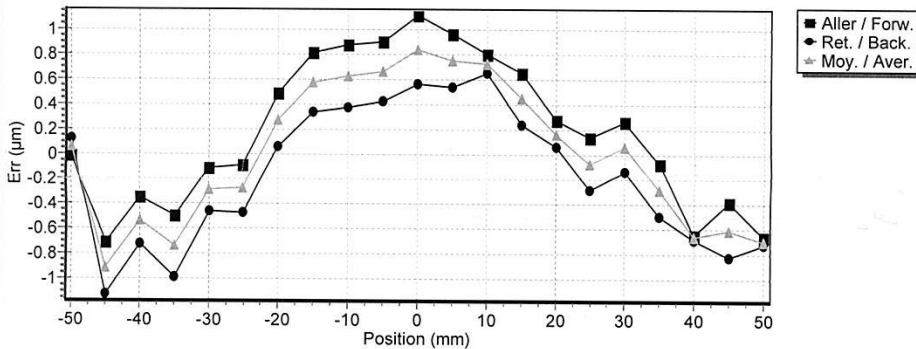
Max (A / F)



Commentaires

Reviewed by:
[Signature]

J-3: Control report for stage 2 (Y axis)

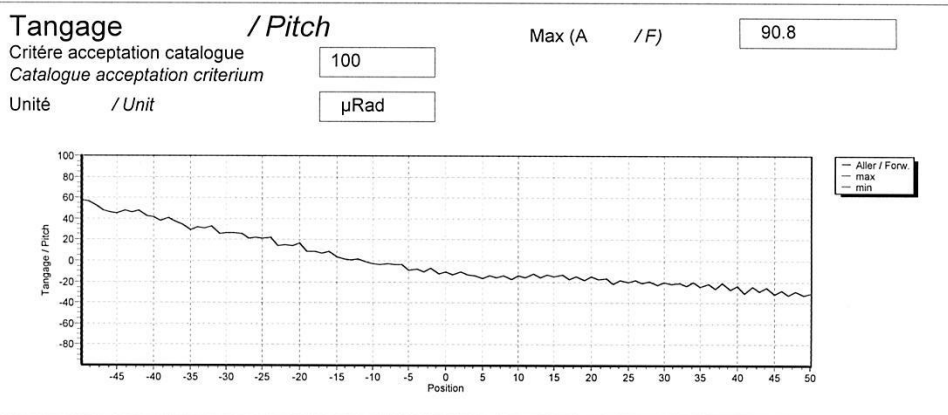
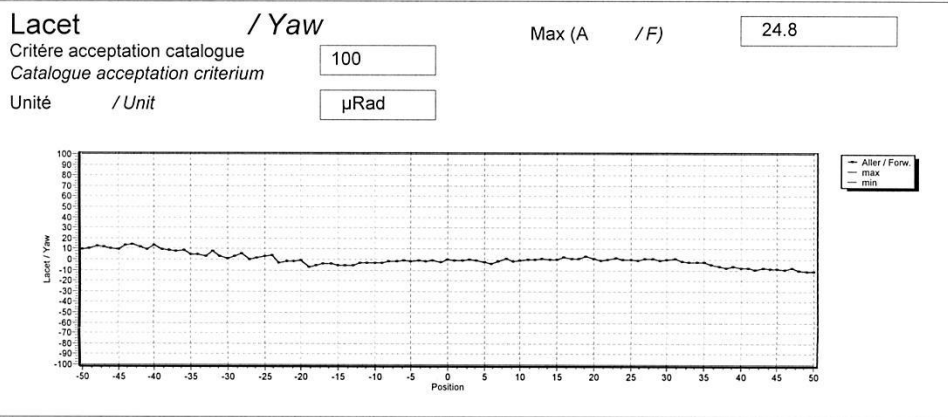
	Rapport de controle <i>Control report</i> 12/12/2012	
 MICRO-CONTROLE une marque du groupe Newport	<h1 style="margin: 0;">INDEXATION</h1>	 Spectra-Physics une division du groupe Newport
Informations / Data		
Nom du produit <i>Product name</i>	<input type="text" value="ILS@ILS100"/>	Nom de l'opérateur <i>Operator name</i>
	<input type="text" value="D MERLET"/>	
Nom du fichier <i>File name</i>	<input type="text" value="12_9180_I2.mes"/>	Instrument <i>Measure tool</i>
		<input type="text" value="Interféromètre Renishaw"/>
N° de série <i>Serial Number</i>	<input type="text" value="12_9180"/>	Identifiant <i>Identifiant</i>
		<input type="text" value="B6 40029"/>
		
Incrément vrai <i>True increment</i>	<input type="text" value="0.0005000255"/>	Unité <i>Unit</i>
Répétabilité <i>Repeatability</i>	<input type="text" value="0.411"/>	<input type="text" value="µm"/>
Précision dans l'axe <i>On axis accuracy</i>	<input type="text" value="1.753"/>	
Précision absolue <i>Absolute accuracy</i>	<input type="text" value="5.246"/>	
Moyenne hystérésis <i>Average hysteresis</i>	<input type="text" value="0.347"/>	
Commentaires		
<i>Reviewed by</i> <i>D.J. 27 Jan 2013</i>		

LACET / TANGAGE Spectra-Physics

une division du groupe Newport

Informations / Data

Nom du produit <i>Product name</i>	<input type="text" value="ILS@ILS100"/>	Nom de l'opérateur <i>Operator name</i>	<input type="text" value="D MERLET"/>
Nom du fichier <i>File name</i>	<input type="text" value="12_9180_L1.mes"/>	Instrument <i>Measure tool</i>	<input type="text" value="LDS"/>
N° de série <i>Serial Number</i>	<input type="text" value="12_9180"/>	Identifiant <i>Identifier</i>	<input type="text" value="B4 41 030"/>



Commentaires *Reviewed by: CJ 22 Jan 2013*

J-4: Control report for stage 3 (Z axis)



Rapport de controle Control report 07/12/2012

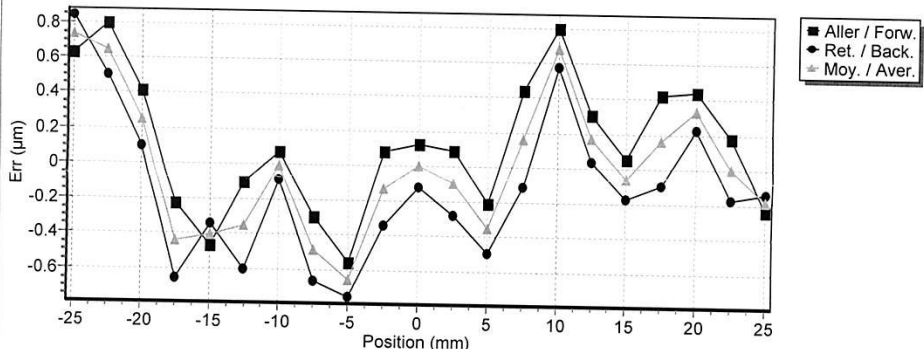
INDEXATION



une division du groupe Newport

Informations / Data

Nom du produit <i>Product name</i>	ILS@ILS50	Nom de l'opérateur <i>Operator name</i>	J TROUVE
Nom du fichier <i>File name</i>	12_9083_12.me5	Instrument <i>Measure tool</i>	Interféromètre Renishaw
N° de série <i>Serial Number</i>	12_9083	Identifiant <i>Identifier</i>	B6 40029



■ Aller / Forw.
● Ret. / Back.
▲ Moy. / Aver.

Incrément vrai <i>True increment</i>	0.0005000304	Unité <i>Unit</i>	µm
Répétabilité <i>Repeatability</i>	0.576		
Précision dans l'axe <i>On axis accuracy</i>	1.389		
Précision absolue <i>Absolute accuracy</i>	3.164		
Moyenne hystérésis <i>Average hysteresis</i>	0.263		

Commentaires *Reviewed by:*
1 of 27 Jan 2013

LACET / TANGAGE  Spectra-Physics
une division du groupe Newport

Informations / Data

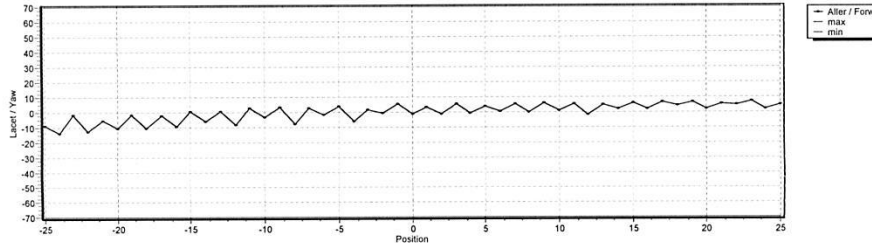
Nom du produit Product name	ILS@ILS50	Nom de l'opérateur Operator name	J TROUVE
Nom du fichier File name	12_9083_L1.mes	Instrument Measure tool	LDS
N° de série Serial Number	12_9083	Identifiant Identifier	B4 41 030

Lacet / Yaw

Critère acceptation catalogue
Catalogue acceptance criterium

Unité / Unit

Max (A / F)

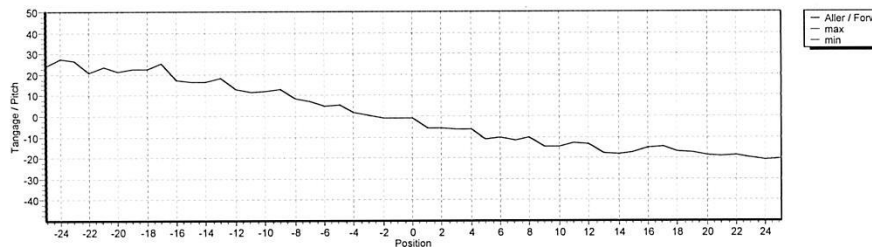


Tangage / Pitch

Critère acceptation catalogue
Catalogue acceptance criterium

Unité / Unit

Max (A / F)



Commentaires

Reviewed by:
n4 22 Jan 2013